UNITED AIRCRAFT CORPORATION

United Aircraft Research Laboratories

EAST HARTFORD, CONNECTICUT

United Aircraft Research Laboratories

UNITED AIRCRAFT CORPORATION

EAST HARTFORD, CONNECTICUT

H-910091-20

Experimental Investigations of Heavy-Gas Containment in R-F Heated and Unheated Two-Component Vortexes

NASA Contract No. NASw-847

REPORTED BY Arthur E. Mensing

Arthur E. Mensing

Jerome F. Jaminet

Jerome F. Jaminet

APPROVED BY James W. Clark

James W. Clark, Chief
Fluid and Systems Dynamics

DATE September 1969

NO. OF PAGES 78

COPY NO. 66.1

FOREWORD

An exploratory experimental and theoretical investigation of gaseous nuclear rocket technology is being conducted by the United Aircraft Research Laboratories under Contract NASw-847 with the joint AEC-NASA Space Nuclear Propulsion Office. The Technical Supervisor of the Contract for NASA is Captain C. E. Franklin (USAF). Results of portions of the investigation conducted during the period between September 15, 1968 and September 15, 1969 are described in the following five reports (including the present report) which comprise the required ninth Interim Summary Technical Report under the Contract:

1. Roman, W. C., J. F. Klein, and P. G. Vogt: Experimental Investigations to Simulate the Thermal Environment, Transparent Walls and Propellant Heating in a Nuclear Light Bulb Engine. United Aircraft Research Laboratories Report H-910091-19, September 1969.

2. Mensing, A. E. and J. F. Jaminet: Experimental Investigations of Heavy-Gas Containment in R-F Heated and Unheated Two-Component Vortexes. United Aircraft Research Laboratories Report H-910091-20, September 1969. (present report)

3. Krascella, N. L.: Theoretical Investigation of the Radiant Emission Spectrum from the Fuel Region of a Nuclear Light Bulb Engine. United Aircraft Research Laboratories Report H-910092-12, September 1969.

4. Latham, T. S., H. E. Bauer, and R. J. Rodgers: Studies of Nuclear Light Bulb Start-up Conditions and Engine Dynamics. United Aircraft Research Laboratories Report H-910375-4, September 1969.

5. Johnson, B. V.: Exploratory Experimental Study of the Effects of Inlet Conditions on the Flow and Containment Characteristics of Coaxial Flows. United Aircraft Research Laboratories Report H-910091-21, September 1969.

Report H-910091-20

Experimental Investigations of Heavy-Gas Containment in R-F Heated and Unheated Two-Component Vortexes

TABLE OF CONTENTS

Report H-910091-20

Experimental Investigations of Heavy-Gas Containment in R-F Heated and Unheated Two-Component Vortexes

SUMMARY

Experimental investigations were conducted in which the amount of heavy gas contained in light-gas vortexes was measured for both heated and unheated (isothermal) vortex flows. In the vortex flows with heat addition, power was added to the flow by r-f induction heating of the gas within the vortex chamber. The light gas, argon, was injected in a tangential direction either from the end walls or from the peripheral wall of the vortex chamber. The vortex flow rates, plasma diameter, and power addition were such as to provide a radial gradient of temperature of approximately 50,000 deg K/in. near the outer edge of the plasma. Xenon was employed as the heavy gas and was injected into the vortex at several different locations. Spectroscopic techniques were used to determine both the temperature distribution and the xenon partial pressures within the plasma.

Tests conducted with unheated vortex flows employed a vortex tube much larger than, but geometrically similar to, the vortex tube used in the heated tests. Air was used as the light gas and mixtures of iodine with helium, nitrogen or sulfur hexafluoride were used as heavy gases. Several different heavy- and light-gas injection configurations were used, and the weight flow rates of both the heavy and light gases were varied. The volume-averaged partial pressures of the heavy gas within the vortexes were determined, as were the radial distributions of the heavy-gas partial pressure.

Comparisons were made of the heavy-gas partial pressures in the heated and unheated flows. For similar geometries and the same light-gas weight flows, the heated vortexes had larger values of the heavy-gas partial pressure in the central regions of the vortex, but less heavy-gas partial pressure at the greater radii. Under the same conditions, the volume averaged heavy-gas partial pressures were about equal in both heated and unheated flows. Radial gradients of static pressure in the heated vortexes were much less than in unheated vortexes having the same flow rates.

RESULTS AND CONCLUSIONS

1. Experiments were conducted in two-component vortex flows in which xenon was injected into an r-f induction-heated argon vortex. Several different methods were used to inject both the argon and xenon into the vortex chamber. Spectroscopic measurements of the light emitted from the plasma were made to determine the plasma temperature and the xenon partial pressure. The primary results of these tests were:

a. The argon plasma diameter was approximately 70 percent of the diameter of the vortex chamber. The peak plasma temperature was approximately 10,000 K and a radial temperature gradient of approximately 50,000 deg K/in. existed near the outside edge of the plasma. Less than 10 percent of the power deposited into the plasma reached the peripheral wall of the vortex chamber.

b. Xenon injected either through the vortex chamber peripheral wall in a radial direction or on the vortex centerline in an axial direction resulted in containment of xenon within the plasma, provided the injection velocity was of the same order of magnitude as the vortex tangential velocity.

c. The presence of a large radial gradient of temperature appears to significantly reduce the xenon partial pressure at the peripheral wall of the vortex chamber.

d. The maximum xenon partial pressures within the plasma region were generally 6 to 7 times the xenon partial pressure that would have existed if the xenon had been uniformly distributed throughout the vortex chamber.

e. For the same argon and xenon flow rates, the method of driving the vortex (i.e., tangential injection of the argon either from the end walls or from the peripheral wall) had no significant effect on the xenon partial pressures within the plasma region.

f. When injected from the surface of the vortex chamber end wall, neither xenon gas nor tungsten particles could be made to enter the plasma in quantities sufficient for spectroscopic measurements.

2. Unheated two-component gas vortex tests were conducted in the high Reynolds number test facility and employed various heavy- and light-gas injection configurations as well as several heavy-gas molecular weights. (The term "unheated" is used to differentiate these tests from the r-f heated tests even though the gases employed were heated to approximately 300 F to avoid condensation of the iodine vapor used to "mark" the heavy gas.) The results of these tests were:

a. With a fixed geometry, increasing the ratio of heavy- to light-gas volume flow rate increased the volume-averaged heavy-gas partial pressure within the vortex. The increase in volume-averaged partial pressure was the same whether the heavy-gas volume flow rate was increased with constant light-gas volume flow rate or the light-gas volume flow rate was decreased with constant heavy-gas volume flow rate. Changes in the heavy-gas molecular weight at a constant ratio of heavy- to light-gas volume flow rate had no effect on the volume-averaged heavy-gas partial pressure.

b. With a fixed geometry and fixed light-gas weight flow, increasing the heavy-gas flow rate increased the heavy-gas partial pressure both in the central core of the vortex and near the peripheral wall of the vortex chamber. However, the ratio of the maximum heavy-gas partial pressure within the vortex to the heavy-gas partial pressure which would exist if the heavy and light gases were fully mixed decreased as the heavy-gas flow rate increased.

c. Injection of the heavy gas in an axial direction through an end wall resulted in less heavy gas stored than did injection of the same flow rate of heavy gas in a radial direction through the peripheral wall. However, for the same heavy- and light-gas flow rates, the ratio of the maximum value of the heavy-gas partial pressure within the vortex to that which would exist if the heavy and light gases were fully mixed was greater with heavy-gas injection through an end wall.

d. With fixed light- and heavy-gas flow rates, increasing the amount of bypass flow (flow withdrawn at the peripheral wall at the ends of the vortex tube) increased the heavy-gas containment parameter by about 60 percent when the bypass flow was varied from 0 to 50 percent. Further increases in bypass flow to greater than 80 percent resulted in little or no additional increases in heavy-gas containment.

3. Comparisons between heated and unheated two-component vortex flows showed that the volume-averaged heavy-gas partial pressures in the heated vortexes were not significantly different from those in the unheated vortexes for the same ratio of heavy-gas flow rate to light-gas flow rate. However, the heavy-gas partial pressures in the central regions of the vortex were greater in heated vortexes than in unheated vortexes, while the heavy-gas partial pressures near the peripheral wall were significantly lower in heated vortexes than in unheated vortexes. The heated vortexes appeared to be much less sensitive to changes in the light-gas injection configurations.

4. Heated vortex flows produced a much smaller radial gradient of pressure than did corresponding unheated vortex flows.

INTRODUCTION

An experimental and theoretical investigation of gaseous nuclear rocket technology is being conducted by the United Aircraft Research Laboratories under Contract NASw-847 administered by the joint AEC-NASA Space Nuclear Propulsion Office. The research performed under this contract is primarily applicable to the vortex-stabilized nuclear light bulb rocket concept described in Ref. 1. In this concept, hydrogen propellant seeded with a small amount of tungsten particles is heated by thermal radiation passing through an internally cooled transparent wall located between gaseous uranium fuel and the propellant. A transparent buffer gas such as neon is injected tangent to the inner surface of the transparent wall to establish a vortex flow which is utilized to isolate the gaseous nuclear fuel from the transparent wall.

A requirement for the operation of any gaseous nuclear reactor is the containment of sufficient nuclear fuel to maintain criticality. In the case of the nuclear light bulb, an additional requirement is that no fuel reach the transparent wall since this would cause the wall to lose transparency.

A number of experimental investigations have been conducted throughout the past several years to determine the containment characteristics of two-component gas vortexes (Refs. 2 through 6). In these investigations, a light gas was used to drive the vortex and a heavy gas was injected separately to simulate gaseous nuclear fuel. Most of the past two-component gas tests were conducted with vortex flows in which no temperature gradient was present.

The experiments conducted in the present investigations had two primary purposes: (1) to investigate the containment of a heavy gas in a vortex flow in which a large temperature gradient is present, and (2) to investigate the vortex flow parameters that affect the heavy-gas containment in an isothermal vortex flow with primary emphasis on establishing flows that are similar to those desired in the full-scale nuclear light bulb engine. In addition, it was desired to make comparisons between the results obtained in isothermal vortex tests and those from similar tests in which a temperature gradient was present to determine the effect of a temperature gradient on the vortex flow patterns.

TEST EQUIPMENT AND PROCEDURES

The two-component vortex tests conducted in this investigation employed two different facilities. The heated vortex tests were conducted using the UARL 80-kw r-f induction heater, while the unheated vortex tests were conducted using the high Reynolds number test facility constructed at UARL under Contract NASw-847. The equipment used in each of these facilities is described in the following two subsections.

Heated Vortex Tests

UARL 80-Kw R-F Induction Heater

The 80-kw r-f induction heater used in the heated vortex tests is basically the same as described in Ref. 7. Briefly, the 80-kw r-f induction heater is a driven system in which a 600-w tunable r-f transmitter drives the grid of the 80-kw power amplifier through a tuned coupling network. The output of the power amplifier is connected to a 2 1/2-turn, 2.7-in.-dia coil through a pi coupling network. The coil turns are spaced approximately 1.0 in. apart and the vortex chamber assembly is inserted within the work coil.

Vortex Models and Light-Gas Injection Systems

Sketches of the two vortex chambers used in these experiments are presented in Fig. 1. Each of the vortex chambers had a 1.26-in.-ID by 1.37-in.-OD (32-mm-ID by 35-mm-OD) fused-silica tube forming the peripheral wall of the vortex chamber. A 1.77-in.-ID by 1.92-in.-OD (45-mm-ID by 49-mm-OD) fused-silica tube was placed around the smaller tube. Cooling water was flowed in the annular region between the two tubes to cool the inner fused-silica tube. The normal water flow rate was 1.2 gpm.

Water-cooled copper end walls were placed inside the smaller fused-silica tube (see Fig. 1). The distance between the end walls was adjustable. A 0.25-in.-ID exhaust duct was located at the center of each end wall, and water-cooled tubing was placed inside each exhaust duct to cool the hot exhaust gases. Water flow rates and inlet and outlet water temperatures were measured for all water coolant flows so that a calorimetric balance could be made.

Two different types of light-gas injection systems were employed. In the system shown in Fig. 1a, which employed end-wall light-gas injection, the light gas (argon) was injected into the vortex chamber in a tangential direction through

eight injectors, four located on each end wall. The injectors consisted of 0.044-in.-ID by 0.062-in.-OD (1.1-mm-ID by 1.5-mm-OD) stainless steel tubing soldered to the end wall at a radius of 0.5 in. (see Fig. 1a). Teflon tubing connected the injectors to two manifolds located several inches away from each end wall. With this light-gas injection system, the end walls were spaced 2.8 in. apart. The light-gas injection area for this configuration was 0.012 sq in. and the scaling parameter, $dL/A_{B,j}$, was 295.

A second system -- peripheral-wall light-gas injection -- was employed in some tests and is shown in Fig. 1b. With this system, the light gas (argon) was injected into the vortex chamber through two rows of 0.010-in.-dia holes. The holes were drilled in a copper injector that was mounted on the fused-silica tube that formed the peripheral wall of the vortex chamber. A slot was cut out of the fused-silica tube so that the copper injector and fused-silica tube formed a smooth surface (see Fig. 1b). The copper injector was fixed to the fused-silica tube with a silicone rubber adhesive sealant (General Electric RTV 102) to provide a leak-proof seal. The holes in each injector led to a common manifold that was connected to the argon supply with teflon tubing. For this system, the light-gas injection area was 0.0127 sq in. and the scaling parameter, $dL/A_{B,j}$, was 345. The light gas was injected at an angle of 20 deg to the tangent of the inner surface of the fused-silica tube. The same end walls discussed previously were used, but the end-wall injectors were removed to provide a smooth end-wall surface. The end walls were spaced 3.5 in. apart (see Fig. 1b) to prevent arcing from the copper injectors to the end walls.

The entire vortex chamber assembly was inserted into the work coil of the 80-kw r-f induction heater. A photograph of the installed assemby (with end-wall light-gas injection) is shown in Fig. 2a and a photograph of the plasma created within the vortex chamber is shown in Fig. 2b. (The camera position was the same for the photographs shown in Figs. 2a and 2b.) For reference, the location of the vortex chamber walls are noted in Fig. 2b.

Heavy-Gas Injection Configurations

Four different configurations were employed to inject the xenon heavy gas into the vortex chamber (see Fig. 2c). The configuration which served as a standard consisted of premixing the xenon with the light-gas argon flow prior to injection into the vortex. The mixing was done far upstream of injection into the vortex chamber. A second method was injection of the heavy gas through a 0.062-in.-ID duct located in one end wall at a radius of 0.36 in.; the heavy gas was injected normal to the end wall.

A peripheral-wall xenon injector (see Fig. 2c) consisted of a 0.040-in.-ID by 0.080-in.-OD (1-mm-ID by 2-mm-OD) fused-silica tube which was fused into the peripheral wall of the vortex chamber. This injector was located midway between the end walls and protruded 0.05 in. into the vortex chamber. The injector tube was connected to the xenon supply by a length of teflon tubing located in the annular coolant passage.

The fourth injection method used was injection of the xenon directly into the plasma through a water-cooled injector. The injector was located on the vortex centerline and protruded 0.60 in. into the vortex chamber (see Fig. 2c). The injector consisted of a 0.18-in.-OD tube having a 0.030-in.-ID port at the center. A large difference between the injector outer and inner diameters was necessary to permit water cooling passages to be incorporated in the probe. This centerline injector was used from only one end wall. During tests, adjustments in the thru-flow control valves were made to insure equal flow from each thru-flow port. These adjustments were necessary to compensate for the partial blockage of the thru-flow port due to the presence of the injector.

Only one heavy-gas injection method was used during any given test; injectors other than the one being used were removed from the vortex chamber. In all tests the heavy gas consisted of xenon mixed with an argon carrier gas. The argon carrier gas was necessary to insure that the injection velocity of the xenon was sufficient to permit it to enter the plasma region. (It was impractical to vary the xenon injection duct area or to increase the xenon flow rate with the existing injection ducts to obtain the required xenon injection velocity). Both the xenon and argon carrier flow rates were measured with calibrated flowmeters. The xenon heavy gas flow rates, argon carrier gas flow rates, and injection velocity are listed in Table I for the various test conditions.

Optical Equipment

Spectroscopic techniques were used to obtain the necessary measurements from which the plasma temperature and xenon partial pressure within the plasma could be determined. A schematic of the optical system used is shown in Fig. 3. A 36-in. focal length lens was positioned 40 in. from the vortex chamber centerline. In this location, the lens formed an image of the plasma on the entrance slit of a 0.25-meter Jarrel-Ash scanning monochromator, positioned 107 in. from the lens. The resulting image was 1.5 times the actual plasma size. Various calibrated neutral density filters were placed in front of the monochromator to reduce the intensity of the entering light. The monochromator was fitted with an EMI 9558C photomultiplier tube having an S-20 response. The monochromator was mounted on a traversing mechanism so that the plasma could be scanned in a vertical direction (the axes of the plasma and vortex were horizontal). The traversing speed was 5 in./min. Both the entrance

and exit slits of the monochromator were 25 microns wide by 1/4 in. long, and were in a horizontal orientation. Data from different axial positions were obtained by rotating the lens slightly, thus moving the image relative to the monochromator slits. Vertical traverses were made at each of the four axial locations noted in Fig. 2c. Care was taken to avoid the r-f work coil when making the traverses.

The output signal from the photomultiplier was fed into a specially constructed amplifier and recorded on a Honeywell 1108 visicorder. Either the signal or the logarithm of the signal could be recorded. A high-speed recorder was used so that the emission spectrum from the plasma could be taken at the maximum scanning speed of the monochromator (i.e., 1000 Å/min). Whenever the emission spectrum was being recorded, the monochromator was not moved; conversely, when the monochromator was being traversed, only a single portion of the spectrum was being recorded. (With the 1180 lines/mm grating that was used, the resolution of the monochromator is about 3 Å).

Test Procedures

A plasma was initiated by evacuating the vortex chamber to a pressure less than 5 torr and turning on the r-f power at a low level to obtain a low-pressure glow discharge. The r-f power, argon flow rate, and pressure within the vortex chamber were then simultaneously increased until the desired operating conditions were reached. Figure 2b is a photograph of the argon plasma at the normal operating conditions.

All tests with a given light-gas injection system were begun with pure argon flow, the same pressure, and the same power into the plasma. (The tests with vortexes having peripheral-wall light-gas injection were conducted at a slightly lower power level than similar tests with end-wall light-gas injection.) After the plasma and coolant flows had reached steady-state conditions, the xenon was injected through the appropriate injector. The presence of xenon in the plasma lowered the plasma impedance and caused an impedance mismatch between the r-f power amplifier and plasma load. No attempt was made to retune the output or to increase the power when the xenon was being injected; consequently, the tests with xenon injection were conducted at power levels less than those with pure argon. The flow and power conditions employed in the various tests conducted in this investigation are listed in Table I.

Since the plasma was confined well away from the fused-silica tube forming the peripheral wall of the vortex chamber (see Fig. 2b), the heat convected to the peripheral wall was quite small (less than 10 percent of the power deposited into the plasma for the conditions used in this investigation). To achieve this condition in an r-f generated plasma required the simultaneous adjustment of flow rate, chamber pressure, r-f power, and r-f tuning. Changes in any of the aforementioned

variables without corresponding changes in the others grossly affected the plasma and caused it to extinguish or change into a mode in which the plasma filled the chamber. This mode caused excessive heating of the fused-silica tube that forms the vortex chamber peripheral wall.

The sketch of the vortex chamber and the confined plasma shown in Fig. 2c includes designations indicating the power dissipated from the plasma. Q_C is the power convected out of the chamber by the hot exhaust gases and is determined calorimetricly from the temperature rise and flow rate of the end-wall coolant. Q_R is the power radiated from the plasma through the coolant water and is determined by a Reeder RBL-500 thermopile having a quartz window. The thermopile was located 104 in. from the plasma. The response of the thermopile was calibrated using an Eppley Laboratory Calibrated Standard of Spectral Irradiance. The radiated power from the plasma was determined from the thermopile reading and the assumption of spherical radiation from the plasma. The actual thermopile reading was increased by 33 percent to account for light blocked by the r-f work coil.

The quantity Q_{CR} is the power absorbed in the peripheral-wall coolant fluid. This power is a combination of radiation from the plasma and conduction through the inner fused silica tube. (Water will absorb almost all radiation above 1.3 microns that passes through the fused-silica tube.) Values of Q_C , Q_R, and Q_{CR} are listed in Table I for the various configurations tested. Also listed in Table I are the power absorbed in the r-f work coil due to resistive heating and the d-c input power. A note following Table I lists the results of a test in which the coolant in the annulus between the fused silica tubes was air instead of water. The power deposited in the air coolant was due only to conduction through the fused-silica tube. The radiated power as determined from the thermopile increased correspondingly. This test showed that, when water was used as the coolant, about 50 percent of Q_{CR} was due to radiation.

Spectral data were obtained for each of the test conditions listed in Table I. These data were obtained by making vertical traverses in each of the four axial positions (see Fig. 2c) of the following portions of the spectrum: (1) the ArI 4300 Å line, (2) the XeI 4671 Å line, and (3) the continuum at approximately 4310 Å. These data, along with calibrations obtained using the Eppley Laboratory Calibrated Standard of Spectral Irradiance, allow the temperature of the plasma and the xenon partial pressure within the plasma to be determined by the method described in a later section.

Unheated Vortex Tests

High Reynolds Number Test Facility

Most of the test equipment employed in the present investigation was used in preceding work under Contract NASw-847 and has been described in detail in Refs. 2, 3, and 6. The essential features of this equipment and modifications made during this report period are presented herein.

The flow system, shown in Fig. 4, consists of three parts: the light-gas (simulated-buffer-gas) supply system, the heavy-gas (simulated-fuel) supply system, and the test section. The light-gas supply system provides a metered weight flow of atmospheric air heated (to prevent condensation of the iodine vapor; see below) in a steam heat exchanger to approximately 270 F. Thermostatically controlled heating tapes on the pipes and heaters within the test section plenum increase the light-gas temperature to approximately 300 F. (The term "unheated", however, is used to differentiate these tests from the r-f heated tests in which energy was deposited directly in the vortex by the surrounding r-f coils.)

A measured weight flow of heavy gas at approximately 300 F is provided by the heavy-gas supply system. The heavy gas is a mixture of a carrier gas and iodine vapor. The iodine vapor is used only in sufficient quantities to permit its detection by optical methods. The iodine generally comprises between 5 and 30 percent by weight of the heavy gas. The molecular weight of the heavy-gas mixture is substantially altered by changing the carrier gas. The desired carrier gas is supplied under pressure to the carrier gas heater which consists of a coil of copper tubing in a 325 F oven. Some of the carrier gas is then bypassed through specially constructed iodine boilers located within the same oven. At 325 F the iodine boilers contain liquid iodine with a vapor pressure of 17 in. Hg. The amount of gaseous iodine in the heavy-gas mixture is controlled by varying the amount of carrier gas bypassed through the boilers. Measurement of the amount of iodine in the mixture is accomplished as the heavy gas passes through the iodine inlet absorptometer or "light box." This absorptometer is discussed in a following subsection.

The test section in which the vortex tube is mounted consists of a 20-in.-ID by 30-in.-long outer cylindrical shell with end flanges. The light gas flows directly into a 4.5-in.-wide annular plenum that is created when the vortex tube is installed.

Vortex Models and Flow Configurations

The 10-in.-ID by 30-in.-long directed-wall-jet vortex tube used in previous investigations (Refs. 2, 3, and 6) was employed in these tests. Two different light-gas injection configurations were used: peripheral-wall light-gas injection

and simulated end-wall light-gas injection (injectors located at the end walls but connected to the peripheral wall). Sketches of the peripheral-wall light-gas injection geometry are shown in Fig. 5. Up to 900 directed-wall-jet inserts (see Fig. 5b) can be installed in the vortex tube. For the tests described herein, two axial rows of 28 inserts each, 180 deg apart, were used (see Fig. 5a). The slot height of the inserts was 0.035 in. and the total injection area, $A_{B,j}$, was 0.98 sq in.

The flow was exhausted from the vortex tube by two means: bypass flow and thru-flow. A separate bypass flow system was installed in the plenum chamber at each end of the vortex tube. Each bypass flow system consisted of a 13/32-in.-ID manifold connected to the vortex tube by 15 equally spaced 3/32-in.-ID tubes (see Fig. 5a). The bypass flow was ducted through the test section end flange to flow-meters. Because the bypass tubes were located very close to the end walls, the resulting flow was considered to be equivalent to the annular axial-bypass configuration used in previous investigations (Ref. 6).

Thru-flow was removed through 1-in.-dia ports at the centers of the end walls. Both bypass flow and thru-flow were exhausted through a common header to the laboratory vacuum system.

Sketches of the simulated end-wall light-gas injection geometry are shown in Fig. 6. This injection configuration consisted of four 0.375-in.-ID injectors (see details in Fig. 6b) equally spaced around the periphery and located approximately 0.5 in. away from each end wall. The total injection area, $A_{B,j}$, was 0.884 sq in. Although the flow passed through the peripheral wall instead of the end walls as in the configuration used in the heated vortex tests (see Fig. 1a), the relative location of the injectors was similar. In tests with this light-gas injection configuration, no bypass flow was used.

Two methods of heavy-gas injection were utilized in these tests: peripheral-wall injection and end-wall injection (sketches of the heavy-gas injection configurations are presented in Fig. 7). Peripheral-wall heavy-gas injection was accomplished using a single injector near the axial mid-plane of the vortex tube (Fig. 7a). The injector consisted of a 0.13-in.-ID by 0.25-in.-OD tube protruding radially inward 0.5-in. from the peripheral wall.

For the end-wall heavy-gas injection configuration, two 0.1-in.-ID tubes were employed (Fig. 7b). The tubes were mounted on opposite sides of the thru-flow duct and the ends of the tubes were flush with the inner surface of one end-wall. The distance between the centers of the injector tubes was 2.9 in. Heavy-gas injection was in the axial direction.

To provide a basis for comparisons between the results of heated and unheated tests, the light-gas and heavy-gas configurations used in the high Reynolds number test facility were scaled as much as possible from those employed in the 80-kw r-f test facility. However, several parameters were not scaled. Among these were the diameters of the thru-flow and heavy-gas injection ports relative to the vortex tube diameter.

Optical Absorption Measurement Systems

As mentioned previously, the density of the iodine in the inlet heavy-gas mixture was determined by means of an iodine absorptometer of "light box" (see Fig. 4). This absorptometer measured the inlet iodine density by alternately sampling (30 times per second) the intensity of a test light beam which passed through windows in the heavy-gas inlet duct and a reference light beam which by-passed the inlet duct. The logarithm of the ratio of the two intensities is proportional to the average iodine density in the duct. A complete discussion of the absorption technique is presented in Appendix I of Ref. 5 and Appendix III of Ref 6.

In addition to the inlet absorptometer, three optical absorption systems were utilized to determine the containment of the heavy gas within the vortex tube. As shown schematically in Fig. 8, these systems consisted of (1) a scanning axial light beam, (2) a fixed centerline light beam, and (3) three fixed chordal light beams.

The axial light beam absorption system was used to determine the radial distribution of the heavy gas as well as the amount of heavy gas in the vortex tube. The amount of light absorbed by the iodine at a given radius of the vortex tube is related to the axially-averaged iodine density (see Appendix I of Ref. 8). The average heavy-gas density can then be calculated from the average iodine density by assuming that the iodine vapor and the carrier gas are fully mixed and that the volume flow rate of the heavy gas mixture is equal to that of the iodine alone. Thus, the heavy-gas density is determined from the relation:

$$\rho_F = \rho_I \left(\frac{W_F}{W_I}\right) \qquad (1)$$

To determine the radial distribution of heavy gas, a scanning light beam was traversed along the upper half of the vertical diameter of the vortex tube from $r/r_1 = 0.2$ to $r/r_1 = 1.0$. A second light beam was then traversed along the lower half of the vertical diameter in the same manner. The amount of iodine in the volume scanned

by the light beam was determined by electronically integrating the logarithm of the light beam intensity during each traverse. Further details of the absorptometer and a discussion of the principles of operation are presented in Appendix III of Ref. 6.

The amount of heavy gas in the core volume not covered by the scanning light beam (i.e., $r/r_1 = 0.2$) was measured using the centerline light system which passes a fixed light beam along the axis of the vortex tube. Fiber optics are utilized as the source and receiver for this light beam (see Fig. 8). To avoid interference with the scanning light system, the centerline light beam was operated by a shutter which opened only during the time when the lower and upper traversing lights beams were off.

Chordal measurements for determining the axial variation of heavy-gas density were made at three axial locations: 25 percent, 50 percent, and 75 percent of the length of the vortex tube (see Fig. 8). The chord at $r/r_1 = 0.625$ was sampled in all three cases. The chordal system also uses fiber optics leading from the same light source and leading to the same photomultiplier as in the centerline light system. Two shutters located in front of the photomultiplier provide sequential sampling of each centerline and chordal light beam.

Test and Data Reduction Procedures

Tests to determine the heavy-gas containment were conducted in the following manner. For a given heavy-gas molecular weight, both the heavy-gas and light-gas weight flow rates were set. After steady-state conditions were obtained, pressures, temperatures, and flow rates were measured. At the same time, a number of traverses (usually 5) of the scanning axial light beam were recorded as well as the outputs of the integrators, centerline light beam, chordal light beams, and inlet iodine absorptometer. Steady-state conditions were verified during this time by monitoring the recorders. The time required for a complete scanning cycle was approximately 18 sec, which is many times the average residence time of the heavy gas within the vortex tube. This process was repeated for each flow condition during a given series of tests. To provide the required baseline data on the light beams, several reference test runs were conducted before and after each series of tests. Reference tests were made with both the light gas and carrier gas flowing, but with no iodine flow.

The total amount of heavy gas contained in the vortex chamber was determined by averaging data obtained from both upper and lower traverses of the scanning light beam. For most tests reported herein, the average value of heavy gas stored differed from the value determined from the individual upper or lower traverse by less than 15 percent.

During this investigation, isothermal vortex test series were conducted by: (1) varying the light-gas flow rate with constant heavy-gas flow rate, (2) varying the heavy-gas flow rate at constant light-gas flow rate, and (3) varying the amount of bypass flow with constant light-gas and heavy-gas flow rates. In addition, some tests were conducted with several different light-gas and heavy-gas injection configurations, and with different heavy-gas molecular weights. In these tests the mixtures used for heavy gases were: helium/iodine ($m_F = 6$), nitrogen/iodine ($m_F = 30$), and sulfur-hexafluoride/iodine ($m_F = 148$). For all of the tests described herein, the heavy-gas and light-gas injection temperatures were approximately 300 F and the static pressure in the vortex chamber was between 0.8 and 1.0 atm. During all tests, equal amounts of thru-flow (and bypass flow) were removed from each end of the vortex chamber. A summary of configurations and operating conditions used is presented in Table II.

DEFINITIONS OF FLUID MECHANICS PARAMETERS

Several non-dimensional fluid mechanics parameters are important in describing both heated and isothermal two-component vortex flows. The parameters employed in this report are defined in this section.

The tangential injection Reynolds number is a measure of the angular momentum of the light gas at injection into the vortex tube. It is defined as

$$Re_j \equiv \frac{\rho_B V_{\phi,j} r_1}{\mu_B} = \frac{W_B r_1}{A_{B,j} \mu_B} \tag{2}$$

where ρ_B and μ_B are the density and laminar viscosity, respectively, of the light gas at injection, r_1 is the radius of the vortex tube, W_B is the light-gas weight flow rate and $v_{\phi,j}$ is the average light-gas injection velocity. The injection Reynolds number was varied by changing the light-gas weight flow rate.

The weight flow rate of the mixture of light gas and heavy gas through the thru-flow ports is expressed in terms of a radial Reynolds number. This Reynolds number is defined as

$$Re_r \equiv \frac{\rho r_1 v_r}{\mu} \tag{3}$$

For isothermal flows, Re_r can be written as

$$Re_r = \frac{W_{TF}}{2\pi \mu_B L} \tag{4}$$

where W_{TF} is the total weight flow rate (light-gas plus heavy-gas weight flow rates) through the thru-flow ports and L is the length of the vortex tube. It is assumed that the laminar viscosity of the thru-flow mixture is equal to the laminar viscosity of the light gas, μ_B.

One measure of the containment characteristics of a confined vortex flow is the average heavy-gas density, $\bar{\rho}_F$ (i.e., a volume-averaged heavy-gas density based on the amount of heavy gas contained within the entire vortex tube). This average density is defined as

$$\overline{\rho}_F \equiv \frac{\mathcal{M}_F}{V} \tag{5}$$

where $\mathcal{M}_F$ is the amount of heavy gas contained in the vortex tube and V is the total volume of the vortex tube.

The average partial pressure of the heavy gas is

$$\overline{P}_F = \frac{\overline{\rho}_F \mathcal{R} T}{m_F} \tag{6}$$

where m_F is the molecular weight of the heavy-gas mixture (iodine plus carrier gas),

$$m_F = \frac{w_F}{w_I/m_I + w_C/m_C} \tag{7}$$

The average partial pressure of the heavy gas is usually non-dimensionalized by the static pressure at the peripheral wall, P_1. The ratio $\overline{P}_F/P_1$ is important since a minimum value (considered to be about 0.2) is required for good performance characteristics of the reference nuclear light bulb engine (see Ref. 9).

If the heavy gas and light gas were fully mixed before injection into the vortex chamber, the heavy gas would be uniformly distributed throughout the vortex chamber, since separation is unlikely. Thus, the ratio of average heavy-gas partial pressure to static pressure for the fully mixed condition, $\overline{P}_F/P_1|_{mix}$ can be considered a reference point for comparison of containment data. A containment parameter, χ, can therefore be defined as:

$$\chi \equiv \frac{\overline{P}_F/P_1}{\overline{P}_F/P_1|_{mix}} \tag{8}$$

From Eq. (6) above and the continuity equation it can be shown that

$$\chi = \frac{\overline{\rho}_F m_B/\rho_B m_F}{w_F m_B/w_B m_F} = \left(\frac{\overline{\rho}_F}{\rho_B}\right)\left(\frac{w_B}{w_F}\right) \tag{9}$$

Thus, for isothermal flows, the containment parameter, X, is identical to the parameter $t_F/t_{F_{min}}$ derived in past investigations (Ref. 6). Some test results in this investigation are discussed in terms of this containment parameter. A containment parameter greater than one occurs when the amount of heavy gas within the vortex chamber is greater than that which would occur if the heavy and light gases were fully mixed. A containment parameter less than one occurs when the amount of heavy gas within the vortex chamber is less than the fully mixed value, and can result when some of the injected heavy gas is "short-circuited" from the heavy-gas injection duct to the vortex-chamber exhaust ducts without entering the main vortex flow region. Although high values of containment parameter are desirable in a full-scale engine to minimize the amount of fuel which must be handled in the fuel recycle system, no specific value must be obtained to establish the feasibility of the engine concept. The primary purpose of the vortex flow is to keep the fuel away from the transparent wall.

A parameter that has been used to scale vortex flows in different vortex geometries is $dL/A_{B,j}$ (see Ref. 10). This parameter was approximately equal to 300 for all light-gas injection configurations tested in both the high Reynolds number test facility and the 80-kw r-f induction heater.

DETERMINATION OF PLASMA TEMPERATURE AND XENON PARTIAL PRESSURE

As part of the investigation on two-component heated vortexes, it was necessary to determine both the temperature of the plasma and the partial pressure of the xenon (i.e., the heavy gas) within the plasma. A technique utilizing spectroscopic measurements of the light emitted from the plasma was used. A schematic of the optical system is presented in Fig. 3. Figure 9 is a reproduction of a typical emission spectrum between 4000 Å and 5000 Å of an argon plasma seeded with xenon. The spectrum shown in Fig. 9 was obtained from a test in which the xenon was premixed with the argon. The xenon flow rate was 2.5 percent of the argon flow rate. Several of the more prominent xenon and argon spectral lines are denoted in Fig. 9. The zero intensity level (obtained by blocking the light entering the monochromator for a short time during the wavelength scan) is also noted in Fig. 9. The slight change in the level of the continuum is due to the response of the photomultiplier tube. (The EMI 9558c photomultiplier has a S-20 response which has maximum sensitivity at about 4200 Å.) Also noted on Fig. 9 are the ArI 4300 Å line which was used to determine plasma temperature and the XeI 4671 Å line which was used to determine the xenon partial pressure.

The procedures used to determine the plasma temperature and xenon partial pressure are described in the following paragraphs. The complete optical system shown in Fig. 3 was calibrated using an Eppley Laboratory Calibrated Standard of Spectral Irradiance. The calibration was necessary so that the relationship between the photomultiplier output signal and the absolute intensity of the light entering the monochromator was known.

The continuum emission along a diameter of a pure argon plasma was measured between wavelengths of 4200 Å and 4300 Å. From the absolute intensity the continuum (determined from the calibration) an average plasma temperature was calculated using the following equation from Ref. 7 (similar equations are also given in Refs. 11 to 14):

$$I_c = 1.13 \times 10^{-31} \bar{g} Z_{eff} \frac{N_e N_+}{T_e^{1/2}} \quad \text{watts/cm}^3 \qquad (10)$$

In Eq. (10), N_e and N_+ are the electron and ion number density, respectively, and are assumed equal for the pure argon plasma; T_e is the electron temperature, and is assumed equal to the gas temperature; Z_{eff}, is the effective charge per ion and is assumed equal to 1.0, and $\bar{g}$ is the Gaunt factor which has a value of approximately 2.3 for argon near 4300 Å (Ref. 7). The plasma is assumed to be in thermodynamic equilibrium

and in charge equilibrium (i.e., $N_e = N_+$). The variation of the continuum intensity, I_c, with temperature for an argon plasma at 1.2 atm pressure calculated using Eq. (10) is shown in Fig. 10. The continuum intensity was chosen for the absolute measurement instead of the line intensity because it was felt the line intensity was subject to much greater error due to uncertainty in the transition probability and due to alteration of line intensity by the inherent broadening of the monochromator. However, in a xenon-argon mixture, the continuum alone cannot be used to determine either the temperature or the xenon partial pressure. (Since continuum intensity is proportional to the electron and ion densities, knowledge of the composition is necessary to determine the temperature, but the temperature is necessary to determine the composition of a gas mixture.) The value of the absolute continuum intensity obtained from a test employing a pure argon plasma was used to determine an average temperature.

Along the same diameter, the maximum value of the ArI 4300 Å line intensity was measured. Using the Boltzmann equation in the form,

$$I_{LINE}^{4300} = K_1 \frac{e^{-E_n/kT}}{T} \qquad (11)$$

The constant, K_1, can be determined from the measured value of the intensity and the previously determined average temperature. For the ArI 4300 Å line, the upper energy level, E_n, has a value of 14.50 ev. In employing Eq. (11) for the determination of K_1 it is assumed that the partition function is equal to 1.0 (a valid assumption below 12,000 K for argon) and that the percent ionization is small (less than one percent for argon at 10,000 K). Since the optical system was unchanged for all tests, the constant determined from Eq. (11) is valid for all tests. (It is assumed that the relative variations of intensity with temperature are the same for both the continuum and line for the temperature range of interest). The variation of the relative intensity of the ArI 4300 Å line at 1.2 atm pressure was calculated from Eq. (11) and the results are presented in Fig. 11.

During a typical test, the monochromator was scanned across the plasma at three different wavelengths; viz., the ArI 4300 Å line, the XeI 4671 Å line (when xenon was used), and the continuum at approximately 4310 Å. Typical traces obtained in a test are presented in Fig. 12a. The intensity of the continuum was subtracted from each of the line intensities and the resultant data were used as input to an Abel inversion program to calculate the line intensities as a function of radius shown in Fig. 12b. Since the relation between the recorded line intensity and the plasma temperature was previously determined, (i.e., the constant K_1) the plasma temperature distribution which corresponds to the intensity distribution shown in Fig. 12b can be obtained using Eq. (11) or Fig. 11.

Determination of the xenon partial pressure also employs the Boltzmann equation and the measured intensity of the XeI 4671 Å line. However, for the xenon the number density of neutral atoms cannot be assumed constant. Thus the Boltzmann equation takes the form

$$I_{LINE}^{4671} = K_2 \frac{P_{xe}^{o}}{T} e^{-E_n/kT} \qquad (12)$$

In Eq. (12) E_n is the upper energy level of the XeI 4671 Å line and has a value of 10.967 ev, P_{xe}^{o} is the pressure (in atm) of the neutral xenon species and T is the gas temperature. It is assumed that xenon and argon temperatures are equal. The partition function is again assumed equal to 1.0 (a valid assumption for xenon below 10,000 K).

Since the xenon may be highly ionized, it is necessary to determine the composition of the argon-xenon mixtures throughout a range of temperatures and xenon partial pressures. The program described in Ref. 15 was used to calculate the partial pressures of the neutral and singly ionized species of xenon throughout a range of temperatures and xenon partial pressures in a argon-xenon mixture. The variation with temperature of the partial pressures of xenon species is presented in Fig. 13. The variations of the relative intensity of the XeI 4671 Å line with temperature were calculated from Eq. (11) using the partial pressure of the neutral xenon species from Fig. 13. These variations are presented in Fig. 14.

To determine the xenon partial pressure at any point in an argon-xenon plasma mixture, Eq. (12) was solved for P_{xe}^{o} using the radial variation of the intensity of the XeI 4671 Å line and the temperature calculated from the ArI 4300 Å line. From the value of P_{xe}^{o} and the temperature, the total xenon partial pressure, P_{xe}, was determined from the composition shown in Fig. 13. However, prior to making any calculations, the constant K_2 in Eq. (12) had to be determined. Values of the transition probability which would have permitted direct calculation of this relationship were not available. Thus, a test was conducted in which spectral emission measurements were made on a known mixture of argon and xenon. (A description of this test is presented in the section entitled DISCUSSION AND RESULTS). The temperature was determined from the ArI 4300 Å line intensity, and the relative intensity of the XeI 4671 Å line was measured. Equation (12) was used to determine the constant K_2. Since no changes were made in the optical system, the constant K_2 was used for all additional test data.

DISCUSSION OF RESULTS

The primary purpose of both the heated and unheated (isothermal) tests was to determine the effects of several geometric and flow variables on the partial pressure, or containment, of the heavy gas in two-component vortexes. In particular, the effect of a large temperature gradient within the vortex was of interest. Because equipment limitations prohibited use of the same geometric configuration in both heated and unheated tests, two different vortex geometries in two different test facilities were employed (see section entitled TEST EQUIPMENT AND PROCEDURES). The following two subsections contain separate discussions of the results obtained from the heated and isothermal vortex tests. The third subsection discusses some comparisons between results obtained from the heated and isothermal vortex tests.

Heated Vortex Tests

Results of Tests Using End-Wall Light-Gas Injection

Tests Employing Argon Only

Experiments were conducted with a vortex chamber having the end-wall light-gas injection configuration shown in Fig. 1a. Tests with pure argon (no xenon injection) resulted in the radial temperature distributions shown in Fig. 15. Temperature distributions are presented for the four axial positions shown in Fig. 2c; position 1 was at 0.2 in. from the left end wall, position 2 was at 1.2 in., position 3 was at 2.0 in., and position 4 was at 2.6 in. (These positions were used for all tests in which the end-wall light-gas injection configuration was employed.) The flow and power conditions for this test are shown in the first column of Table I. Also noted in Fig. 15 is the location of the vortex-tube peripheral wall. The plasma diameter is approximately 70 percent of the vortex-tube diameter; the plasma was confined well away from the peripheral wall. It is estimated that the temperature gradient at the outer edge of the plasma was between 40,000 and 60,000 deg K/in. Temperatures in the central region (i.e., away from the end walls, positions 2 and 3) were considerably greater than those near the end walls (positions 1 and 4). In addition, the peak temperatures of approximately 10,000 K did not occur on the plasma centerline, but at a radius about halfway between the centerline and the plasma edge. This phenomenon is typical of r-f generated plasmas (Refs. 7 and 16). The temperature at the centerline cannot be accurately determined due to a singularity in the Abel inversion equation. Also, a total temperature range of approximately 2000 K is the maximum that can be obtained with the present instrumentation due to the large intensity change associated with this temperature difference (see Fig. 11).

Additional tests were conducted to provide data for direct comparison with the unheated-vortex data. In particular, measurements of the end-wall, peripheral-wall, and centerline static pressure distributions were made with and without heat addition. The data from these tests are discussed subsequently in the subsection entitled "Comparison of Results of Heated and Unheated Tests."

Test With Xenon Premixed

A test was conducted employing the end-wall light-gas injection configuration (Fig. 1a) in which xenon was premixed with the argon prior to injection into the vortex chamber. The xenon and argon weight flow rates were measured so that the xenon partial pressure within the vortex chamber was predetermined. The results of this test were necessary to determine the relationship between the XeI 4671 Å line intensity and the xenon partial pressure (see preceding section). The flow and power conditions are given in the second column of Table I. The presence of xenon in the plasma lowered the reflected impedance of the plasma causing an impedance mismatch between the r-f power amplifier and the plasma load. This mismatch resulted in less power deposited into the plasma with the xenon-argon mixture than with argon alone (see Table I). The radial distributions of the plasma temperature and xenon partial pressure are presented in Fig 16. The decrease in power deposited in the plasma caused correspondingly lower plasma temperatures (compare Fig. 16a with Fig. 15). The peak plasma temperature decreased about 900 K. The temperature gradient at the outer edge of the plasma also decreased with the presence of xenon. However, the plasma was still confined well away from the peripheral wall and no increase in the heating of the peripheral wall was evident.

This test was made to determine the constant in the equation relating the intensity of the XeI 4671 Å to the temperature and pressure (i.e., Eq. (12)). Since the xenon and argon were premixed prior to injection, the xenon partial pressure within the vortex chamber was equal to the fully mixed value of 0.011 atm. (It was assumed that no separation of the xenon and argon occurred within the vortex chamber.) From the XeI 4671 Å line intensity measurements, the temperatures obtained from Fig. 16a, and the known value of the xenon partial pressure, the constant in Eq. (12) was calculated at forty different radial and axial positions. The forty values were averaged to determine one value of the constant, and this average value, along with the temperatures of Fig. 16a and the measured intensities of the XeI 4671 Å line, was used to calculate the xenon partial pressure within the plasma region. The results of these calculations are presented in Fig. 16b. It was, of course, expected that all the curves shown in Fig. 16b would lie on a single horizontal line. The variation shown is probably due to experimental errors resulting from the complex procedure necessary for determining the xenon partial pressure. In general, the variations shown in Fig. 16b are small considering that the intensity of the XeI 4671 Å line varies approximately linearly with pressure but exponentially with temperature (see Fig. 14). That is, small errors in the determination of temperature could show up as large errors in the calculation of xenon partial pressure.

Tests With Peripheral-Wall Xenon Injection

Tests were conducted in which the xenon was injected into the argon plasma through the peripheral wall (see Fig. 2c). Figure 17 presents the data obtained, and the third column of Table I gives the flow and power conditions for these tests. Again, the presence of the xenon caused a reduction in the power deposited and a lower peak plasma temperature. In addition, the temperature near the centerline was reduced much more than in previous tests, and there was less of an axial gradient. The xenon partial pressure distributions presented in Fig. 17b show a definite increase near the vortex centerline. This could occur if the xenon injection velocity was sufficient to allow the xenon to penetrate the outer regions of the plasma before it was able to spread in an axial direction. Also included on Fig. Fig. 17b is the value of the xenon partial pressure that would be obtained if the xenon were evenly distributed through the vortex chamber or, in other words, fully mixed. The measured xenon partial pressures are well above this value, thus showing that some containment occurred.

Tests With Xenon Injection at Vortex Centerline

Figure 18 presents similar results for a plasma in which the xenon was injected through the probe on the vortex centerline (see Fig. 2c). (Whenever this heavy-gas injection configuration was used, only partial measurements for position 1 were obtained due to light blockage by the probe). As shown in Fig. 18a, the peak plasma temperature of 9500 K which occurred was midway between that of a pure argon plasma and that obtained with xenon injection through the peripheral wall. However, the plasma temperature near the centerline was decidedly reduced and the peak plasma temperature occurred at a larger radius than in previous tests. The flow and power conditions for this test are listed in the fourth column of Table I. The injection of xenon caused only a small reduction in total power, primarily because most of the xenon was located near the vortex center and thus had only a small effect on the plasma impedance. The xenon partial pressure distributions presented in Fig. 18b show a high concentration of xenon near the vortex centerline with very little xenon at the outer regions of the plasma. For comparison, the fully mixed value (i.e., the partial pressure that would exist if the xenon were evenly distributed throughout the vortex chamber) is included in Fig. 18b.

Tests With End-Wall Heavy-Gas Injection

Some tests were attempted in which the heavy gas was injected normal to the end wall through a duct in the end wall located at a radius of 0.36 in. from the centerline (see Fig. 2c). In these tests two different types of "heavy gas" were employed: (1) xenon with an argon carrier gas, and (2) tungsten particles with

an argon carrier gas. (A particle feed system similar to that described in Ref. 16 was used to dispense the tungsten particles. The difference between the system used in this study and that of Ref. 16 was in the method of particle agitation within the particle storage chamber. A vibrating diaphragm was used to agitate the particles in the present studies, while the method of Ref. 16 employed spinning blades.) The heavy-gas injection velocities were varied from approximately ten to several hundred feet per second. In none of these tests was the heavy gas within the plasma region sufficiently dense to allow spectroscopic measurements to be made. At the higher injection velocities, the vortex appeared to "breakdown" and the plasma could no longer be confined away from the peripheral wall. Isothermal vortex tests results reported in Ref. 5 also showed vortex "breakdown" at large heavy-gas injection velocities. Similar tests conducted in an isothermal vortex configuration (see a following subsection) showed that the heavy-gas, when injected from the end-wall, appeared to "short circuit" the vortex containment region and be quickly swept out of the vortex chamber. Thus, injection of the heavy gas through an end wall appears to be a poor method for depositing heavy gas into the plasma region, at least for the particular radial locations employed, and no further attempts were made to obtain data with this configuration.

Results of Tests Using Peripheral-Wall Light-Gas Injection

Tests Employing Argon Only

Two-component isothermal vortex tests (Refs. 2, 3, and 4) conducted previously have always employed light-gas injection from the peripheral wall of the vortex chamber. It is believed that this type of injection causes the least disturbance to the desired vortex flow patterns and, hence, results in a minimum amount of turbulence. Consequently, two-component tests were conducted in heated vortex flows employing the peripheral-wall light-gas injection configuration shown in Fig. 1b. The first of these tests used argon only (i.e., no heavy-gas injection), and the resultant radial temperature distributions within the plasma are presented in Fig. 19. The flow and power conditions are listed in the fifth column of Table I. It is important to remember that r-f considerations (specifically arcing between the injector and end walls) necessitated moving the end walls 3.5 in. apart for this configuration, compared with 2.8 in. for the end-wall light-gas injection configuration. The temperature profiles shown in Fig. 19 are quite similar to those of Fig. 15 (with end-wall light-gas injection) with two possible exceptions. The peripheral-wall light-gas injection configuration (see Fig. 1b) resulted in a slightly smaller diameter plasma and the temperature decrease near the centerline was less pronounced than with the end-wall light-gas injection configuration. However, there are similarities between the data of Fig. 19 and 15; a peak plasma temperature of about 10,000 K, a decrease of about 500 K near the end walls of the vortex chamber (positions 1 and 4), and a smaller plasma size near the end walls.

Again, the plasma was confined well away from the peripheral wall of the vortex chamber and the temperature gradients near the edge of the plasma were approximately 50,000 deg K/in.

Tests With Peripheral-Wall Xenon Injection

Tests were conducted employing the peripheral-wall light-gas injection configuration (Fig. 1b) and the peripheral-wall heavy-gas injection configuration (Fig. 2c). Figure 20 presents the radial variations of temperature and xenon partial pressure obtained from these tests. The flow and power conditions employed are given in the sixth column of Table I. As was noted previously, xenon injected from the peripheral wall decreased the power that was deposited in the plasma and, consequently, the plasma temperature. The presence of xenon also decreased the radial temperature gradient. The xenon partial pressure data presented in Fig. 20b show trends similar to those obtained with end-wall light-gas injection; an increase in xenon partial pressure near the vortex centerline. However, the radial gradient of the xenon partial pressure was much less with peripheral-wall light-gas injection (compare Fig. 20b with Fig. 17b). For comparison, the fully mixed value of xenon partial pressure is also shown in Fig. 20b.

Tests With Xenon Injection on Vortex Centerline

Figure 21 presents the radial distributions of temperature and xenon partial pressure obtained with the xenon injected through the probe on the vortex centerline (see Fig. 2c). Corresponding flow and power conditions for this configuration are given in the seventh column of Table I. As was noted previously, this heavy-gas injection system had a smaller effect on the peak plasma temperature than did heavy-gas injection through the peripheral wall. In addition, the temperature gradient at the edge of the plasma remained nearly the same as that obtained with no xenon injection (compare Figs. 21a and 19). The radial variations of xenon partial pressure for this configuration are presented in Fig. 21b. The xenon partial pressures are lower than was anticipated since this light-gas injection configuration was believed to provide good containment. The same heavy-gas injection system, but with end-wall light-gas injection, showed xenon containment superior to that shown in Fig. 21b (compare Figs. 18b with 21b). The reasons for the low values shown in Fig. 21b are not understood. However, the results show that the amount of xenon was decidedly less at the end of the vortex chamber opposite the xenon injection location. Thus, it is possible that the xenon injection velocity was too low and that an appreciable amount of xenon was not entering the plasma but was flowing around the probe tip and out the thru-flow port. This condition had been noted previously in preliminary testing when attempts were made to inject xenon at low velocities with no carrier gas. However, it is not understood why greater xenon injection velocities would have to be used with peripheral-wall light-gas injection than with end-wall light-gas injection.

Unheated Vortex Tests

Several series of two-component gas tests were conducted using the high Reynolds number test facility. These tests employed several different heavy- and light-gas injection configurations, and tests were conducted throughout a range of heavy- and light-gas injection flow rates. Most of the data from these tests are presented with the heavy-gas partial pressure (either volume-averaged or local) and the containment parameter considered as the dependent variables. The heavy-gas partial pressure was non-dimensionalized by the static pressure at the peripheral wall of the vortex chamber. Results of these tests are discussed in the following subsections.

Results of Tests Using the Peripheral-Wall Light-Gas Injection Configuration

Tests With Different Light-Gas Injection Weight Flow Rates

A series of tests was conducted with the vortex configuration having peripheral-wall light-gas injection (see Fig. 5) and peripheral-wall heavy-gas injection (see Fig. 7a). In these tests, the heavy-gas flow rate was held constant and the light-gas flow rate was varied. Since the vortex chamber has a fixed geometry, the injection Reynolds number is directly proportional to the light-gas flow rate. The tests employed heavy gases having three different molecular weights as described in the section entitled TEST EQUIPMENT AND PROCEDURES. Results obtained from these tests are presented in Figs. 22 to 25.

Figure 22 presents the variation of the volume-averaged heavy-gas partial pressure ratio with injection Reynolds number for three heavy-gas molecular weights. Corresponding radial Reynolds numbers and light-gas flow rates are shown on the abscissa. (For vortex flows with no bypass, Re_j, Re_r, and W_B are proportional.) The dashed lines indicate the partial pressure that would result if the heavy gas and light gas were fully mixed prior to injection ($\bar{P}_F/P_1 \mid_{mix}$). The arrows denote the data points for which partial pressure distributions are presented in Figs. 23, 24, and 25. From Fig. 22 it can be seen that the heavy-gas partial pressure increases with decreasing heavy-gas molecular weight (e.g., SF_6 and I_2 vs He and I_2) and decreasing injection Reynolds number for the particular heavy-gas flow rates employed in the tests.

A trend of decreasing amounts of heavy gas at the peripheral wall with increasing injection Reynolds number is indicated in the radial distributions of heavy-gas partial pressure presented in Figs. 23, 24, and 25. (For a given heavy-gas molecular weight, the heavy-gas flow rate was held constant.) However, there appears to be no discernable effect of the heavy-gas molecular weight on the amount of heavy gas at the peripheral wall. This result is contrary to that reported in Refs. 2 and 3 and may be attributed to differences in the method of heavy-gas injection and the injection velocities employed in these tests.

The partial pressures at the axis of the vortex tube ($r/r_1 = 0$), as indicated in Figs. 23 through 25, may be slightly in error, especially at lower light-gas flow rates. The centerline light beam passes through a 6-in.-length of the thru-flow pipe at each end of the vortex tube. Thus, it is possible that the amount of heavy gas in the core of the vortex is approximately 25 percent less than that indicated in Figs. 23 through 25.

Several additional tests were conducted with three peripheral-wall heavy-gas injectors (0.13-in.-ID by 0.25-in.-OD). These injectors were located at 25 percent, 50 percent, and 75 percent of the vortex tube length, measured from the left end wall. The heavy gas was a mixture of nitrogen and iodine vapor. Heavy-gas injection with this configuration resulted in an average heavy-gas partial pressure from one-and-one-half to three times that measured in the tests with the single heavy-gas injector. Further testing with multiple heavy-gas injectors should be undertaken in an effort to achieve high heavy-gas partial pressures.

Tests With Different Heavy-Gas Injection Weight Flow Rates

Tests were conducted with a configuration having peripheral-wall light-gas and peripheral-wall heavy-gas injection in which the heavy-gas flow rate was varied while the light-gas flow rate was held constant. The volume-averaged heavy-gas partial pressures obtained in the tests are shown in Fig. 26 for a range of the light- to heavy-gas weight flow rate ratio, W_B/W_F, and for three different heavy-gas molecular weights. The dashed lines indicate the fully mixed condition and the arrows denote the data points for which radial heavy-gas partial pressure distributions are presented in Fig. 27.

The test results presented in Fig. 26 confirm a trend observed previously (see Fig. 13 of Ref. 3) that the average heavy-gas partial pressure increases with decreasing W_B/W_F -- that is, the average heavy-gas partial pressure increases as the heavy-gas flow rate increases. However, the heavy-gas containment (indicated by the vertical distance of the data above the fully mixed lines) generally decreased as this occurred. The radial distribution of local partial pressure for the nitrogen/iodine mixture (Fig. 27) indicates that a considerable increase in the heavy-gas partial pressure in the central core volume occurred when the heavy-gas weight-flow was increased. The partial pressure at the peripheral wall also increased when the heavy-gas flow rate was increased.

The data shown in Fig. 22 (light-gas flow rate varied) and in Fig. 26 (heavy-gas flow rate varied) are combined in Fig. 28. This figure presents the variation of heavy-gas partial pressure ratio with the ratio of heavy-gas to light-gas volume flow rates at injection. From Fig. 28 it can be seen that the increase of average heavy-gas partial pressure is similar for all three heavy-gas molecular weights when either the volume flow rate of the heavy gas is increased or the volume flow rate of the light gas is decreased.

Tests With Different Bypass Weight Flow Rates

Tests were conducted in which the amount of axial bypass flow (see bypass geometry in Fig. 5a) was varied. In these tests, the heavy-gas and light-gas weight flow rates were held constant. The tests employed both end-wall and peripheral-wall heavy-gas injection, and a nitrogen/iodine mixture as the heavy-gas. Results of these tests are shown in Fig. 29. Peripheral-wall light-gas injection was used in both cases.

As also indicated in a previous study (Ref. 3), a greater average heavy-gas partial pressure can be achieved with axial bypass. As the amount of axial bypass is increased, the increase in heavy-gas partial pressure is approximately twice as much for end-wall heavy-gas injection as for peripheral-wall heavy-gas injection (see Fig. 29). This is to be expected since axial bypass flow decreases the amount of heavy-gas "short circuited" from the end-wall injectors directly to the thru-flow ports, provided W_B remains constant. The present data indicate little increase in heavy-gas partial pressure with greater than 50 percent bypass flow. Also, it can be seen by comparing the two radial distributions of heavy gas shown in Fig. 30 with the curve in Fig. 24 for $Re_j = 2.8 \times 10^5$ that increasing bypass flow resulted in no significant difference in the amount of heavy gas at the peripheral wall. However, the ratio of the peak heavy-gas partial pressure to the heavy-gas partial pressure at the peripheral wall increased considerably with increased bypass flow.

No decrease in heavy-gas partial pressure for radial Reynolds numbers below 100 was noted for either end-wall or peripheral-wall heavy-gas injection (see Fig. 29). The decrease shown in Fig. 13 of Ref. 3 may be the result of the extremely high bypass fractions tested rather than only the effect of the variation in radial Reynolds number.

Results of Tests Employing Different Light- and Heavy-Gas Injection Configurations

Heavy-gas containment data for the two light-gas injection configurations (end-wall (Fig. 6) and peripheral-wall (Fig. 5)), both having end-wall heavy-gas injection, are shown in Fig. 31. These data are presented in terms of the heavy-gas containment parameter, χ, defined in the section DEFINITION OF FLUID MECHANICS PARAMETERS. In these tests the heavy-gas flow rate was held constant, while the light-gas flow rate was varied. The arrows denote tests for which radial distributions of heavy-gas partial pressure are presented in Fig. 32.

The data in Fig. 31 indicate that the two different light-gas injection methods resulted in no significant differences in heavy-gas containment. However, a significant effect on heavy-gas containment with different heavy-gas injection configurations is indicated by comparison with data obtained from tests with peripheral-wall light-gas injection and peripheral-wall heavy-gas injection, determined from the data presented in Fig. 22. With end-wall heavy-gas injection, it is apparent that much of

the heavy-gas is being convected directly into the end-wall boundary layer and out the thru-flow ports (i.e., "short circuited"). This has also been observed in past investigations, even when the end-wall heavy-gas injection ports were located at a larger radius ($r/r_1 = 0.5$) as in Refs. 2 and 3. For example, if the fully mixed line (for fully mixed conditions $\bar{\rho}_F/\rho_B = W_F/W_B$) is added to Fig. 48 in Ref. 2, all previous end-wall heavy-gas injection data are also at less than the fully mixed containment conditions ($\chi < 1.0$).

These results do not eliminate end-wall heavy-gas injection from consideration as a desirable injection method for the nuclear light bulb engine. An important mitigating factor can be seen in the partial pressure distributions in Fig. 32. For similar injection Reynolds numbers, the tests conducted with end-wall heavy-gas injection resulted in lesser amounts of heavy gas at the peripheral wall than for the peripheral-wall heavy-gas injection configuration (compare Fig. 32 with Fig. 24).

Results of Chordal Measurements

The chordal measurements with both end-wall and peripheral-wall heavy-gas injection revealed an axial variation of heavy-gas density. The heavy gas is concentrated near the axial midplane of the vortex tube and decreases more or less symmetrically toward the end walls at all injection Reynolds numbers. Measurements of the heavy-gas density along a chord located at 62.5 percent of tube radius showed that the amount of heavy gas at an axial position 25 percent of the vortex tube length from the end walls was approximately 25 percent (for end-wall heavy-gas injection) and 60 percent (for peripheral-wall heavy-gas injection) less than the amount of heavy gas at the axial midplane.

Comparison of Results of Heated and Unheated Tests

Results Obtained with the Same Vortex Tube Geometry

Several tests were conducted in which the xenon partial pressure at the peripheral wall was measured both with and without heat addition to the vortex flow. The vortex tube used was the same model for the r-f tests having the end-wall light-gas injection configuration shown in Fig. 1a. A sample of gas was withdrawn at the peripheral wall of the vortex chamber, approximately 1/4 in. from the midplane. The sample was analyzed (both a gas chromatagraph and a mass spectrometer were used) to determine the xenon concentration at the wall. These tests were conducted with the configurations and flow conditions listed in columns 3 and 4 of Table I. Samples were also taken during isothermal tests with identical vortex configurations and flow conditions but with no heat addition to the vortex.

The results of these tests were: (1) with xenon injected through the peripheral wall, the xenon partial pressure at the peripheral wall was 8.4×10^{-4} atm with r-f heating and 59×10^{-4} atm with no heating (the fully mixed value was 55×10^{-4} atm) and (2) with xenon injected through the centerline probe, the xenon partial pressure at the peripheral wall was 1.0×10^{-4} atm with r-f heating and 5.1×10^{-4} atm with no heating (the fully mixed value was 73×10^{-4} atm). Thus, the presence of the strong temperature gradient had the effect of reducing the diffusion of xenon to the peripheral wall.

Static pressure distributions in both the axial and radial directions were also measured with this light-gas injection configuration but with no xenon injection. Measurements were made both with and without heat added to the vortex flow. Figure 33 presents the distributions of static pressure along the peripheral wall, along the vortex centerline, and along one end wall of the vortex chamber. For comparison, similar pressure distributions obtained in tests with the same geometry and argon flow rate but with no heating are also shown. The reference pressure for all distributions shown in Fig. 33 was taken as the peripheral-wall static pressure at the axial midplane. The absolute value of the reference pressure is 1.2 atm (490 in. of water).

The axial pressure distribution along the peripheral wall is shown in Fig. 33a. A slight pressure decrease occurs near each end wall, and the value is independent of whether the plasma is present or not. The axial pressure distribution along the vortex centerline is shown in Fig. 33b. These pressures were measured with a water-cooled probe inserted through the thru-flow ports along the vortex centerline. The pressure with heating is nearly constant while, with no heating, the presence increases significantly away from the end wall. The radial distributions of static pressure measured on the end wall are presented in Fig. 33c. Note that there are large differences in the radial pressure gradients between the heated and unheated vortex flows. By employing the radial momentum equation,

$$\frac{dP}{dr} = \frac{\rho v_\phi^2}{r} \tag{13}$$

and using the curves of Fig. 33c to obtain dP/dr, it can be shown that the tangential velocity, v_ϕ, is approximately the same in both the heated and unheated vortexes. For the heated vortex, the density at a given radius, r, was calculated from an average temperature at the same radius from the values shown in Fig. 15.

On the basis of the differences in pressure distributions between the heated and unheated cases, it is probable (although not certain) that significant differences in flow patterns may exist for these two vortexes. The flow in the end-wall boundary

layer is strongly dependent upon the radial gradient of pressure at the end wall; the larger the pressure gradient, the greater the amount of boundary layer, or secondary, flow (Ref. 17). Since the end walls are highly cooled and the plasma is small at the end wall (see Fig. 2b), it can be assumed that the density of the end-wall boundary layer flow is unaffected by the presence of the plasma. Thus, the small pressure gradient in the heated case (as compared to the unheated case) must result in less secondary flow. However, because the total thru-flow was constant, the radial flow external to the boundary layer (the primary flow) must be greater in heated vortexes than in unheated vortexes.

Results Obtained with Different Vortex Tube Geometries

By necessity, most of the heated and isothermal containment tests were conducted in vortex chambers of vastly differing sizes (see Figs. 1 and 5). Equipment limitations prohibited making isothermal containment tests in the 1.26-in.-ID vortex chamber employed in the r-f heated tests and, or course, heated tests were not possible in the 10-in.-ID vortex chamber used in the isothermal containment tests. However, since some of the tests were conducted in vortex chambers that were geometrically similar in many respects and at equal Reynolds numbers, it is of interest to compare results from some of these tests.

Figure 34 presents the radial distributions of heavy-gas partial pressures obtained from both the heated and unheated vortex flows. As previously discussed, the heated tests were made in a 1.26-in.-ID vortex chamber in which energy was added by r-f coils while the unheated tests were made in a 10-in.-ID vortex chamber. These tests employed similar peripheral-wall light-gas injection geometries and the injection Reynolds number was approximately 100,000 for both. The scaling parameter, $dL/A_{B,j}$, was approximately 300 for both vortex chambers. The heavy gas was injected radially inward through a duct in the peripheral wall. The molecular weight of the heavy gas was several times that of the light gas (3.5 in the heated tests and 5.0 in the unheated tests). One notable difference was the ratio of light- to heavy-gas flow rates (W_B/W_F = 66 for the heated tests and 46 for the unheated tests).

In Fig. 34, the curve for the heated tests was obtained by averaging the four axial distributions shown in Fig. 20, while the curve for the unheated tests was transferred from Fig. 25. The results of heated tests show that more heavy gas is present near the center of the vortex, but less is present at the larger radii, than in the isothermal tests. In the heated tests, the amount of heavy gas at radius ratios greater than 0.75 could not be measured. Two possible radial distributions between r/r_1 = 0.75 and r/r_1 = 1.0 are sketched in Fig. 34 (curves A and B).

Figure 35 presents a comparison of the average heavy-gas partial pressure obtained in heated an unheated tests. The cross hatched area represents the range of data presented in Fig. 28 for the unheated vortex tests. The two data points for the heated vortex tests were obtained by integrating the data of Fig. 34 with respect to $(r/r_1)^2$. Two points were obtained because of the two curves for the partial pressure at radius ratios between 0.75 and 1.0 (fig. 34). Samples of the gas composition made at the peripheral wall (see discussion in previous subsection) indicate that the lower value might be more accurate, but further data are needed to verify this. The small difference between the average heavy-gas partial pressure and the fully mixed value indicates that convective flows into and out of the plasma region are large. Note, however, that the rate of fuel loss from the vortex in a nuclear light bulb engine is relatively unimportant; the main purpose of the vortex is to keep the fuel off the peripheral wall. The conclusion from the data in Fig. 35 is that the average partial pressure of the heavy gas is relatively independent of the presence of a strong temperature gradient in the vortex flow.

Figure 36 shows the effect of the heavy- to light-gas volume flow ratio on the peak local heavy-gas partial pressure for heated and unheated vortexes. The data for the unheated tests were obtained using the 10-in.-ID vortex tube having peripheral-wall light-gas injection and peripheral-wall heavy-gas injection. The data for the heated tests were obtained with the small r-f model with several geometries. For a description of the geometry, reference should be made to the particular figure from which the data were obtained. For the heated tests, the peak value of the heavy-gas partial pressure was obtained by averaging the four axial stations.

The results shown on Fig. 36 indicate that, for unheated vortex flows, the amount of heavy-gas separation (i.e., the ratio of peak heavy-gas partial pressure to fully mixed heavy-gas partial pressure) is low at high values of the heavy- to light-gas volume flow rate ratio, but increases as the volume flow ratio decreases. It appears that a maximum heavy-gas separation occurs at a volume flow rate ratio of about 0.01, but more data are needed to verify this. As noted on Fig. 36, the maximum value of heavy-gas partial pressure divided by the fully mixed heavy-gas partial pressure occurs approximately at a ratio of heavy-gas injection velocity to light-gas injection velocity of unity. If this quantity is raised to a value of 10, the ratio of maximum heavy-gas partial pressure to fully mixed pressure decreases. It was observed during the performance of the tests that the large heavy-gas injection velocities appeared to "tear apart" the vortex, resulting in a uniform heavy-gas distribution throughout the vortex chamber. It is apparent from these results that future tests designed to increase the average heavy-gas partial pressure be conducted with an increase in fuel injection area in order to minimize fuel injection velocity.

The results of the heated tests show that ratios of the peak heavy-gas partial pressure to the fully mixed heavy-gas partial pressure are between 6.0 and 7.0, somewhat greater than similar values obtained from unheated tests. However, data were not taken at high values of the volume flow rate ratio to determine if the same trend exists in both the heated and unheated vortex flows. The data presented in Fig. 36, and gas samples taken at the peripheral wall of a heated vortex, indicate that the temperature gradient suppresses the flow of heavy gas to the peripheral wall. This result is important for the nuclear light bulb engine concept where the primary purpose of the vortex flow is to prevent nuclear fuel from reaching the transparent peripheral wall.

REFERENCES

1. McLafferty, G. H. and H. E. Bauer: Studies of Specific Nuclear Light Bulb and Open-Cycle Vortex-Stabilized Gaseous Nuclear Rocket Engines. United Aircraft Research Laboratories Report F-910093-37, prepared under Contract NASw-847, September 1967. Also issued as NASA CR-1030, 1968.

2. Kendall, J. S., W. C. Roman, and P. G. Vogt: Initial Radio-Frequency Gas Heating Experiments to Simulate the Thermal Environment in a Nuclear Light Bulb Reactor. UARL Report G-910091-17, prepared under Contract NASw-847, September 1968. Also issued as NASA CR-1311.

3. Kendall, J. S.: Experimental Investigation of Heavy-Gas Containment in Constant Temperature Radial-Inflow Vortexes. UARL Report F-910091-15, prepared under Contract NASw-847, September 1967.

4. Mensing, A. E. and J. S. Kendall: Experimental Investigation of the Effect of Heavy- to Light-Gas Density Ratio on Two-Component Vortex Tube Containment Characteristics. UARL Report D-910091-9, prepared under Contract NASw-847, September 1965.

5. Mensing, A. E. and J. S. Kendall: Experimental Investigation of Containment of a Heavy Gas in a Jet-Driven Light-Gas Vortex. UARL Report D-910091-4, prepared under Contract NASw-847, March 1965.

6. Kendall, J. S., A. E. Mensing, and B. V. Johnson: Containment Experiments in Vortex Tubes with Radial Outflow and Large Superimposed Axial Flows. UARL Report F-910091-12, prepared under Contract NASw-847, May 1967. Also issued as NASA CR-993.

7. Marteney, P. J., A. E. Mensing, and N. L. Krascella: Experimental Investigation of the Spectral Emission Characteristics of Argon-Tungsten and Argon-Uranium Induction Heated Plasmas. UARL Report G-910092-11, prepared under Contract NASw-847, September 1968. Also issued as NASA CR-1314.

8. Mensing, A. E. and J. S. Kendall: Experimental Investigation of Containment of Gaseous Iodine in a Jet-Driven Vortex. Air Force Systems Command Report RTD-TDR-63-1093, prepared by United Aircraft Research Laboratories under Contract AF 04(611)-8189, November 1963.

9. Latham, T. S.: Nuclear Studies of the Nuclear Light Bulb Rocket Engine. UARL Report G-910375, prepared under Contract NASw-847, September 1968. Also issued as NASA CR-1315.

REFERENCES (Continued)

10. McLafferty, G. H.: Private Communication.

11. Goldfarb, V. M. and S. V. Dresvin: Optical Investigation of the Distribution of Temperature and Electron Density in an Argon Plasma. Soviet Physics, High Temperature Physics (Translation), Vol. 3, p. 303, 1965.

12. Robinson, D. and P. D. Lenn: Plasma Diagnostics by Spectroscopic Methods. Applied Optics, Vol. 6, p. 983, 1967.

13. Corliss, C. H. and J. B. Shumaker, Jr.: Transition Probabilities in Argon I. Journal of Research of the National Bureau of Standards-A, Vol. 71A, p. 575, 1967.

14. Scholz, P. D. and T. P. Anderson: Local Thermodynamic Equilibrium in an RF Argon Plasma. Journal of Quantitative Spectroscopy and Radiative Transfer, Vol. 8, p. 1411, 1968.

15. McMahon, D. G. and R. Roback: Machine Computation of Chemical Equilibrium in Reacting Systems. In Kinetics, Equilibria, and Performance of High Temperature Systems. Proceedings of the First Conference Western States sections of the Combustion Institute, Los Angeles, California, November 1959; edited by G. S. Bahn and E. E. Zukoski, Butterworths, Washington 1960.

16. Roman, W. C., J. F. Klein, and P. G. Vogt: Experimental Investigation to Simulate the Thermal Environment, Transparent Walls, and Propellant Heating in a Nuclear Light Bulb Engine. UARL Report H-910091-19, prepared under Contract NASw-847, September 1969.

17. Anderson, O.: Theoretical Solutions for the Secondary Flow on the End-Wall of a Vortex Tube. UARL Report R-2494-1, prepared under Contract AF 04(611)-7448, November 1961.

LIST OF SYMBOLS

$A_{B,j}$	Light-gas injection area, sq in.
$A_{F,j}$	Heavy-gas injection area, sq in.
c_B	Light-gas specific heat, kw/lb-deg K
d	Diameter of vortex chamber, in.
E_{coil}	Peak r-f voltage across work coil, volts
E_n	Upper energy level, ev
f	Frequency, Hz
$\bar{g}$	Gaunt factor, dimensionless
I_c	Intensity of continuum radiation, watts/cm^3-ster
I_{line}	Intensity of radiation of a single line, arbitrary units
I_x	Intensity of radiation measured from chord, watts/cm^2
k	Boltzmann constant, 1.38 x 10^{-16} erg/deg K
K_1, K_2	Constants used in Eqs. (11) and (12)
L	Length of vortex chamber, in. or ft
m_B	Molecular weight of light gas (simulated buffer gas)
m_C	Molecular weight of carrier gas
m_F	Molecular weight of heavy gas (simulated fuel)
m_I	Molecular weight of iodine vapor, m_I = 254
N	Number density, cm^{-3}
N_e	Number density of electrons, cm^{-3}
N_+	Number density of singly ionized atoms, cm^{-3}

LIST OF SYMBOLS (Continued)

P	Static pressure, atm
P_F	Heavy-gas partial pressure, atm
$\bar{P}_F$	Volume-averaged heavy-gas partial pressure, atm
P_r	Static pressure on end wall, in.H_2O
P_{xe}	Xenon partial pressure, atm
P_{xe}^{o}	Partial pressure of unionized xenon, atm
P_{xe}^{+}	Partial pressure of singly ionized xenon, atm
P_W	Static pressure at midplane on peripheral wall, in.H_2O
P_Z	Static pressure in axial direction, in. H_2O
P_1	Static pressure at vortex chamber peripheral wall, atm
Q_{coil}	Power deposited in r-f work coil, kw
Q_C	Power convected out of thru-flow ducts, kw
Q_{CR}	Power deposited in peripheral-wall coolant, kw
Q_{DC}	D-C Power to r-f power amplifier, kw
Q_R	Power radiated, kw
Q_T	Total power deposited in plasma, kw
r	Radius, in. or ft
r_1	Radius of vortex chamber, in. or ft
$\mathcal{R}$	Universal gas constant, ft-lb/lb-mole-deg R
Re_j	Injection Reynolds number, (Eq. (2)), dimensionless
Re_r	Radial Reynolds number, (Eq. (4)), dimensionless

LIST OF SYMBOLS (Continued)

t_F	Heavy-gas time constant, $\mathcal{M}_F/W_F$, sec
$t_{F_{min}}$	Heavy-gas time constant for fully mixed flow, sec
T	Temperature, deg R or deg K
T_e	Electron temperature, deg K
T_{TF}	Average temperature of gas exhaust out of thru-flow ducts, deg K
$v_{\phi,j}$	Injection velocity of light gas, ft/sec
v_x	Injection velocity of xenon, ft/sec
V	Volume of vortex chamber, ft^3
W_B	Weight flow of light gas, lb/sec
W_{TF}	Weight flow of light gas removed through thru-flow ports, lb/sec
W_C	Weight flow of carrier gas, lb/sec
W_F	Weight flow of heavy gas, lb/sec
W_I	Weight flow of iodine vapor, lb/sec
W_x	Weight flow of xenon, lb/sec
$\mathcal{M}_F$	Total amount of heavy gas in vortex chamber, lb
x	Perpendicular distance from chord to centerline, in.
z	Axial distance measured from left end wall, in.
Z_{eff}	Effective ionic charge, dimensionless
Z_p	Reflected impedance, ohms
λ	Wavelength, angstroms
μ_B	Viscosity of light gas, lb/ft-sec

LIST OF SYMBOLS (Continued)

μ_B	Density of light gas, lb/ft^3
$\bar{\rho}_F$	Volume-averaged density of heavy gas, lb/ft^3
χ	Heavy-gas containment parameter, dimensionless

Subscripts

chord	Refers to measurements on a chord
mix	Refers to conditions where heavy and light gases are fully mixed

Superscripts

4300	Denotes ArI 4300 Å line
4671	Denotes XeI 4671 Å line

TABLE I

TEST CONFIGURATIONS AND OPERATING CONDITIONS FOR HEATED VORTEX TESTS

UARL 80-KW R-F Induction Heater

Configuration (See Note 1 for Abbrevations)

	EW Ar No Xe	EW Ar Premixed Xe	EW Ar PW Xe	EW Ar CL Xe	PW Ar No Xe	PW Ar PW Xe	PW Ar CL Xe
Figure Where Data are Presented	15, 33	16	17, 36	18, 36	19	20, 34, 35 36	21
Flow Conditions							
Light Gas	Argon	Argon	Argon	Argon	Argon	Argon	Argon
Injection Flow Rate, W_B - lb/sec	3.3×10^{-3}	3.3×10^{-3}	3.3×10^{-3}	3.3×10^{-3}	3.3×10^{-3}	3.3×10^{-3}	3.3×10^{-3}
Injection Velocity, $v_{B,j}$ - ft/sec	360	360	360	360	300	300	300
Injection Reynolds Number, Re_j	1.15×10^5	1.15×10^5	1.15×10^5	1.15×10^5	0.97×10^5	0.97×10^5	0.97×10^5
Vortex Pressure, P - atm	1.2	1.2	1.2	1.2	1.2	1.2	1.2
Heavy-Gas	---	Xe	Xe + Ar	Xe + Ar	---	Xe + Ar	Xe + Ar
Xenon Flow Rate, W_x - lb/sec	0	8.8×10^{-5}	5.5×10^{-5}	8.2×10^{-5}	0	5.1×10^{-5}	8.3×10^{-5}
Argon Carrier Flow Rate, W_C - lb/sec	0	0	12.5×10^{-5}	10.0×10^{-5}	0	5.5×10^{-5}	13.0×10^{-5}
Xenon Injection Velocity, $v_{x,j}$ - ft/sec	0	---	130	210	---	60	250
Weight Flow Rate Ratio of Xenon/Argon, W_x/W_B	0	0.027	0.016	0.024	0	0.015	0.025
Power Conditions							
Power Deposited in Plasma, $Q_T = Q_R + Q_{CR} + Q_C$ - kw	9.3	6.7	7.2	9.6	7.8	6.4	6.9
Power Radiated from Plasma, Q_R - kw	1.47	0.60	0.66	1.20	1.32	0.57	0.90
Power to Peripheral Wall Coolant, Q_{CR} - kw	0.6(2)	0.5	0.4	0.5	1.0	0.5	0.7
Power Convected out of Vortex, Q_C - kw	7.2	5.6	6.1	7.9	5.5	5.3	5.3
Average Exhaust Gas Temperature, $T_{TF} = Q_C/W_B C_B$ - deg K	8900	7300	7700	9200	7100	6800	6800
Power Deposited in R-F Work Coil, Q_{coil} - kw	2.1	1.2	1.2	1.8	1.7	1.2	1.1
R-F Conditions							
R-F Driving Frequency, f - mHz	7.25	7.25	7.25	7.25	7.25	7.25	7.25
D-C Plate Power, Q_{DC} - kw	25.0	21.6	20.3	24.4	18.0	16.1	17.3
R-F Peak Coil Voltage, E_{coil} - volts	6700	4800	5000	5650	6170	4330	5170
Reflected Impedance, $Z_p = E_{coil}^2/2(Q_T + Q_{coil})$ - ohms	1960	1430	1500	1410	2010	1220	1670

Note 1.

EW Ar - Argon injected tangentially through end-wall injectors (see Fig. 1a)
PW Ar - Argon injected tangentially through peripheral-wall injectors (see Fig. 1b)
No Xe - No xenon used
Premixed Xe - Xenon mixed with argon upstream of vortex
PW Xe - Xenon injected radially through port in peripheral wall (see Fig. 2c)
CL Xe - Xenon injected axially at vortex centerline (see Fig. 2c)

Note 2.

A test in which the peripheral-wall coolant fluid was air instead of water resulted in the following: $Q_{CR} = 0.3$ kw and $Q_R = 1.75$ kw. All the increase in Q_R occurred at wavelengths greater than 1.0 micron.

TABLE II

TEST CONFIGURATIONS AND OPERATING CONDITIONS FOR UNHEATED TESTS

High Reynolds Number Test Facility

Light-Gas Injection Configuration	Heavy-Gas Injection Configuration	Light-Gas Flow Rate W_B - lb/sec	Injection Reynolds Number Re_j	Radial Reynolds Number Re_r	Heavy-Gas Flow Rate W_F - lb/sec	Percent Bypass Flow	W_B/W_F	Heavy Gas	Heavy-Gas to Light Gas Injection Velocity Ratio, $v_{F,j}/v_{B,j}$	Data Shown on Figure
Peripheral Wall $A_{B,j}$=0.98 in.^{2}	Peripheral Wall $A_{F,j}$= 0.013 in.^{2}	0.0067 * ↓ 0.075	25,000 ↓ 280,000	26.2 ↓ 294	0.4 x 10^{-3}	0	6 → 185	He + I_2	1.7 → 15.2	22,
					1.1 x 10^{-3}			N_2 + I_2	1.1 → 12.6	
					0.81 x 10^{-3}			SF_6 + I_2	0.15 → 1.34	28
		0.008 * ↓ 0.075	30,000 ↓ 280,000	31.5 ↓ 294	0.4 x 10^{-3}		20 → 180	He + I_2	1.7 → 15.2	23
					1.21 x 10^{-3}		6.6 → 62	N_2 + I_2	1.1 → 12.6	24
					0.80 x 10^{-3}		10 → 94	SF_6 + I_2	0.15 → 1.34	25
		0.059	220,000	231	0.13 x 10^{-3} * ↓ 4.2 x 10^{-3}		14 → 450	He + I_2	0.5 → 8.8	26,
								N_2 + I_2	0.2 → 2.5	28
								SF_6 + I_2	0.07 → 1.05	
		0.059	220,000	231	1.6 x 10^{-3} *		41	N_2 + I_2	0.2 → 1.9	27
					0.65 x 10^{-3} *		94			
					0.16 x 10^{-3} *		360			
		0.06	225,000	235 → 35	1.23 x 10^{-3}	0 → 83 *	49		1.47	29
				20.2		14.4 *				30
				40.3		83 *				
	End Wall $A_{F,j}$ = 0.016 in.^{2}	0.009 * ↓ 0.075	25,000 ↓ 280,000	36.8 ↓ 294	1.3 x 10^{-3}	0	6 ↓ 58		1.1 → 9.3	31
					1.6 x 10^{-3}					
		0.018 * ↓ 0.064	67,000 ↓ 240,000	75 ↓ 253	1.3 x 10^{-3}		14 ↓ 48		1.3 → 4.2	32
		0.06	225,000	235 → 35	1.21 x 10^{-3}	0 → 83 *	49		1.23	29
End Wall $A_{B,j}$=0.88 in.^{2}		0.024 * ↓ 0.065	90,000 ↓ 245,000	94 ↓ 256	1.6 x 10^{-3}	0	15 ↓ 41		1.3 → 3.4	31

* Primary Test Variable

H-910091-20

SKETCHES OF VORTEX CHAMBERS USED IN 80-KW R-F HEATER SHOWING LIGHT-GAS INJECTION SYSTEMS

a. END-WALL LIGHT-GAS INJECTION

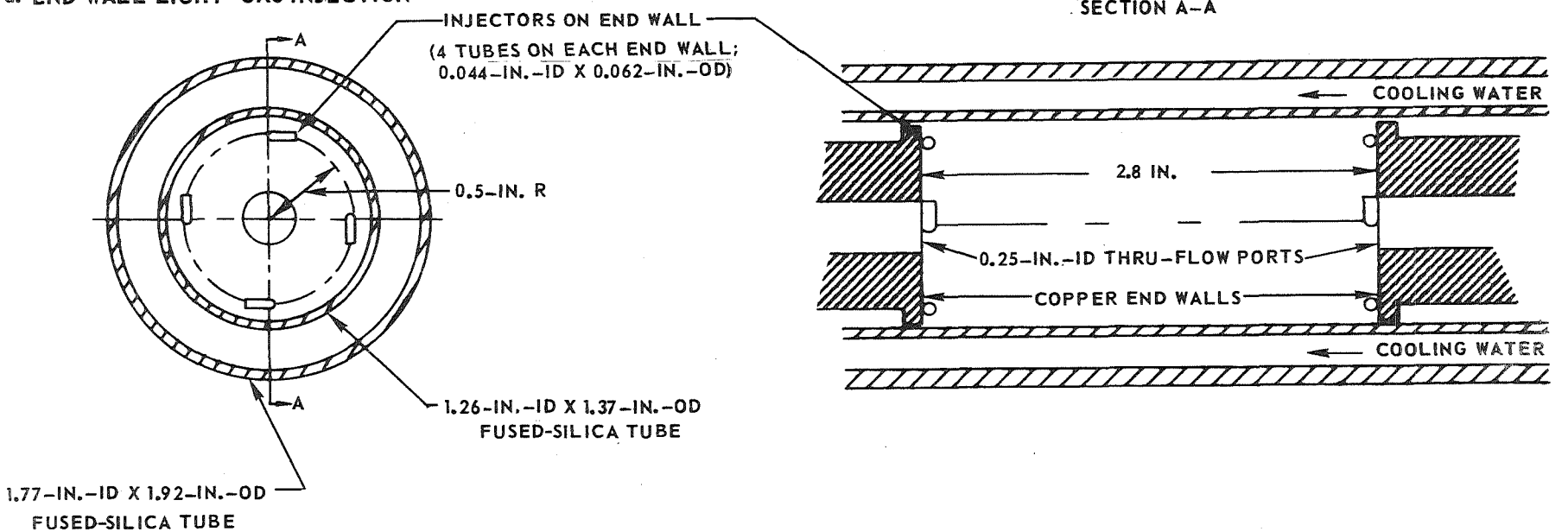

b. PERIPHERAL-WALL LIGHT-GAS INJECTION

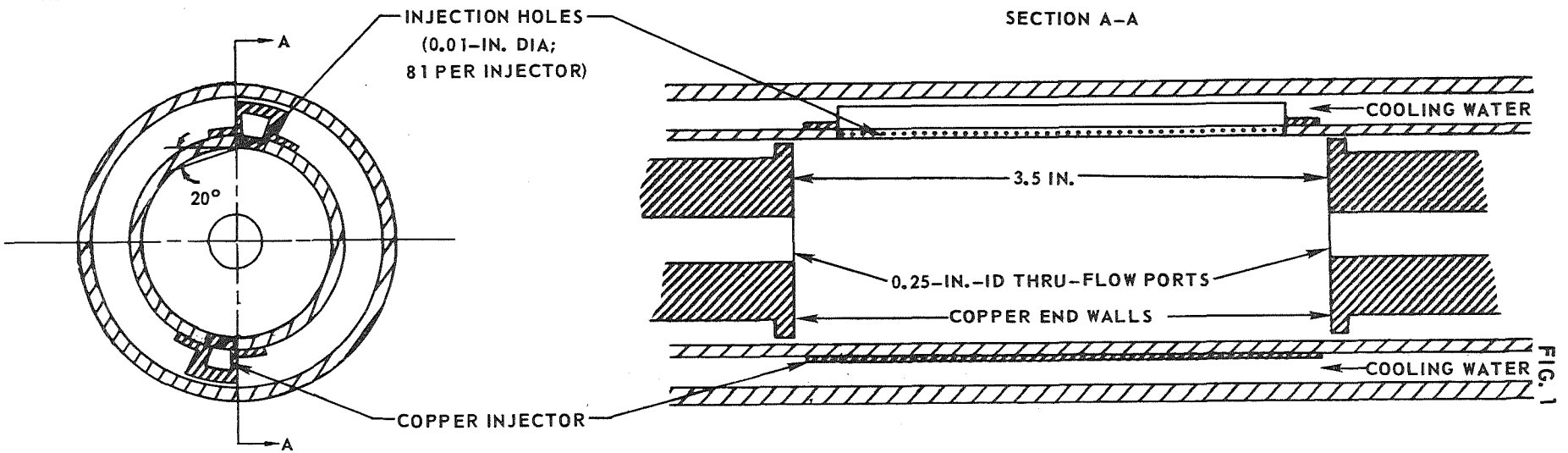

FIG. 1

TWO-COMPONENT VORTEX TEST ASSEMBLY FOR 80-KW R-F INDUCTION HEATER

SEE FIG. 1 FOR DETAILS OF LIGHT-GAS INJECTION CONFIGURATIONS
SEE TABLE I FOR TEST CONDITIONS

a. PHOTOGRAPH OF ASSEMBLY

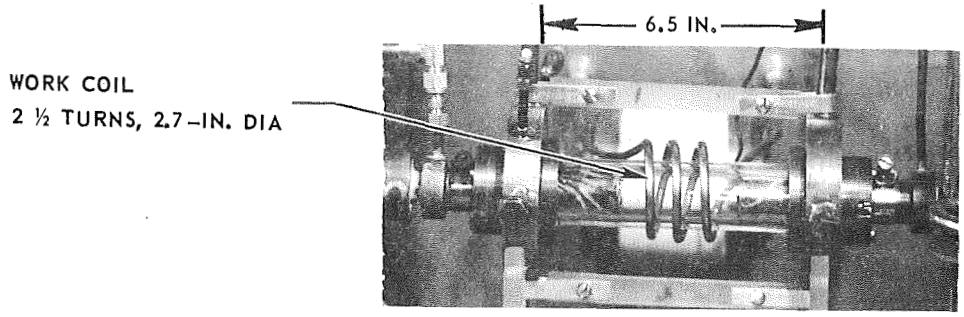

b. PHOTOGRAPH OF PLASMA

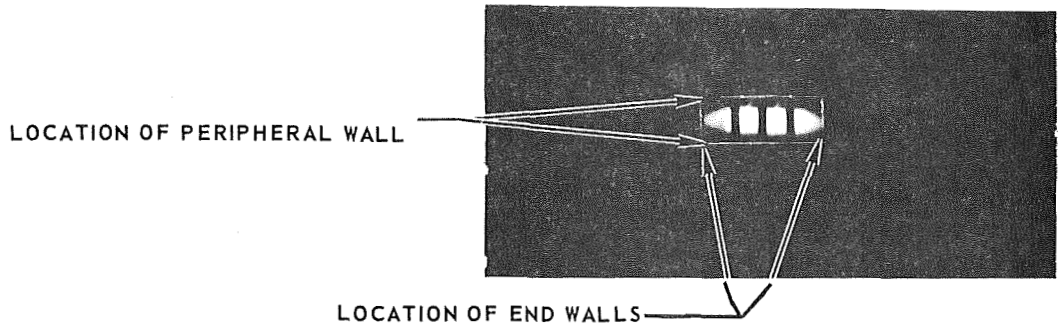

c. SKETCH OF VORTEX CHAMBER SHOWING XENON (HEAVY-GAS) INJECTION LOCATIONS, POWER LOSSES, AND CHORDAL SCANNING POSITIONS

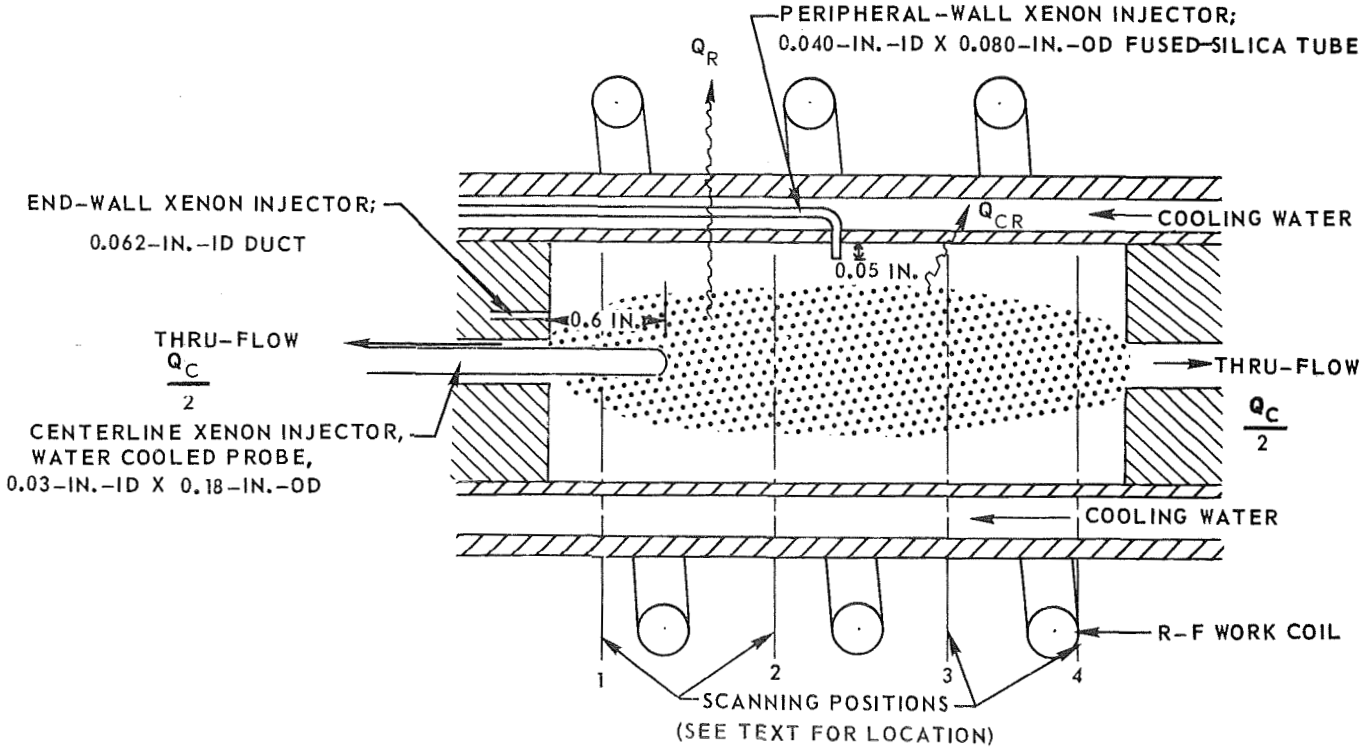

SCHEMATIC OF OPTICAL SYSTEM USED FOR SPECTRAL MEASUREMENTS

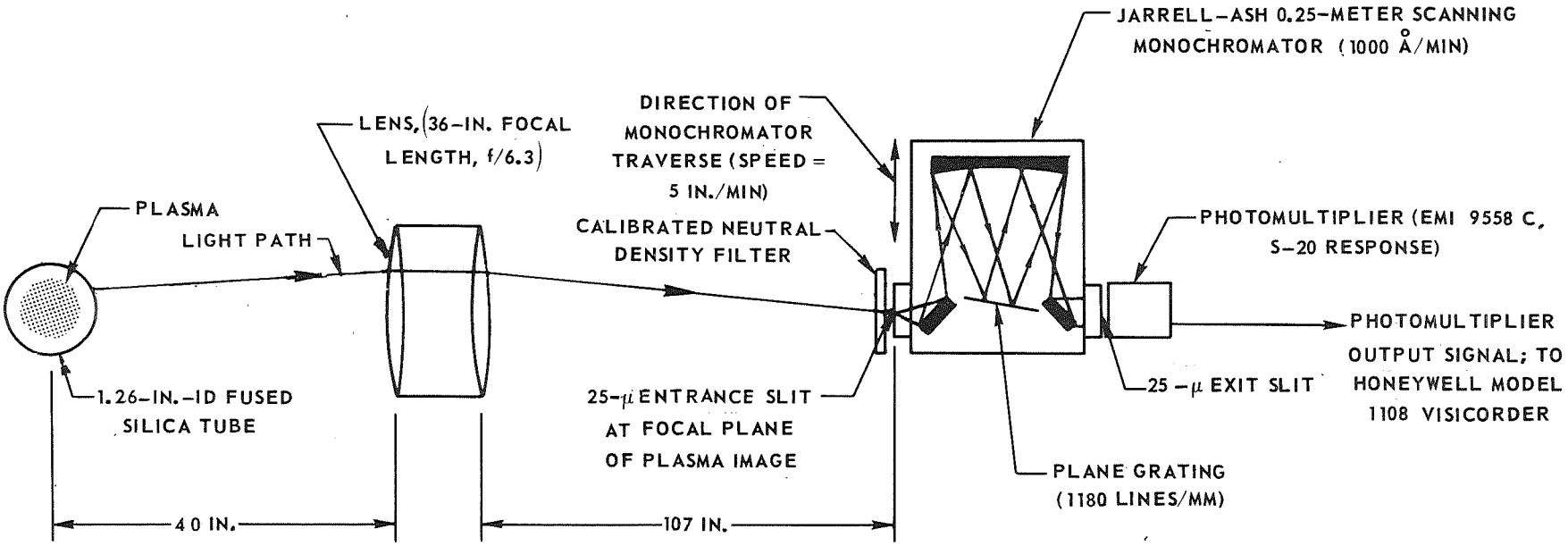

FIG. 3

SCHEMATIC DIAGRAM OF FLOW SYSTEMS IN HIGH REYNOLDS NUMBER TEST FACILITY

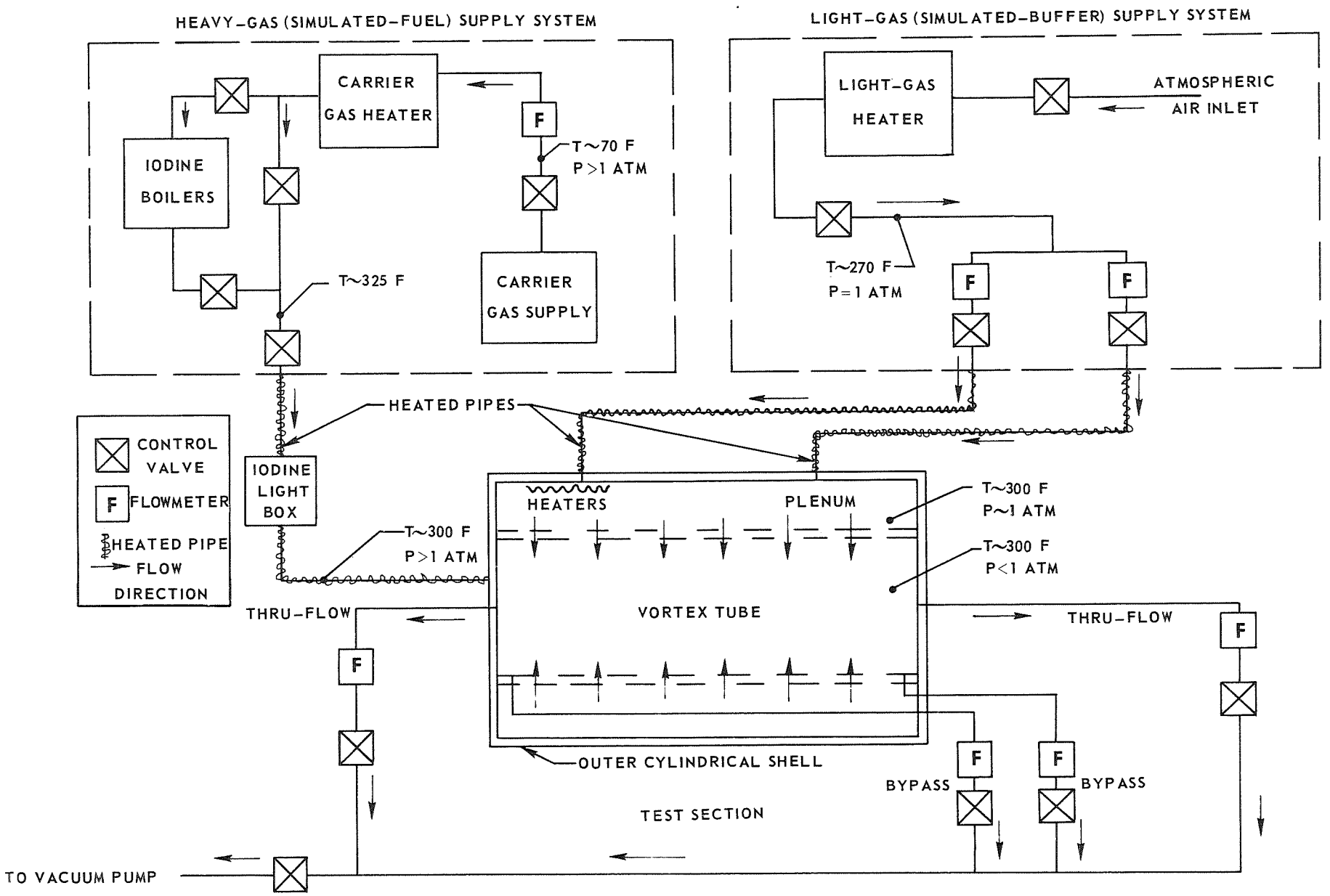

FIG. 4

GEOMETRY OF VORTEX TUBE WITH PERIPHERAL-WALL LIGHT-GAS INJECTION

HIGH REYNOLDS NUMBER TEST FACILITY

a) VORTEX TUBE

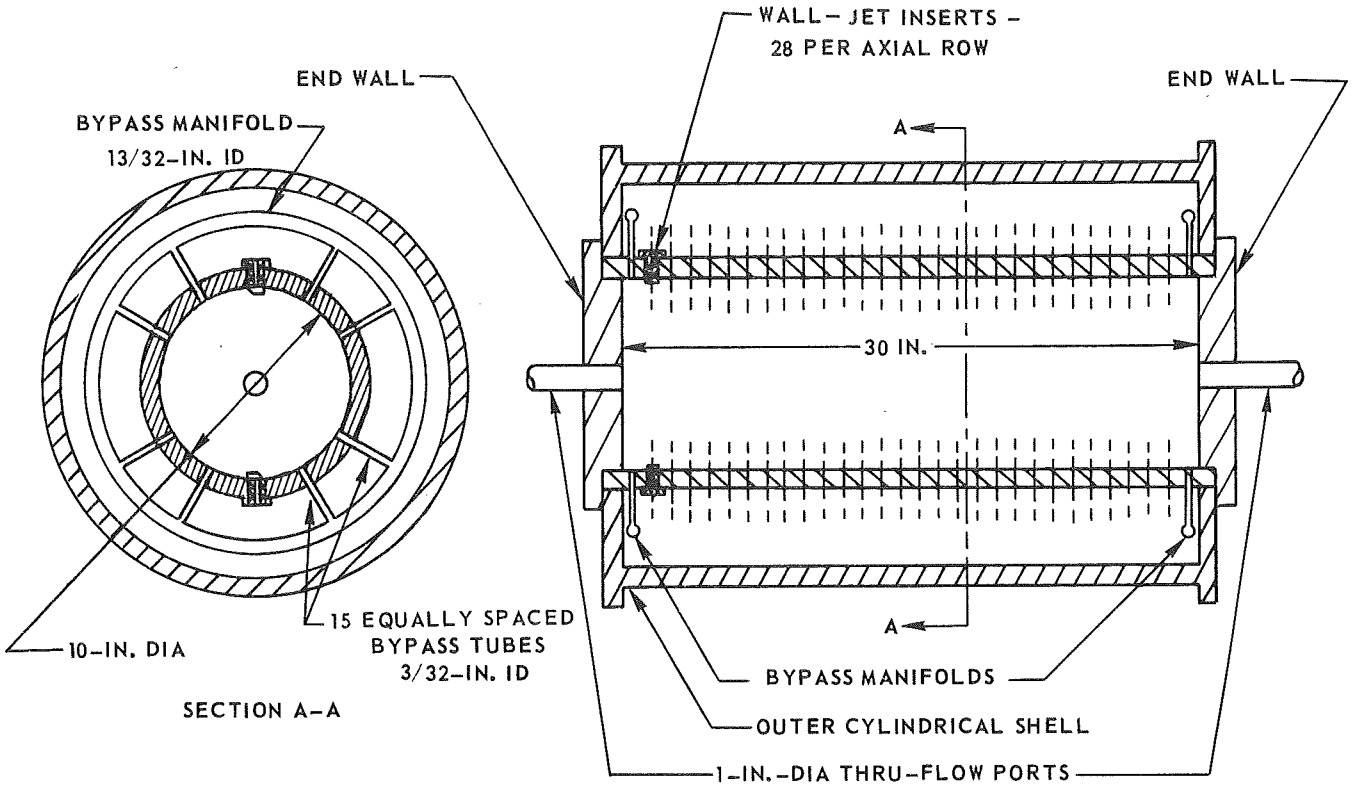

b) DETAILS OF DIRECTED-WALL-JET INSERTS

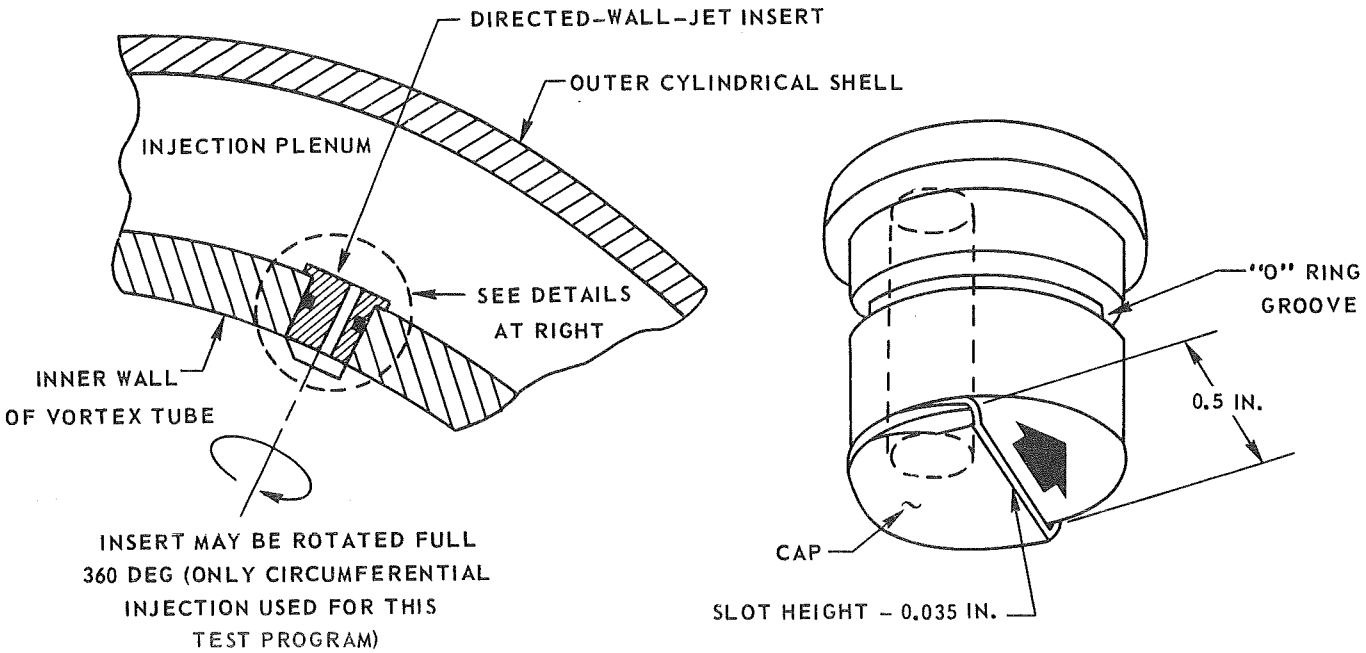

H-910091-20

FIG. 6

GEOMETRY OF VORTEX TUBE WITH LIGHT-GAS INJECTION THROUGH DUCTS LOCATED NEAR THE END-WALLS (SIMULATED END-WALL INJECTION)

HIGH REYNOLDS NUMBER TEST FACILITY

a) VORTEX TUBE

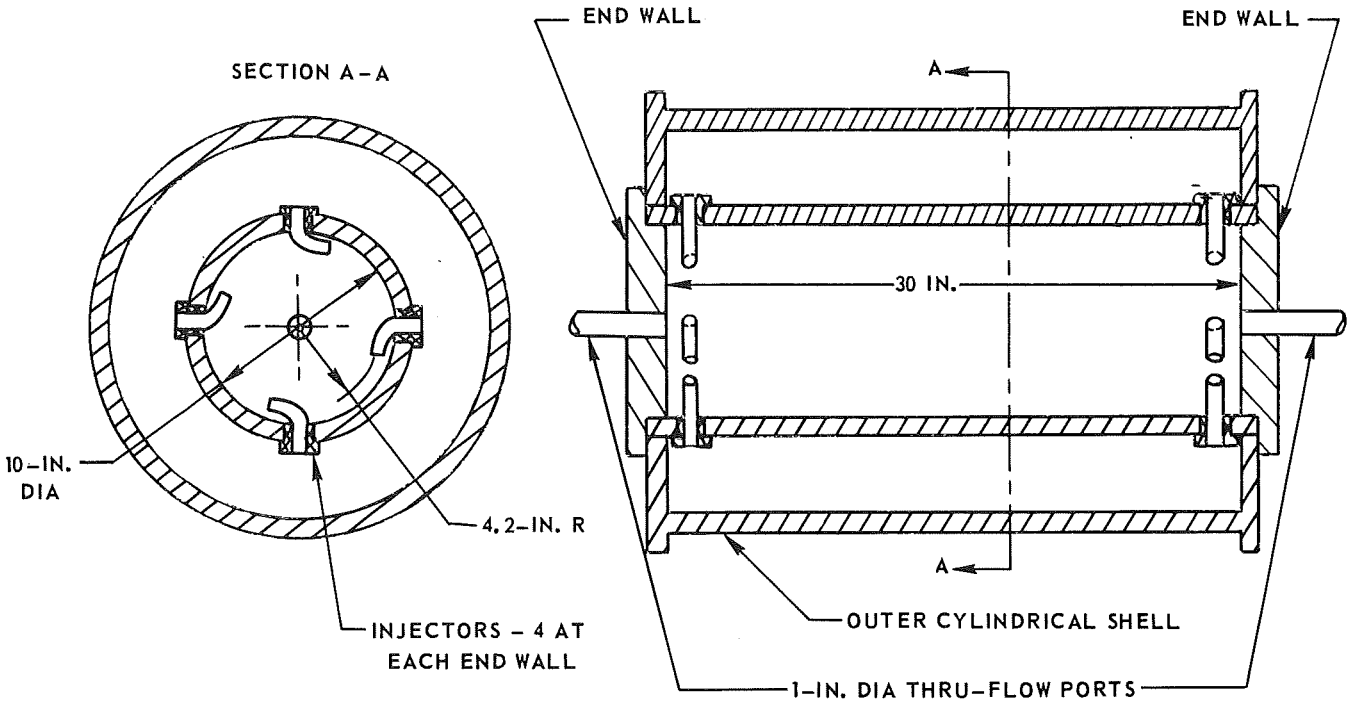

b) DETAILS OF INJECTOR

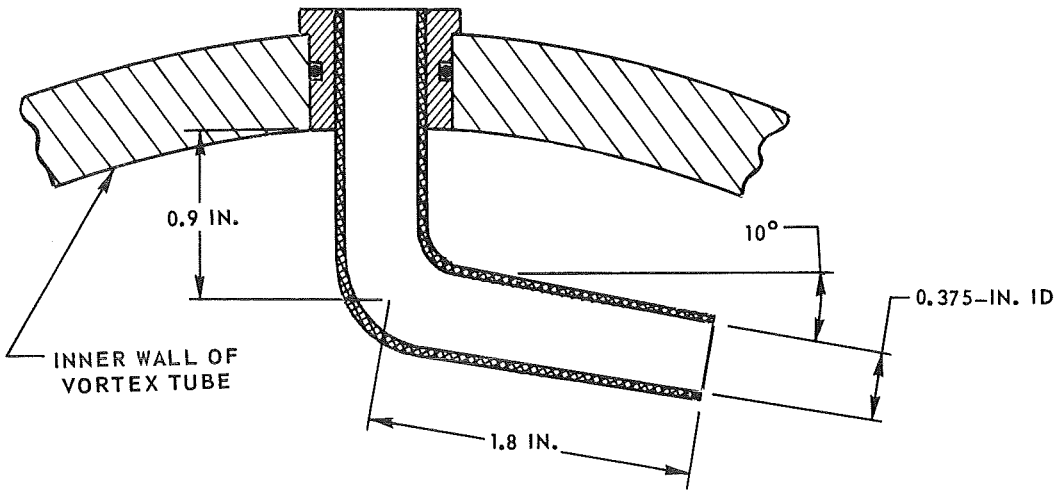

FIG. 7

HEAVY-GAS INJECTION CONFIGURATIONS

HIGH REYNOLDS NUMBER TEST FACILITY

a) PERIPHERAL-WALL HEAVY-GAS INJECTION

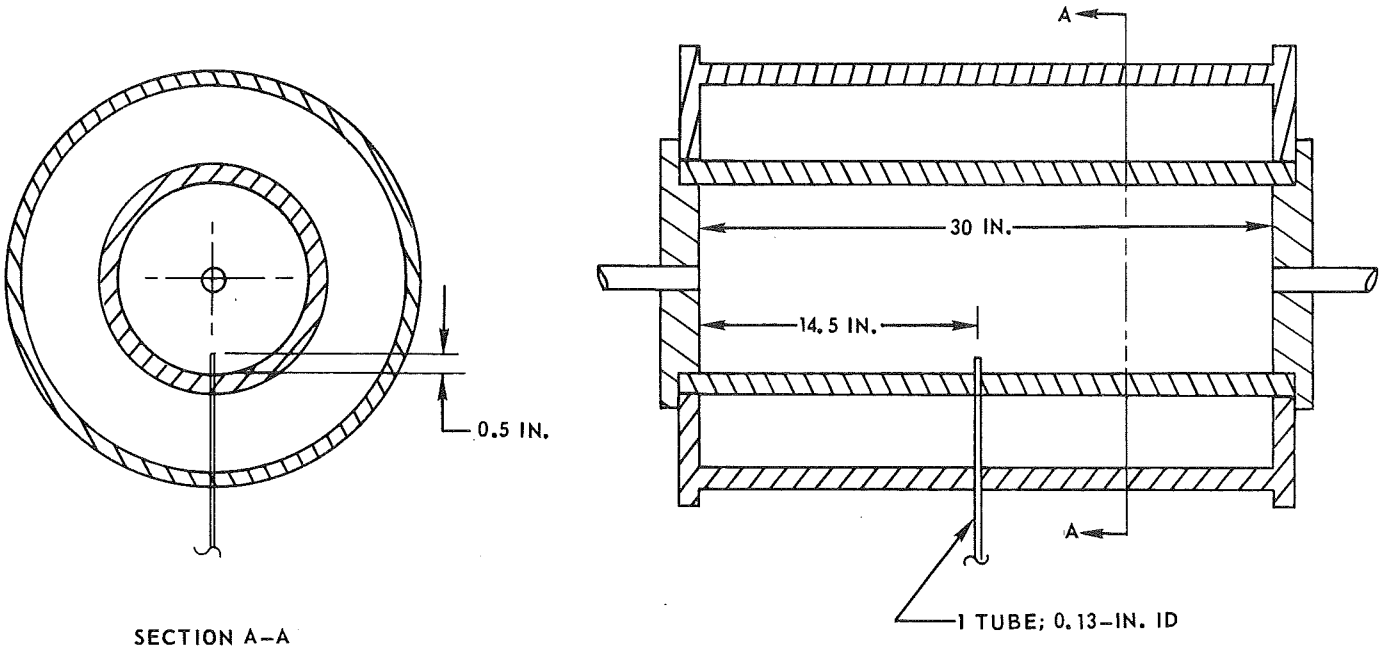

SECTION A-A

b) END-WALL HEAVY- GAS INJECTION

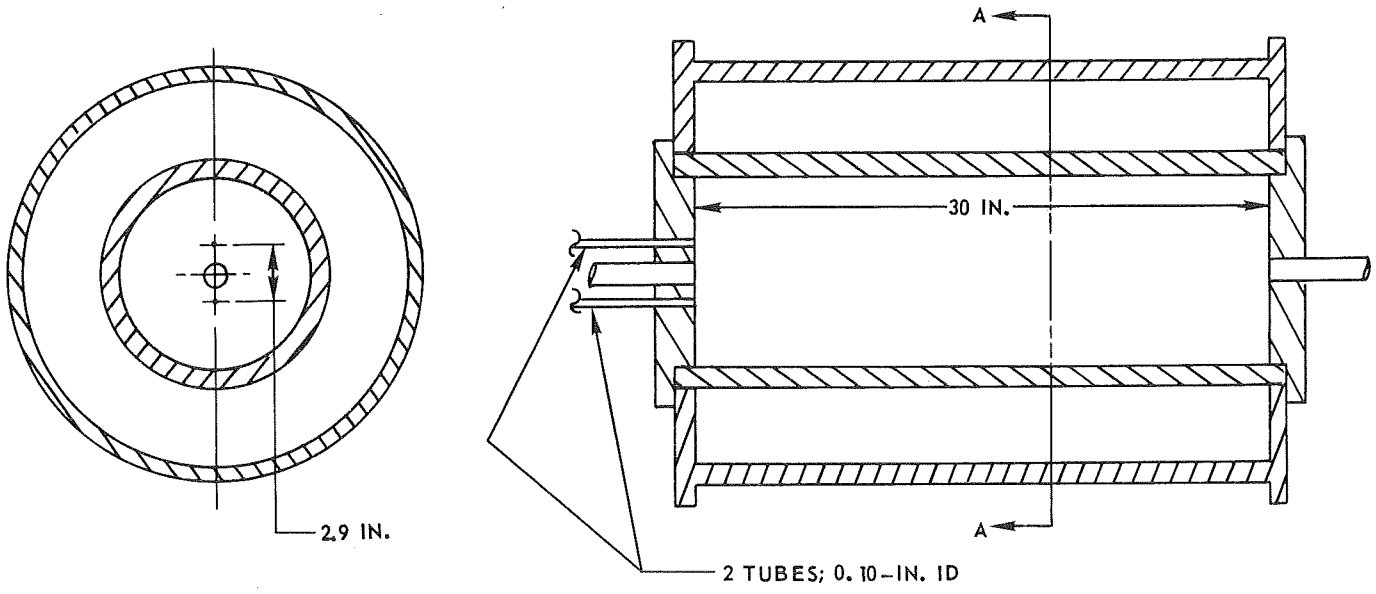

SECTION A-A

SCHEMATIC DIAGRAM OF OPTICAL SYSTEM IN HIGH REYNOLDS NUMBER TEST FACILITY

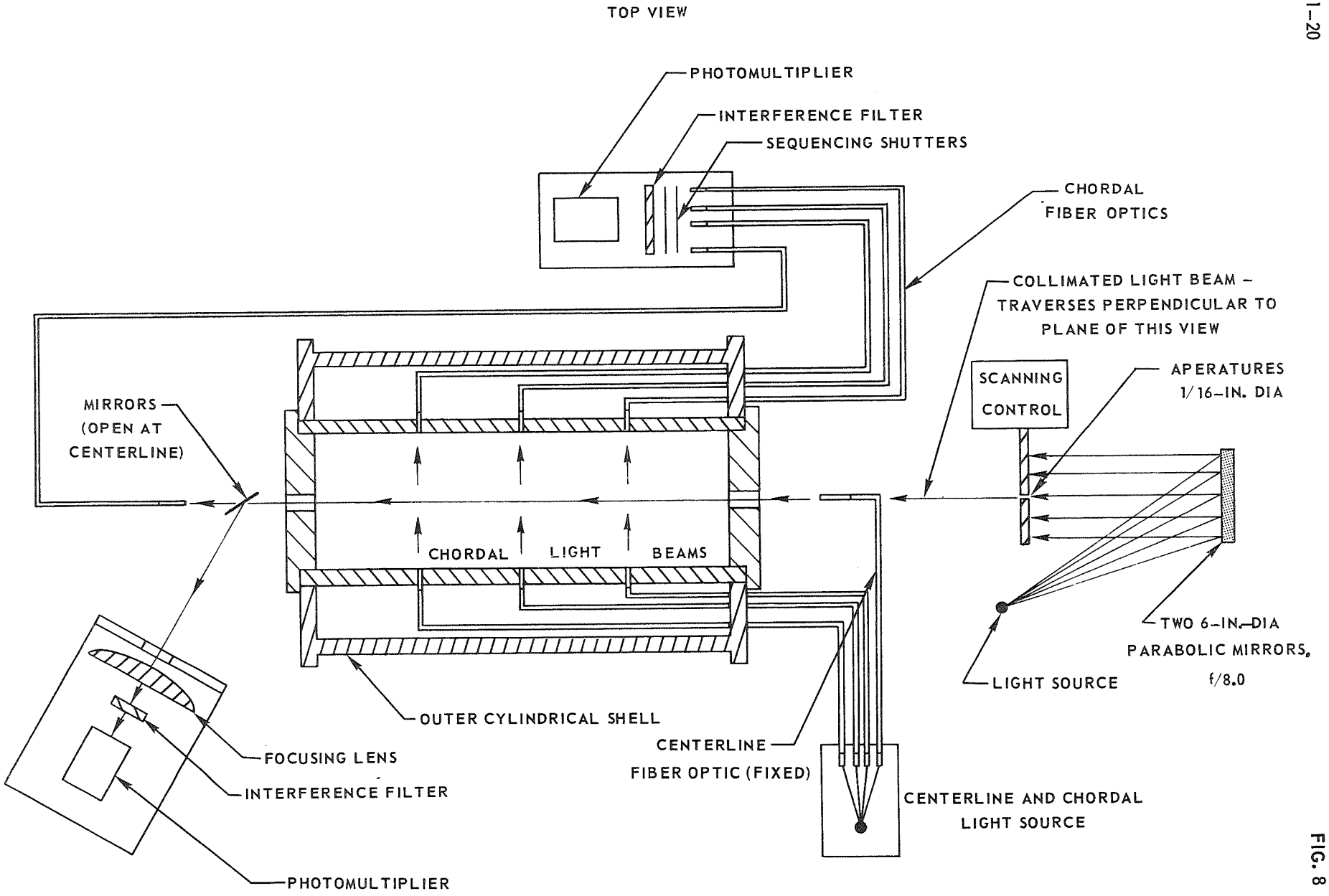

FIG. 8

TYPICAL EMISSION SPECTRUM BETWEEN 4000 Å AND 5000 Å OF AN ARGON PLASMA SEEDED WITH XENON

UNCORRECTED FOR PHOTOMULTIPLIER RESPONSE

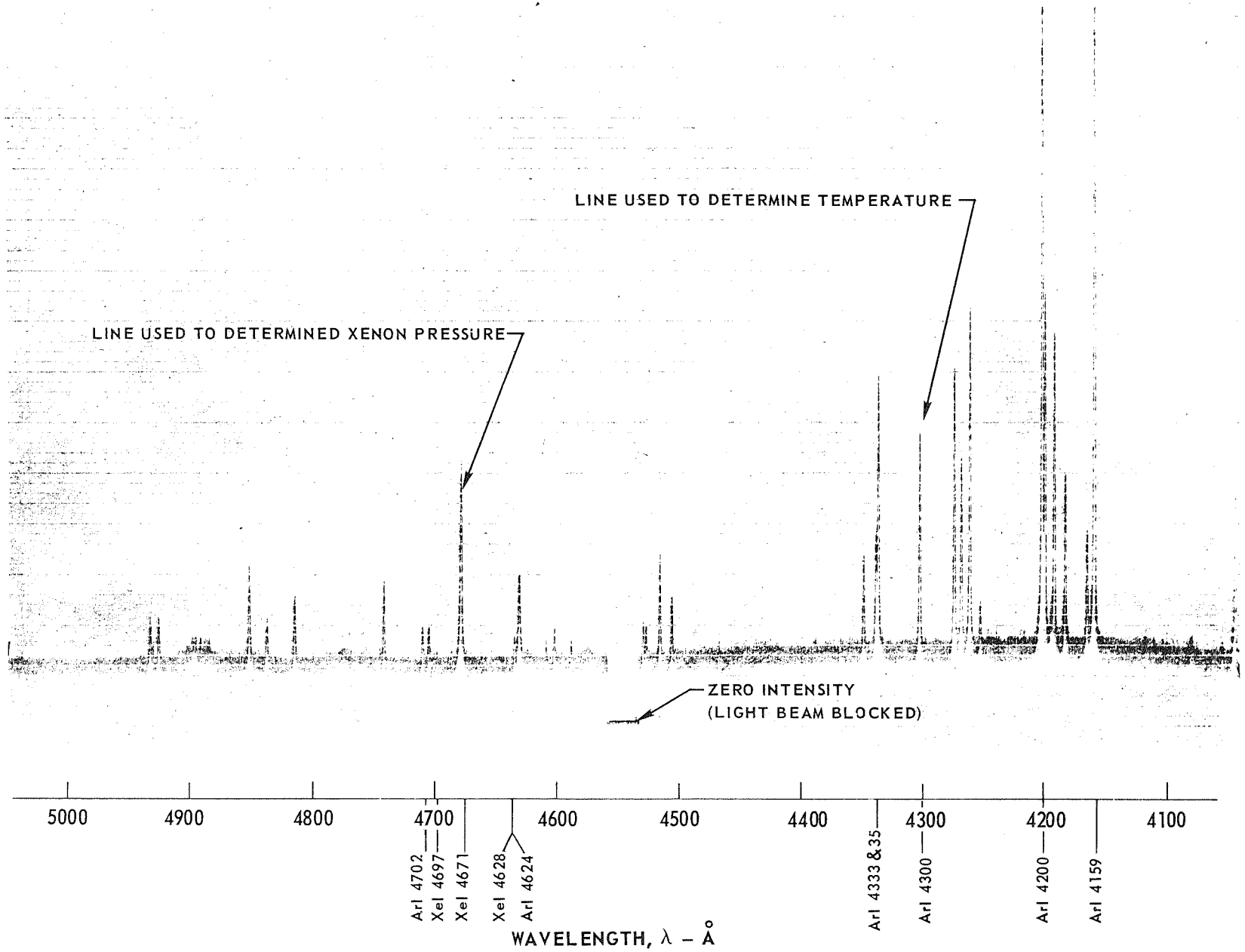

FIG. 9

FIG. 10

CALCULATED VARIATION WITH TEMPERATURE OF THE TOTAL ARGON CONTINUUM RADIATION BETWEEN 4200 Å AND 4300 Å AT A PRESSURE OF 1.2 ATM

CALCULATED FROM EQ. 10

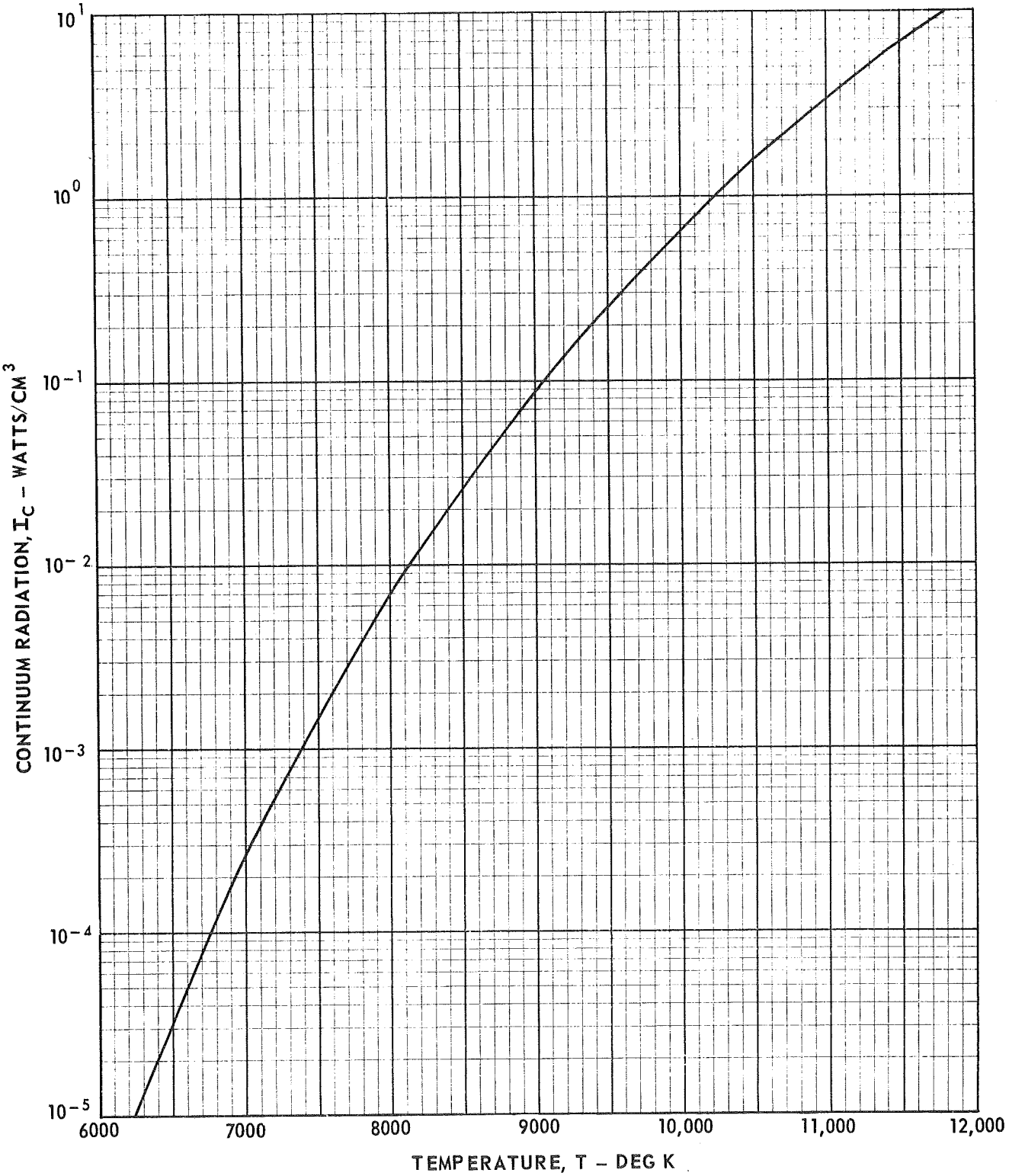

CALCULATED VARIATION WITH TEMPERATURE OF THE INTENSITY OF THE ARGON I 4300 Å LINE AT A PRESSURE OF 1.2 ATM

CALCULATED FROM EQ. 11

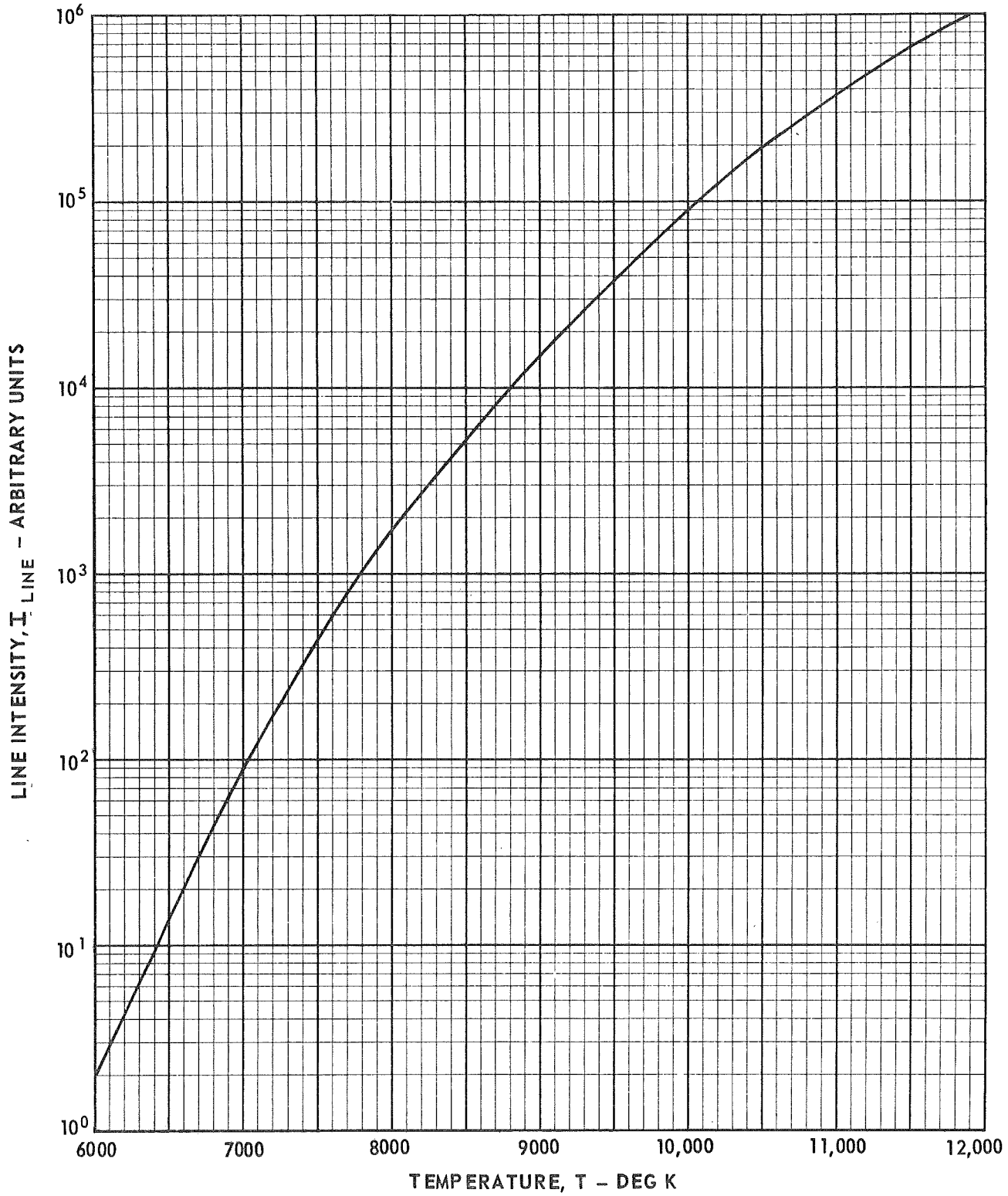

FIG. 12

TYPICAL CHORDAL AND RADIAL VARIATIONS IN INTENSITY OF CONTINUUM, AN ARGON LINE AND A XENON LINE IN ARGON PLASMA WITH XENON INJECTION

PERIPHERAL-WALL LIGHT-GAS INJECTION
PERIPHERAL-WALL HEAVY-GAS INJECTION

a. CHORDAL VARIATIONS

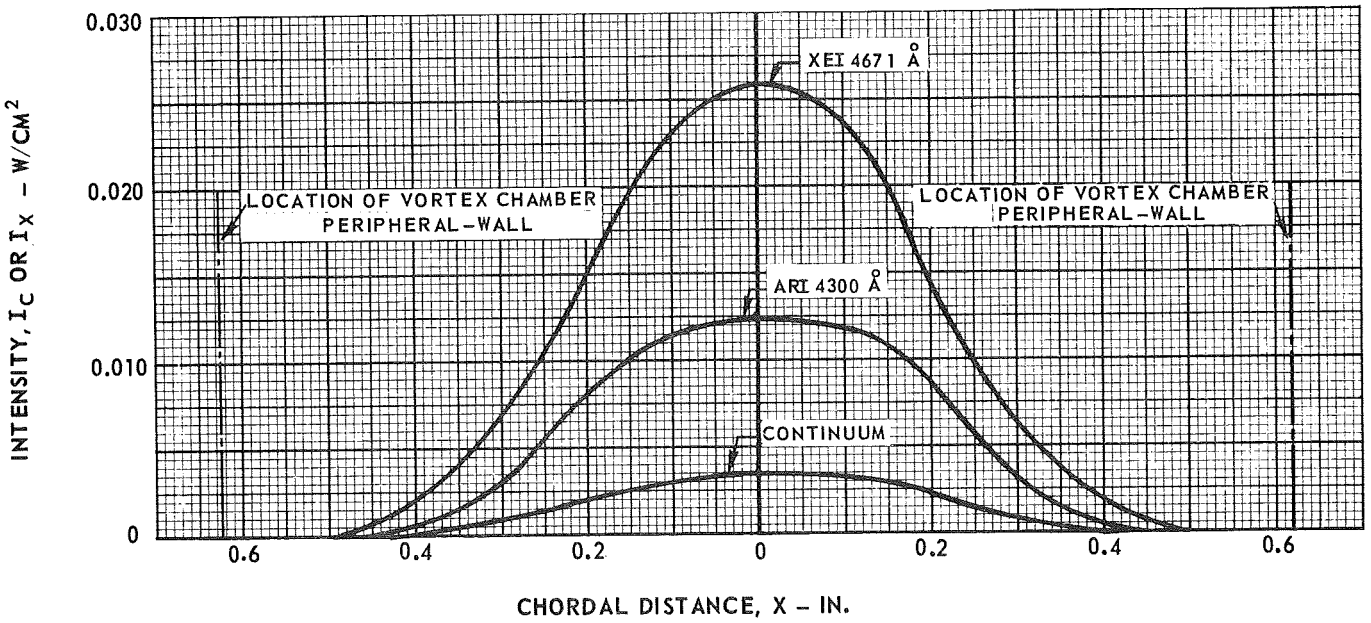

b. RADIAL VARIATIONS

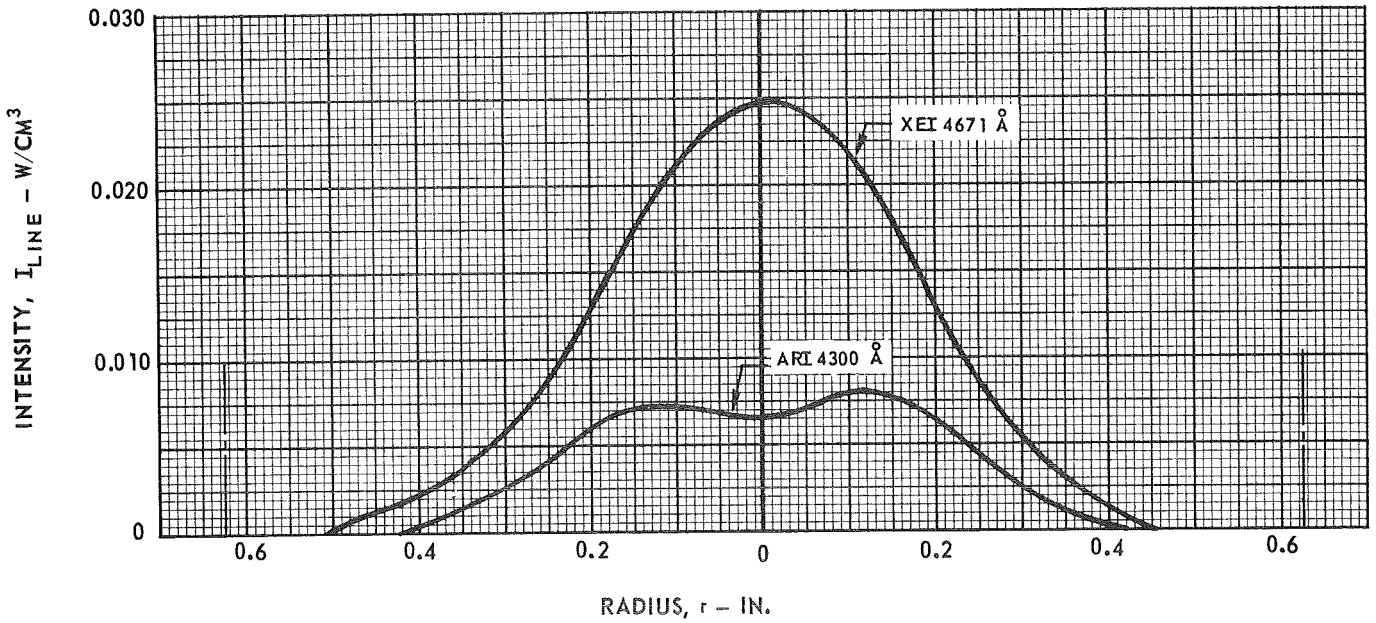

FIG. 13

COMPOSITION OF XENON IN AN EQUILIBRIUM ARGON-XENON MIXTURE

TOTAL PRESSURE = 1.2 ATM

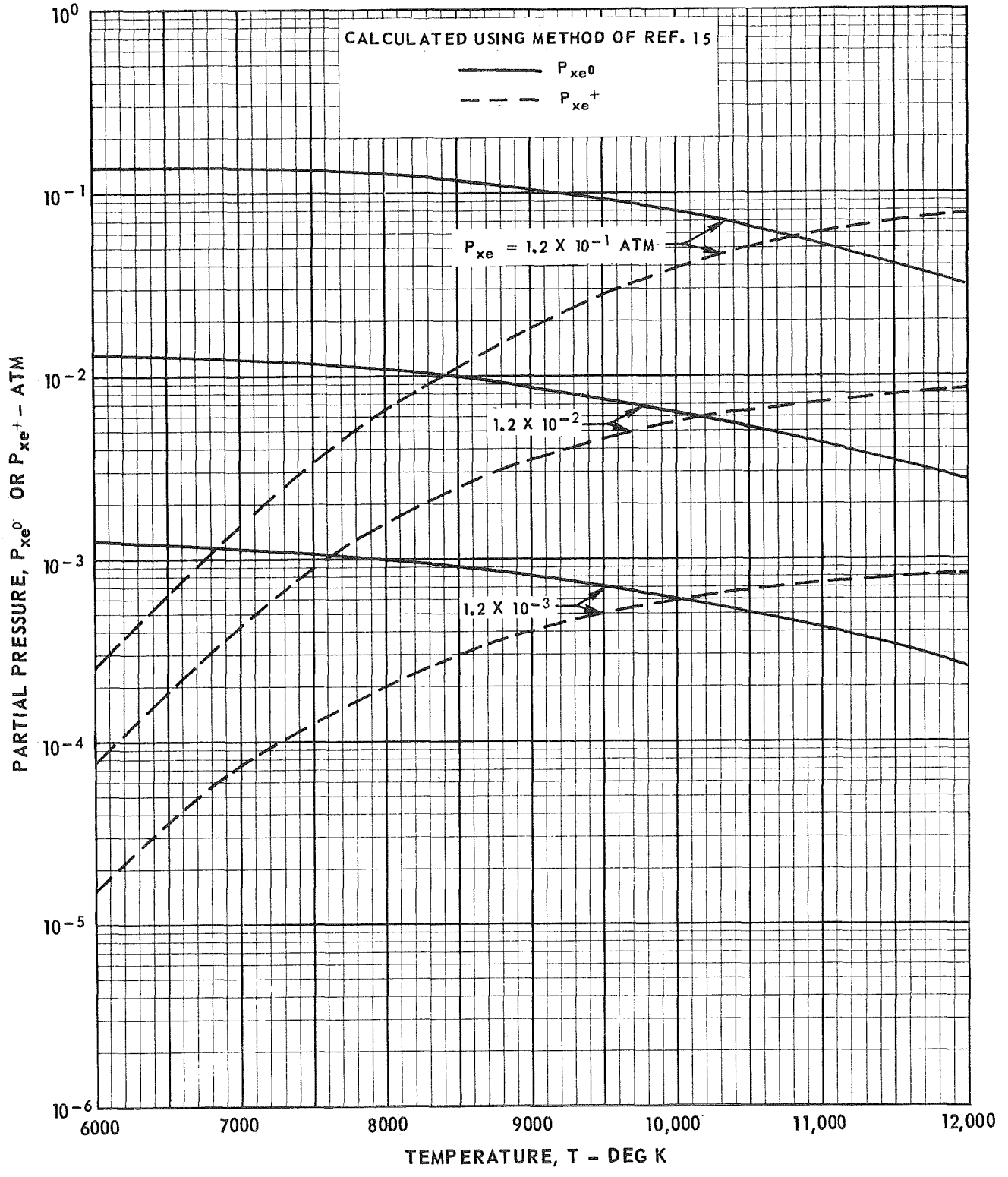

FIG. 14

CALCULATED VARIATION WITH TEMPERATURE OF THE INTENSITY OF THE XENON I 4671 Å LINE IN AN ARGON-XENON MIXTURE

CALCULATED FROM EQ. 12 USING COMPOSITION OF FIG. 13

TOTAL PRESSURE = 1.2 ATM

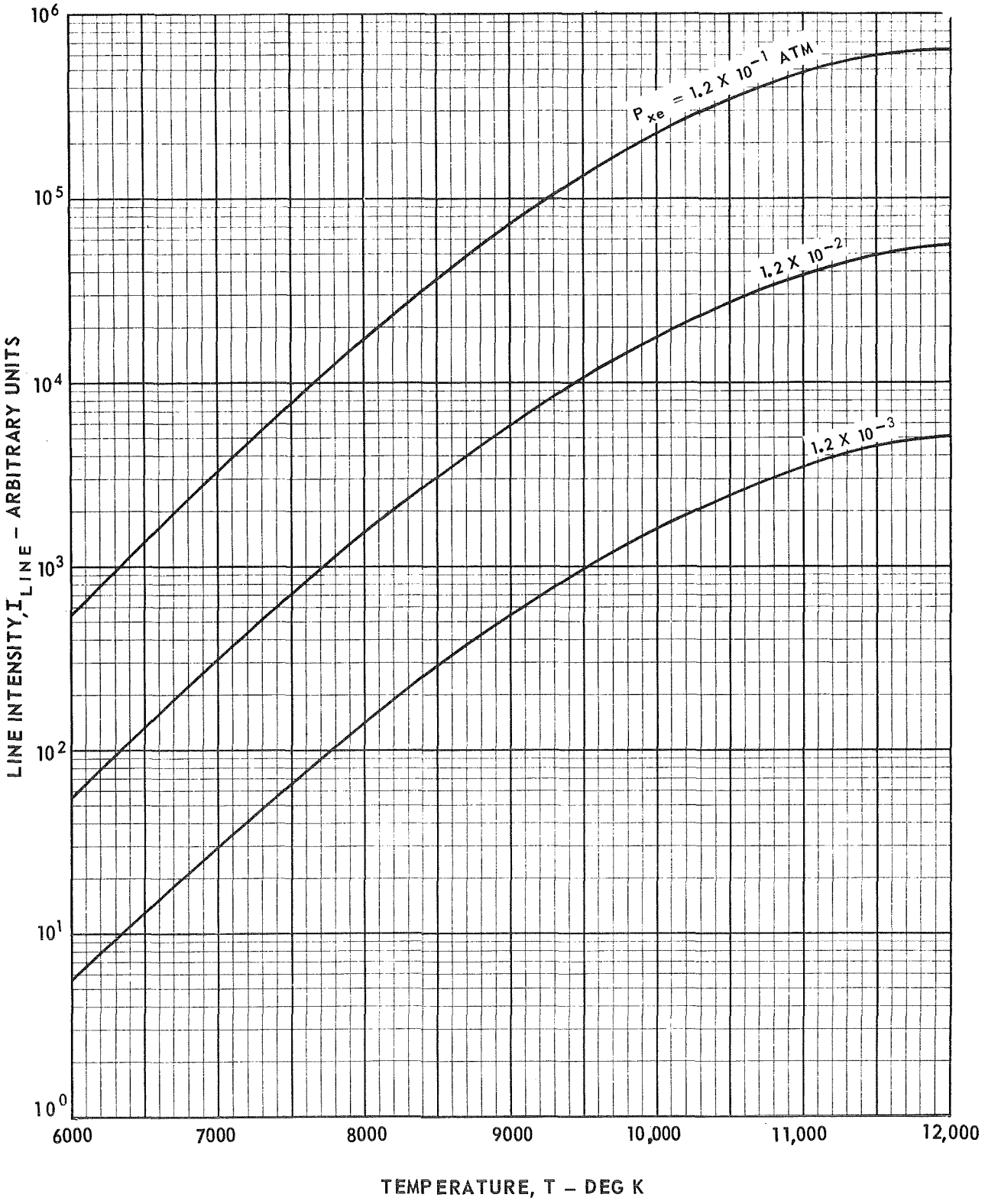

RADIAL DISTRIBUTIONS OF TEMPERATURE FOR AN END-WALL-DRIVEN ARGON PLASMA VORTEX

TEMPERATURE DETERMINED FROM INTENSITY OF ARI 4300 Å LINE
SEE FIG. 1a FOR ARGON INJECTION CONFIGURATION
SEE TABLE I FOR FLOW AND POWER CONDITIONS

LINE	AXIAL POSITION (SEE FIG. 2c)
———	1
— · —	2
– – – –	3
— — —	4

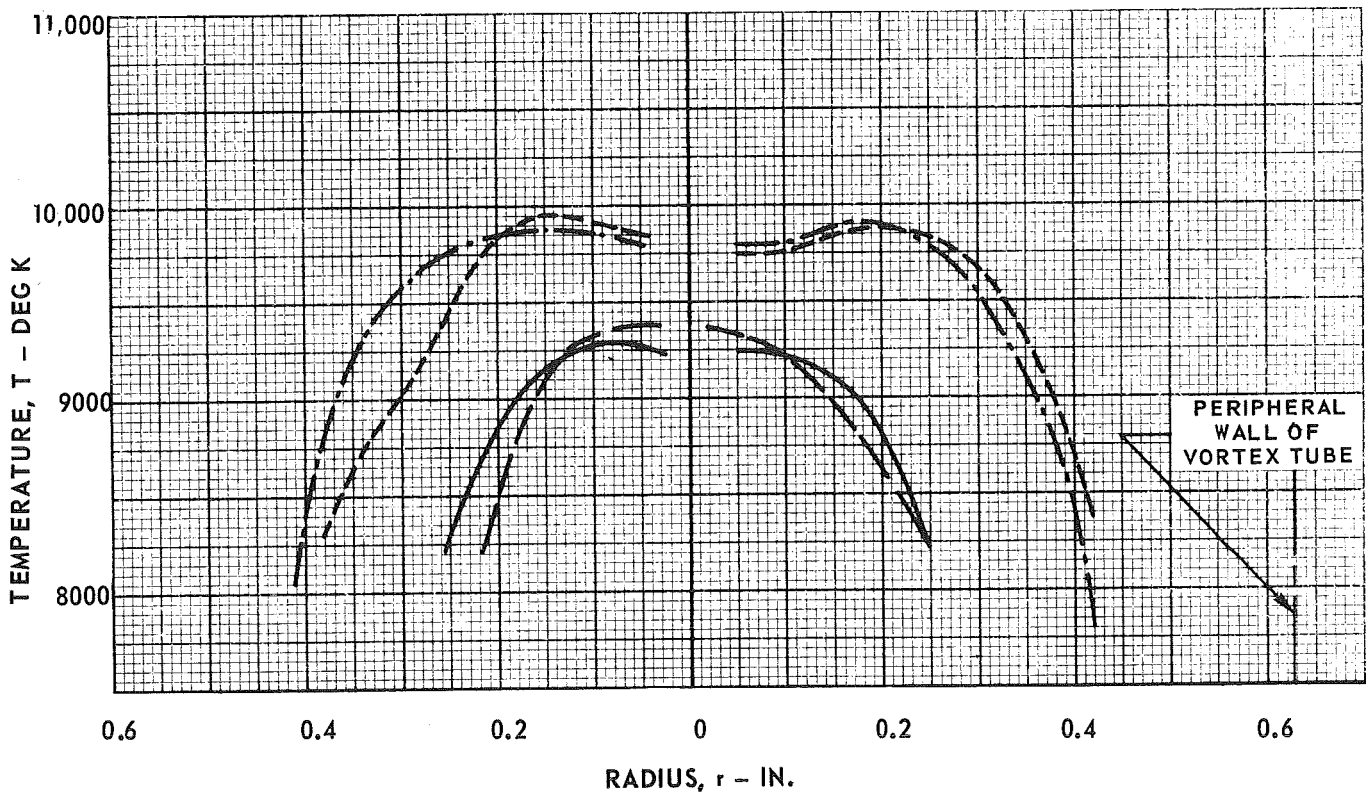

RADIAL DISTRIBUTIONS OF TEMPERATURE AND XENON PARTIAL PRESSURE FOR AN END-WALL-DRIVEN ARGON PLASMA VORTEX PREMIXED WITH XENON

SEE FIG. 1a FOR ARGON INJECTION CONFIGURATION
SEE TABLE I FOR FLOW AND POWER CONDITIONS

LINE	AXIAL POSITION (SEE FIG. 2c)
———	1
——·——	2
– – – –	3
—— ——	4

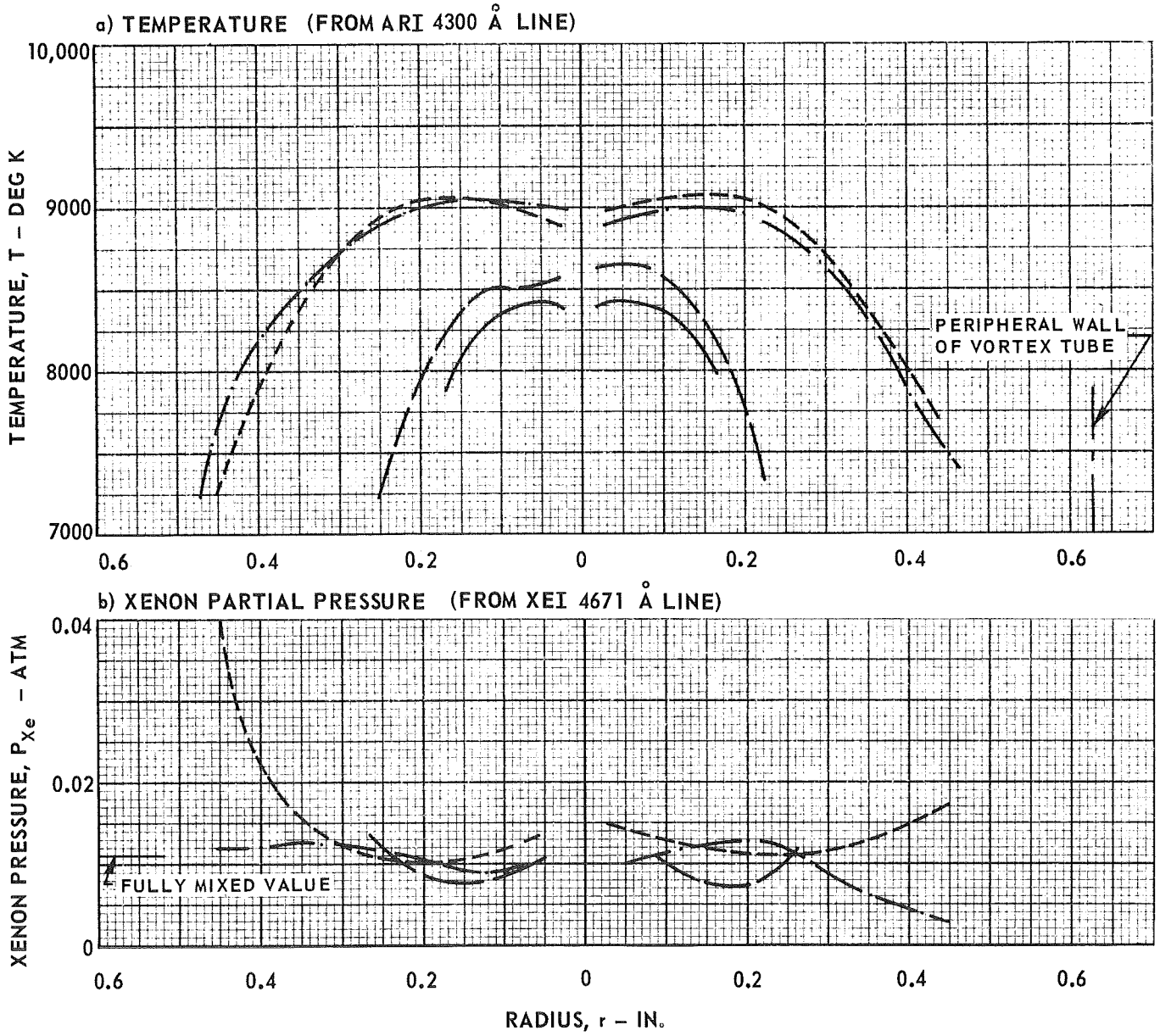

H-910091-20

FIG. 17

RADIAL DISTRIBUTIONS OF TEMPERATURE AND XENON PARTIAL PRESSURE FOR AN END-WALL-DRIVEN ARGON PLASMA VORTEX WITH PERIPHERAL-WALL XENON INJECTION

XENON INJECTED RADIALLY INWARD THROUGH PERIPHERAL WALL (SEE FIG. 2c)
SEE FIG. 1a FOR ARGON INJECTION CONFIGURATION
SEE TABLE I FOR FLOW AND POWER CONDITIONS

LINE	AXIAL POSITION (SEE FIG. 2c)
———	1
—·—	2
– – –	3
—— ——	4

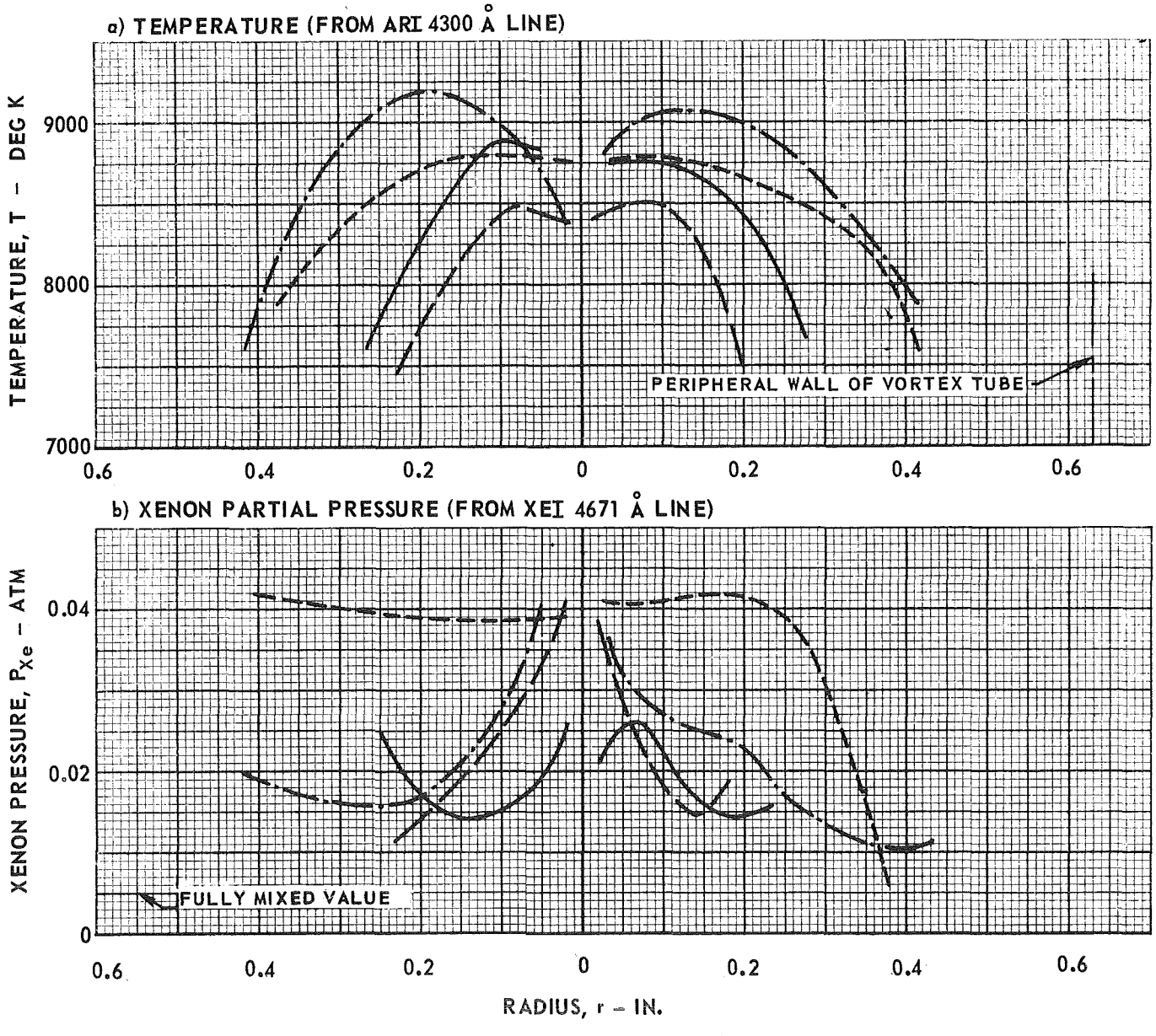

FIG. 18

RADIAL DISTRIBUTIONS OF TEMPERATURE AND XENON PARTIAL PRESSURE FOR AN END-WALL-DRIVEN ARGON PLASMA VORTEX WITH CENTERLINE XENON INJECTION

XENON INJECTED AXIALLY THROUGH PROBE ON VORTEX CENTERLINE (SEE FIG. 2c)
SEE FIG. 1a FOR ARGON INJECTION CONFIGURATION
SEE TABLE I FOR FLOW AND POWER CONDITIONS

LINE	AXIAL POSITION (SEE FIG. 2c)
———	1
—·—	2
– – –	3
—— ——	4

a) TEMPERATURE (FROM ARI 4300 Å LINE)

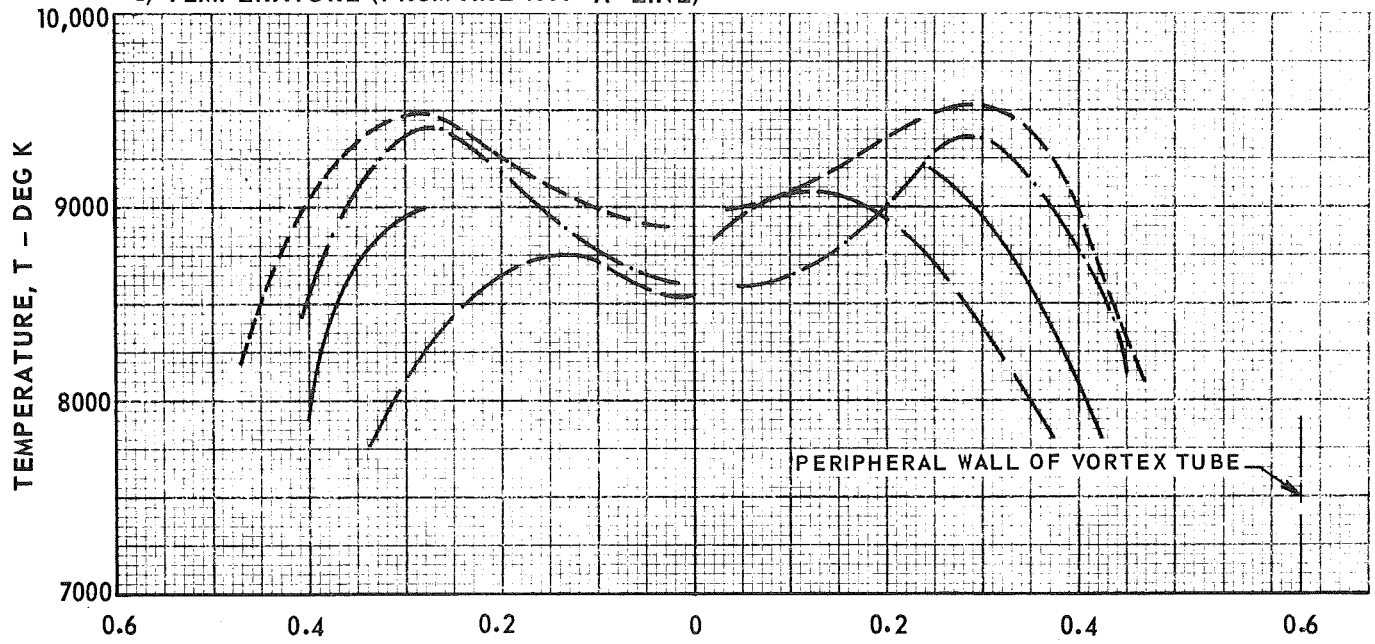

b) XENON PARTIAL PRESSURE (FROM XEI 4671 Å LINE)

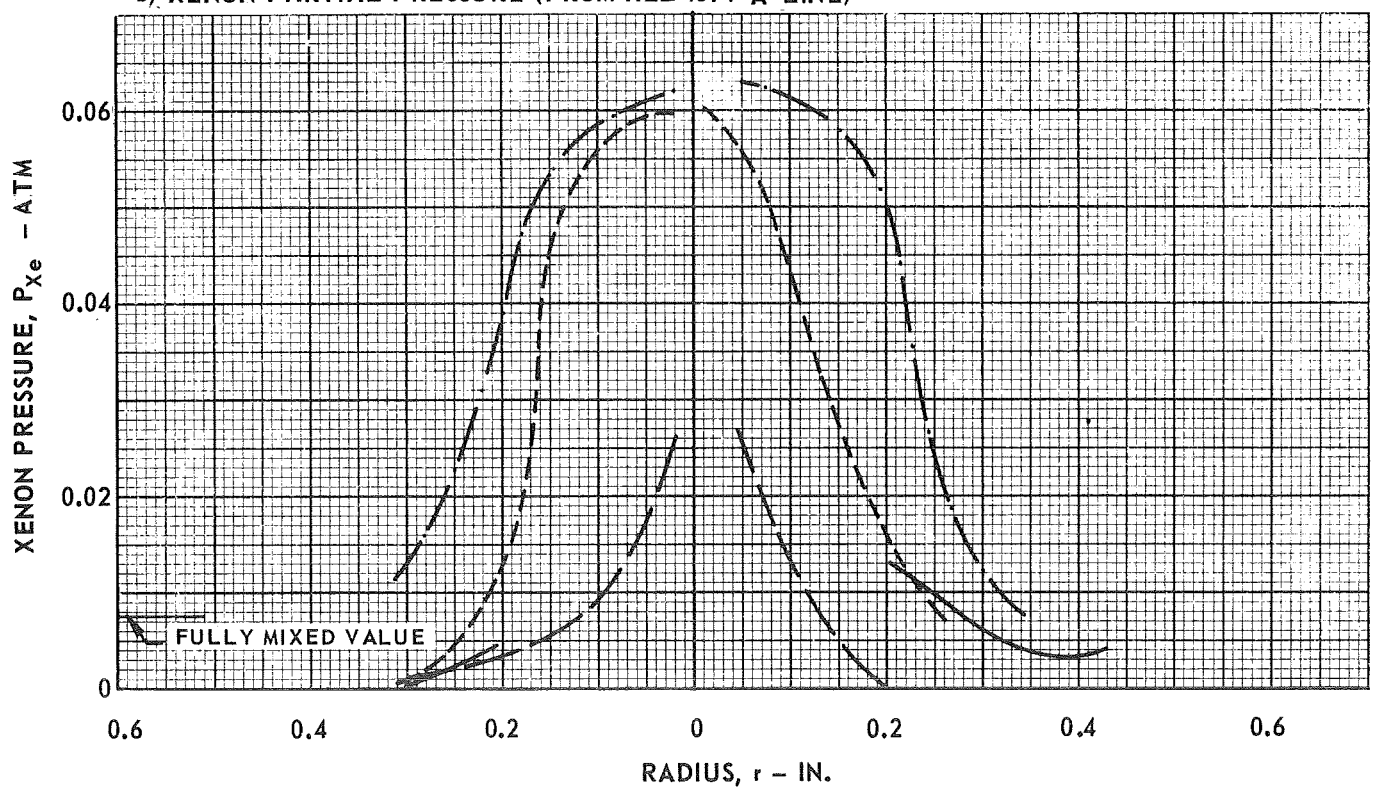

RADIAL DISTRIBUTIONS OF TEMPERATURE FOR A PERIPHERAL-WALL-DRIVEN ARGON PLASMA VORTEX

TEMPERATURE DETERMINED FROM INTENSITY OF ARI 4300 Å LINE
SEE FIG. 1b FOR ARGON INJECTION CONFIGURATION
SEE TABLE I FOR FLOW AND POWER CONDITIONS

LINE	AXIAL POSITION (SEE FIG. 2c)
———	1
——·——	2
– – – –	3
—— ——	4

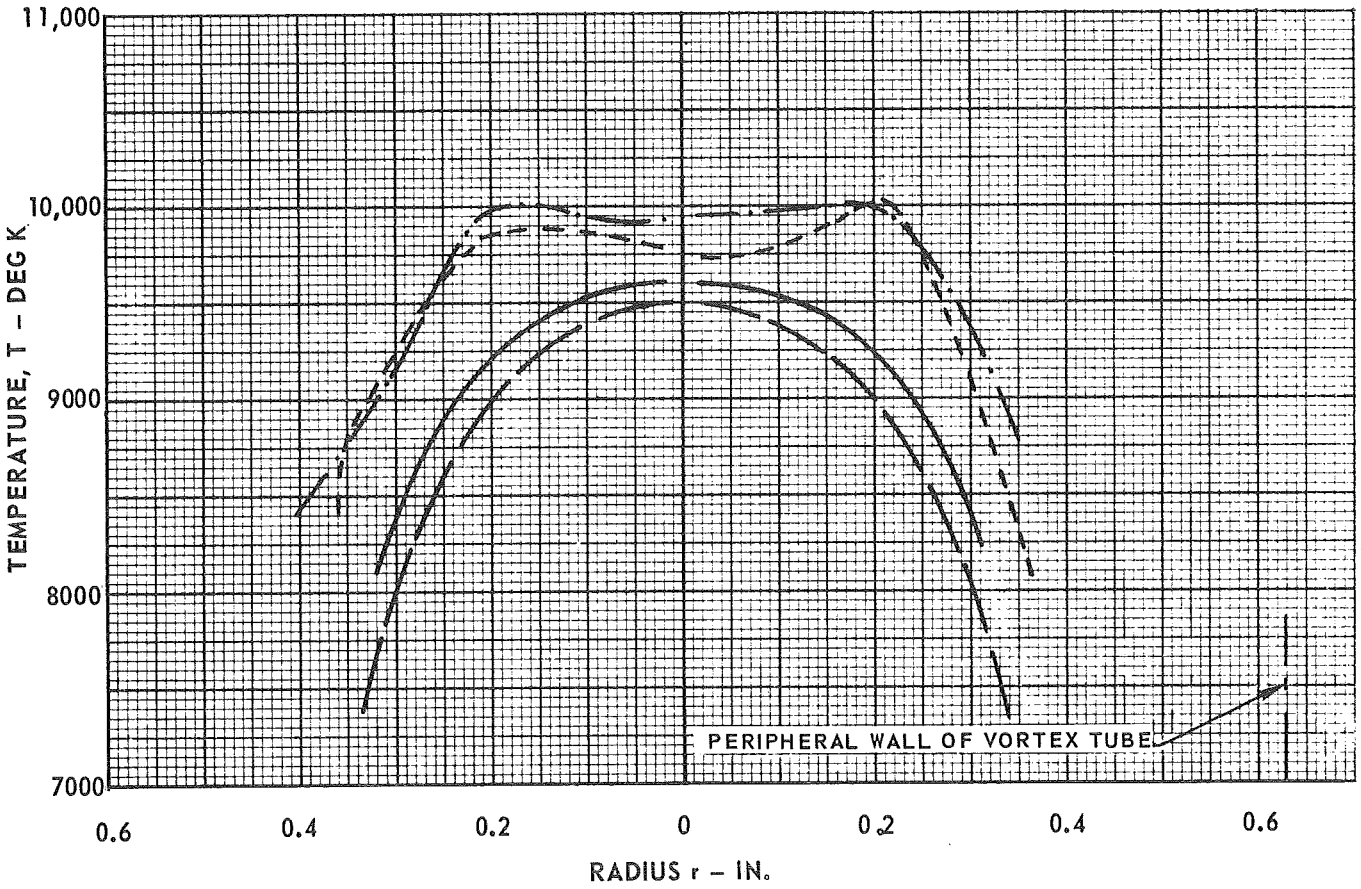

H-910091-20

FIG. 20

RADIAL DISTRIBUTIONS OF TEMPERATURE AND XENON PARTIAL PRESSURE FOR A PERIPHERAL-WALL-DRIVEN ARGON PLASMA VORTEX WITH PERIPHERAL-WALL XENON INJECTION

XENON INJECTED RADIALLY INWARD THROUGH PERIPHERAL WALL (SEE FIG. 2c)
SEE FIG. 1b FOR ARGON INJECTION CONFIGURATION
SEE TABLE I FOR FLOW POWER CONDITIONS

LINE	AXIAL POSITION (SEE FIG. 2c)
———	1
—·—	2
– – –	3
—— ——	4

a) TEMPERATURE (FROM ARI 4300 Å LINE)

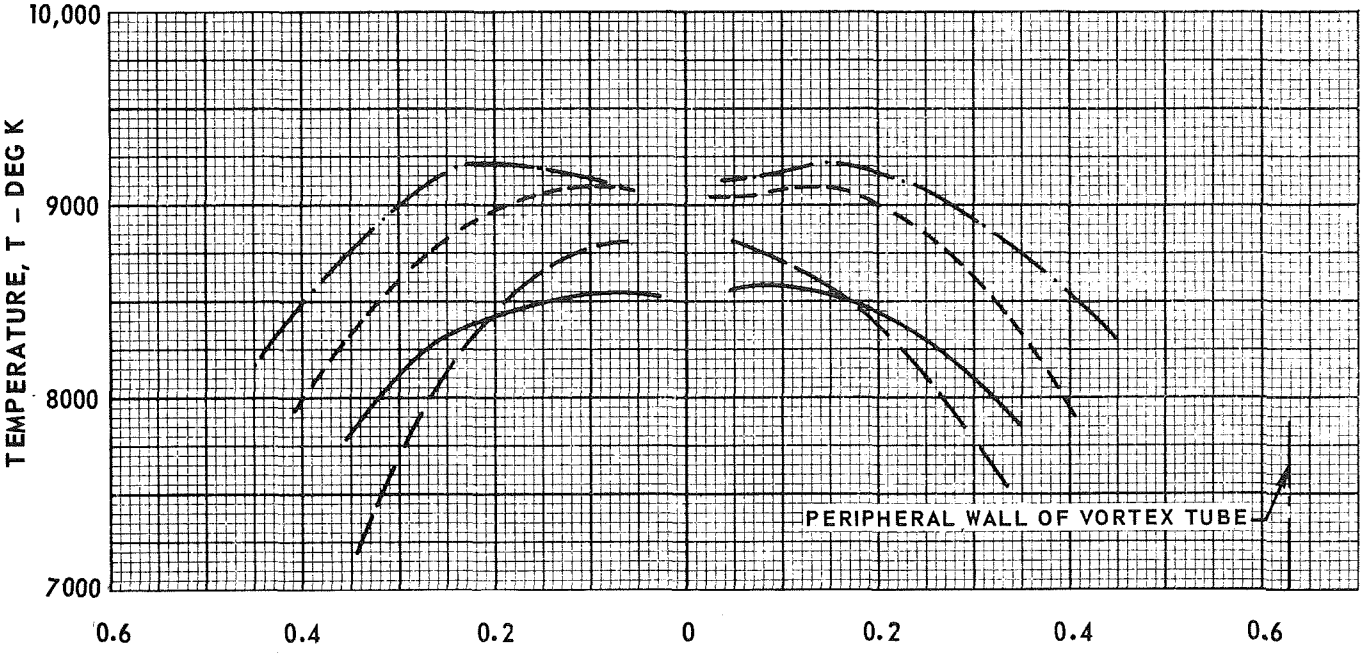

b) XENON PARTIAL PRESSURE (FROM XEI 4671 Å LINE)

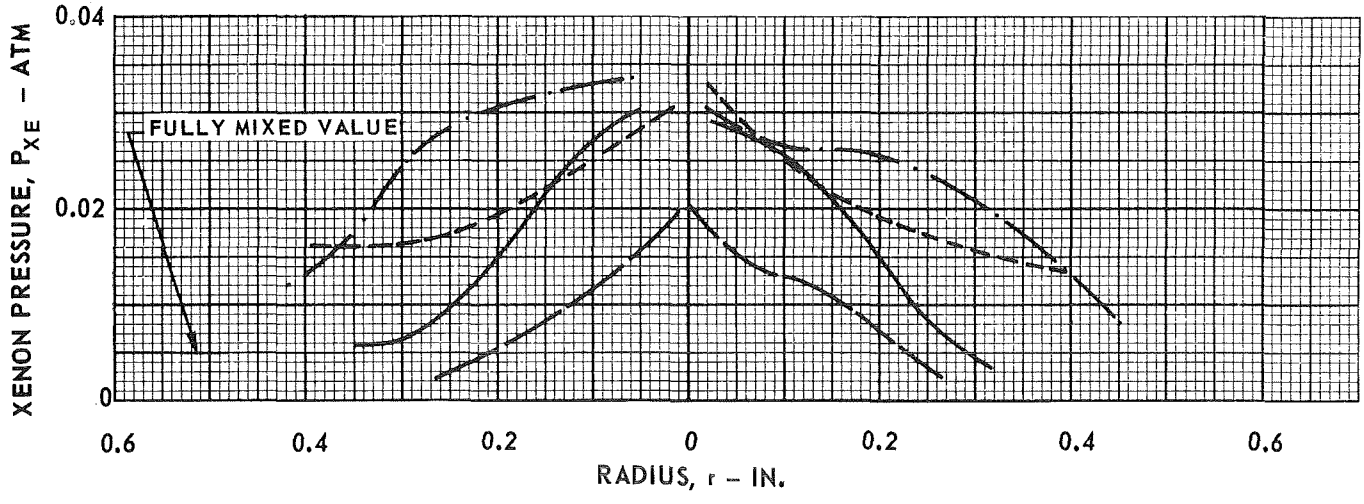

RADIAL DISTRIBUTIONS OF TEMPERATURE AND XENON PARTIAL PRESSURE FOR A PERIPHERAL-WALL-DRIVEN ARGON PLASMA VORTEX WITH CENTERLINE XENON INJECTION

XENON INJECTED AXIALLY THROUGH PROBE ON VORTEX CENTERLINE (SEE FIG. 2c)
SEE FIG. 1b FOR ARGON INJECTION CONFIGURATION
SEE TABLE I FOR FLOW AND POWER CONDITIONS

LINE	AXIAL POSITION (SEE FIG. 2c)
———	1
—·—	2
– – –	3
—— ——	4

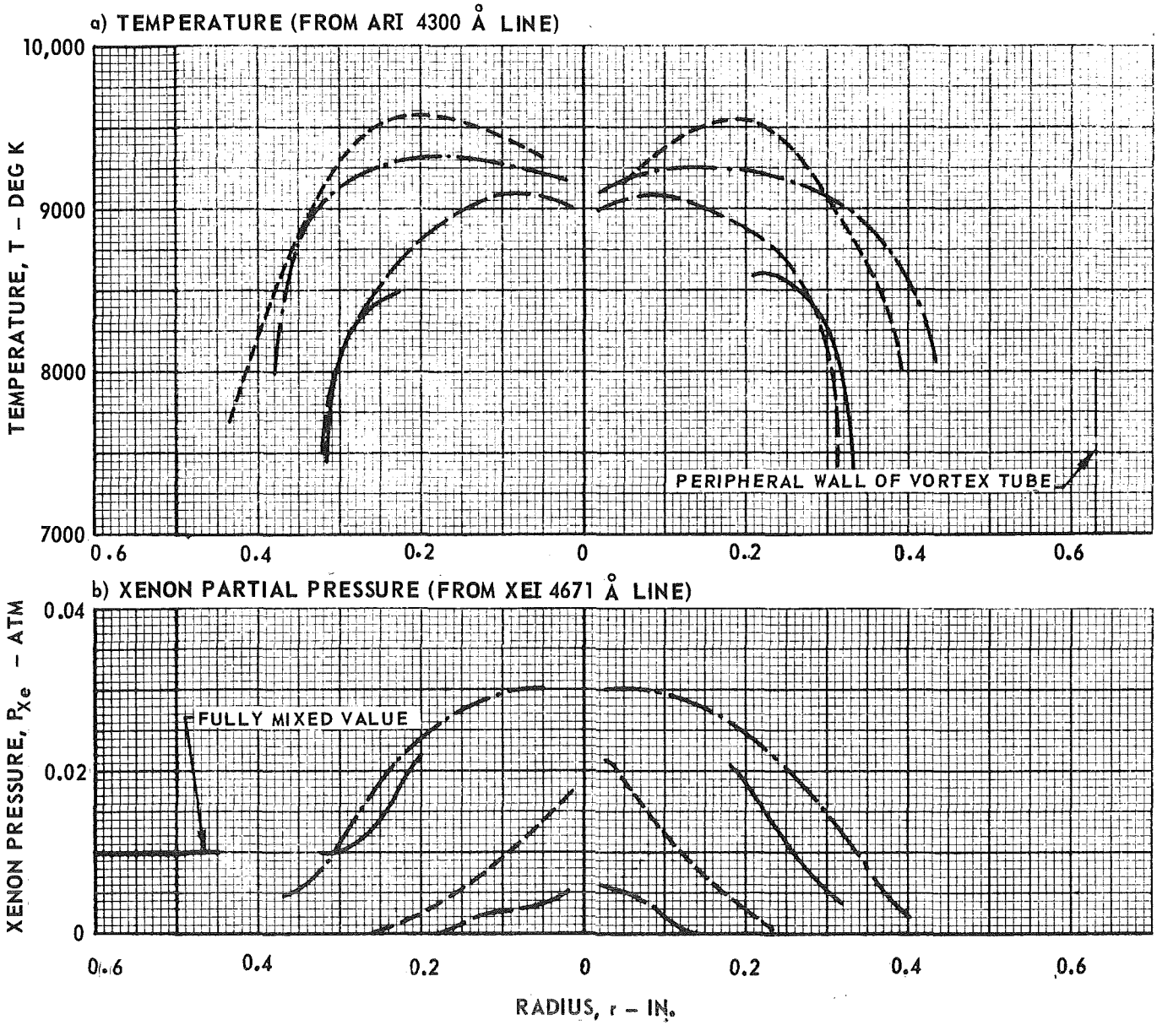

FIG. 22

EFFECTS OF REYNOLDS NUMBER AND HEAVY-GAS MOLECULAR WEIGHT ON THE AVERAGE HEAVY-GAS PARTIAL PRESSURE IN THE HIGH REYNOLDS NUMBER TEST FACILITY

PERIPHERAL-WALL LIGHT-GAS INJECTION (SEE FIG. 5)
PERIPHERAL-WALL HEAVY-GAS INJECTION (SEE FIG. 7a)
ARROWS INDICATE POINTS FOR WHICH RADIAL DISTRIBUTIONS ARE PRESENTED IN FIGS. 23, 24, AND 25
SEE TABLE II FOR OPERATING CONDITIONS

SYMBOL	HEAVY GAS	W_F-LB/SEC	FULLY MIXED (SEE TEXT)
△	$He + I_2$	0.4×10^{-3}	— · — · — · —
○	$N_2 + I_2$	1.1×10^{-3}	- - - - - - - - - -
□	$SF_6 + I_2$	0.8×10^{-3}	— — — —

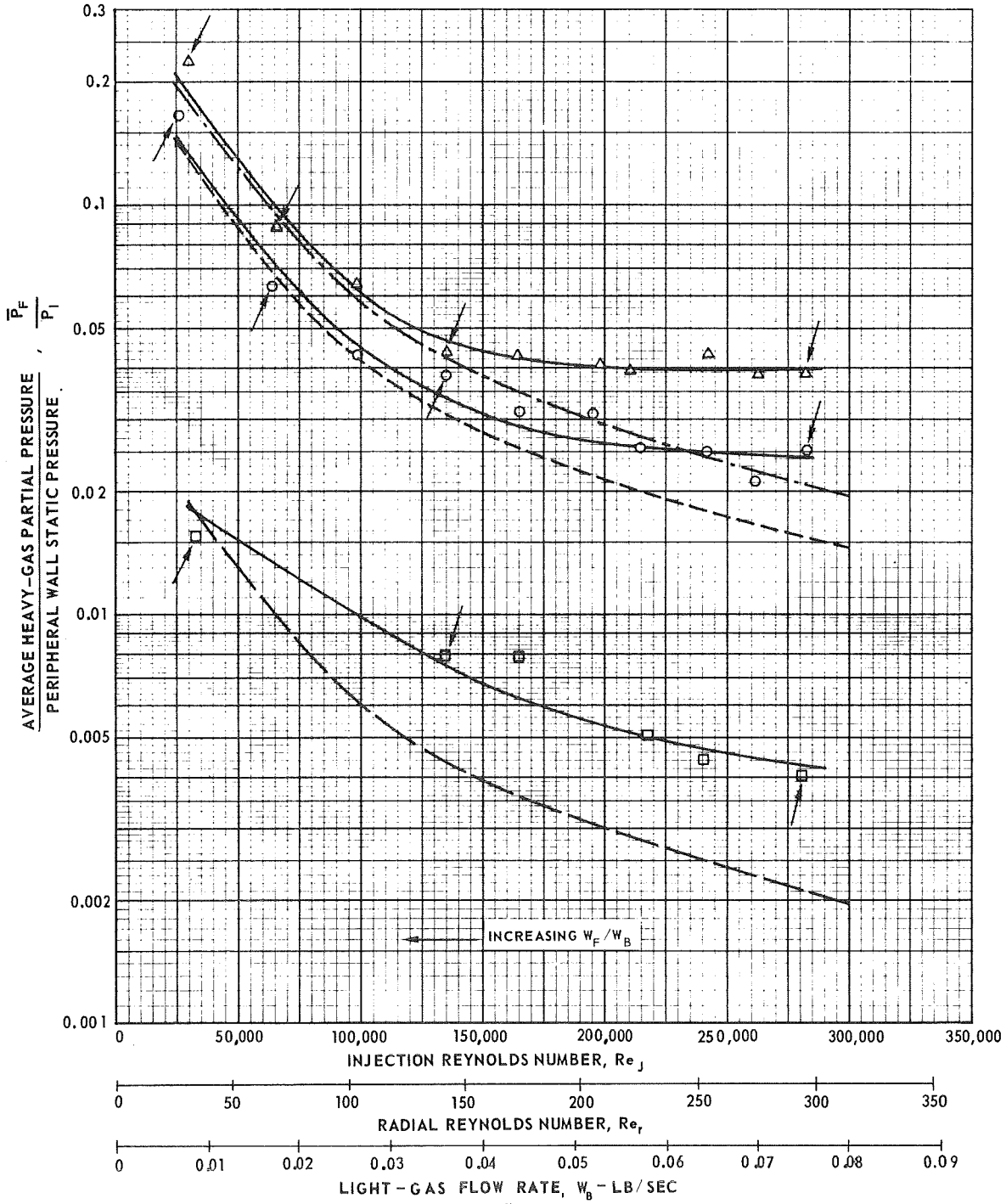

FIG. 23

RADIAL DISTRIBUTIONS OF HEAVY-GAS PARTIAL PRESSURE AT SEVERAL INJECTION REYNOLDS NUMBERS -- HELIUM/IODINE HEAVY GAS

PERIPHERAL-WALL LIGHT-GAS INJECTION (SEE FIG. 5)
PERIPHERAL-WALL HEAVY-GAS INJECTION (SEE FIG. 7a)
CONSTANT HEAVY-GAS FLOW RATE, $W_F = 0.4 \times 10^{-3}$ LB/SEC
SEE TABLE II FOR OPERATING CONDITIONS

SYM	Re_j	$\overline{P_F}/P_1$	$\overline{P_F}/P_1\|_{MIX}$
○	0.3×10^5	— —	0.20
⬭	0.65×10^5	·····	0.096
□	1.3×10^5	— · —	0.041
◇	2.7×10^5	— — —	0.021

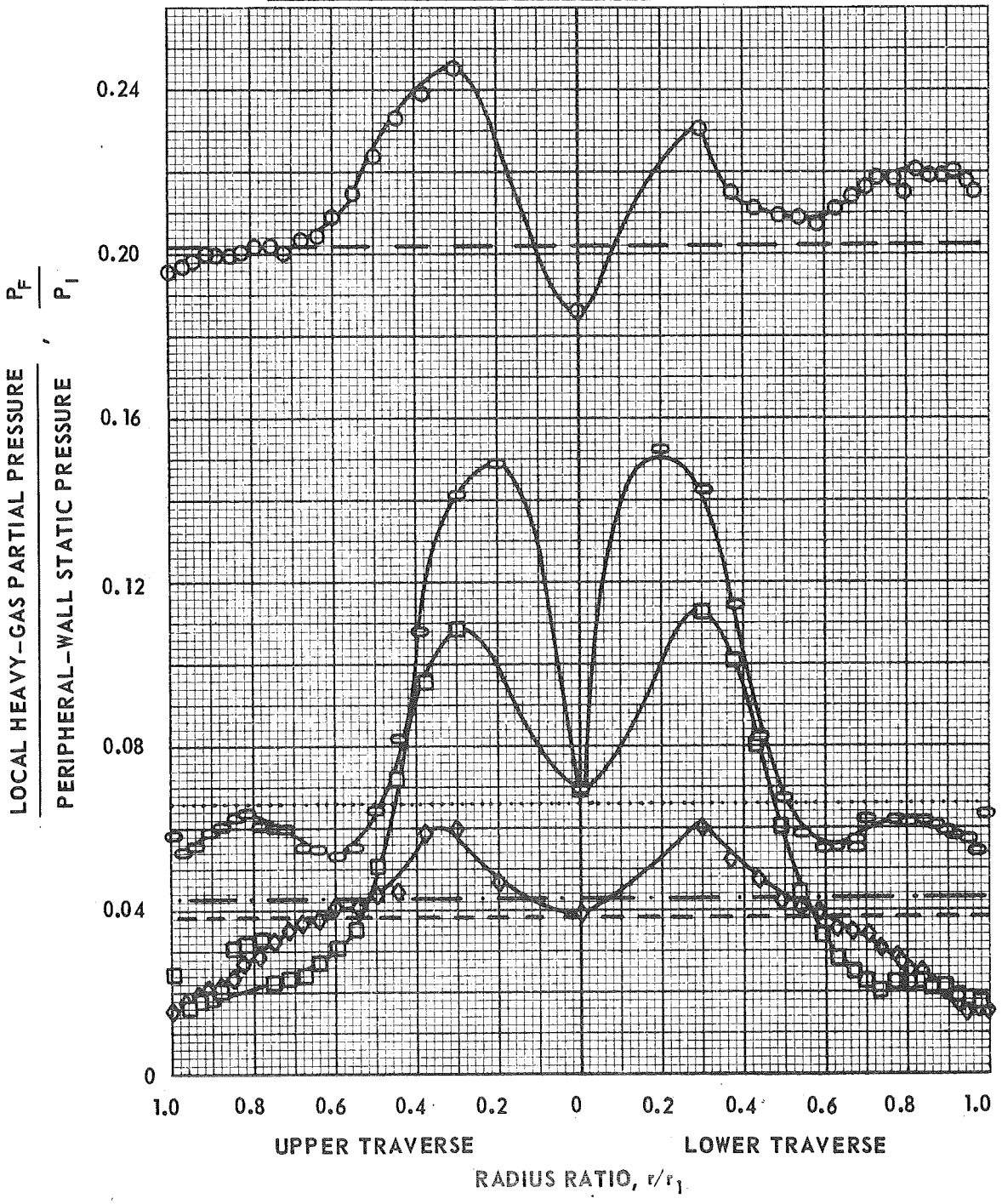

FIG. 24

RADIAL DISTRIBUTIONS OF HEAVY-GAS PARTIAL PRESSURE AT SEVERAL INJECTION REYNOLDS NUMBERS -- NITROGEN/IODINE HEAVY GAS

PERIPHERAL-WALL LIGHT-GAS INJECTION (SEE FIG. 5)
PERIPHERAL-WALL HEAVY-GAS INJECTION (SEE FIG. 7a)
CONSTANT HEAVY-GAS FLOW RATE, $W_F = 1.2 \times 10^{-3}$ LB/SEC
SEE TABLE III FOR OPERATING CONDITIONS

SYMBOL	Re_j	$\overline{P}_F/P_I$	$\overline{P}_F/P_I\|_{MIX}$
—○—	0.3×10^5	—·—	0.07
—⬭—	0.63×10^5	----------	0.032
—□—	1.3×10^5	— —	0.016
—◇—	2.8×10^5	— — — —	0.17

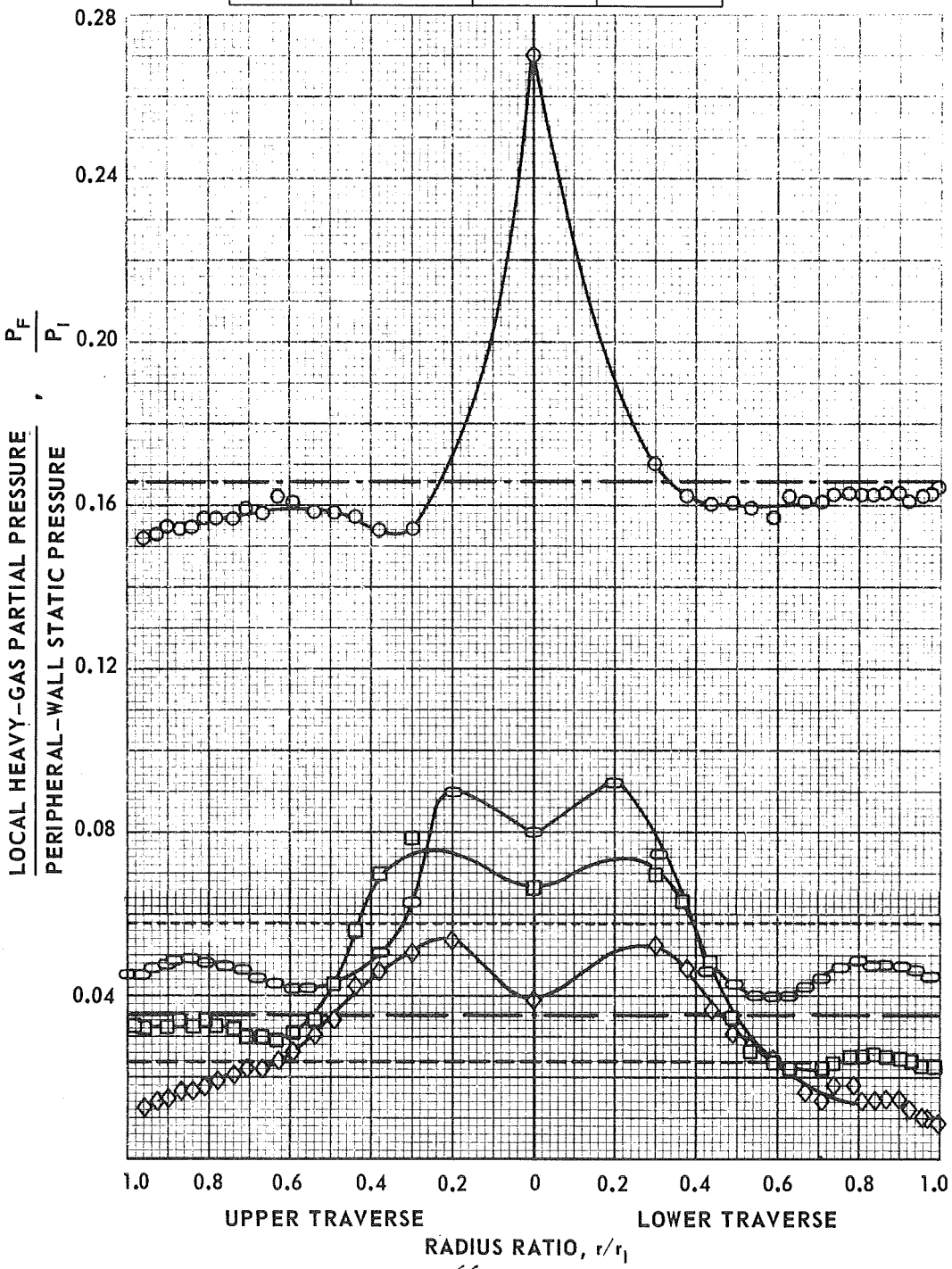

FIG. 25

RADIAL DISTRIBUTIONS OF HEAVY-GAS PARTIAL PRESSURE AT SEVERAL INJECTION REYNOLDS NUMBERS -- SULFUR-HEXAFLUORIDE/IODINE HEAVY GAS

PERIPHERAL-WALL LIGHT-GAS INJECTION (SEE FIG. 5)
PERIPHERAL-WALL HEAVY-GAS INJECTION (SEE FIG. 7a)
CONSTANT HEAVY-GAS FLOW RATE, $W_F \simeq 0.8 \times 10^{-3}$ LB/SEC
SEE TABLE III FOR OPERATING CONDITIONS

SYMBOL	Rej	$\overline{P}_F/P_1$	$\overline{P}_F/P_1 \mid_{MIX}$
—○—	0.3×10^5	—·—·	0.018
—□—	1.3×10^5	— — —	0.0044
—◇—	2.8×10^5	- - - - -	0.0020

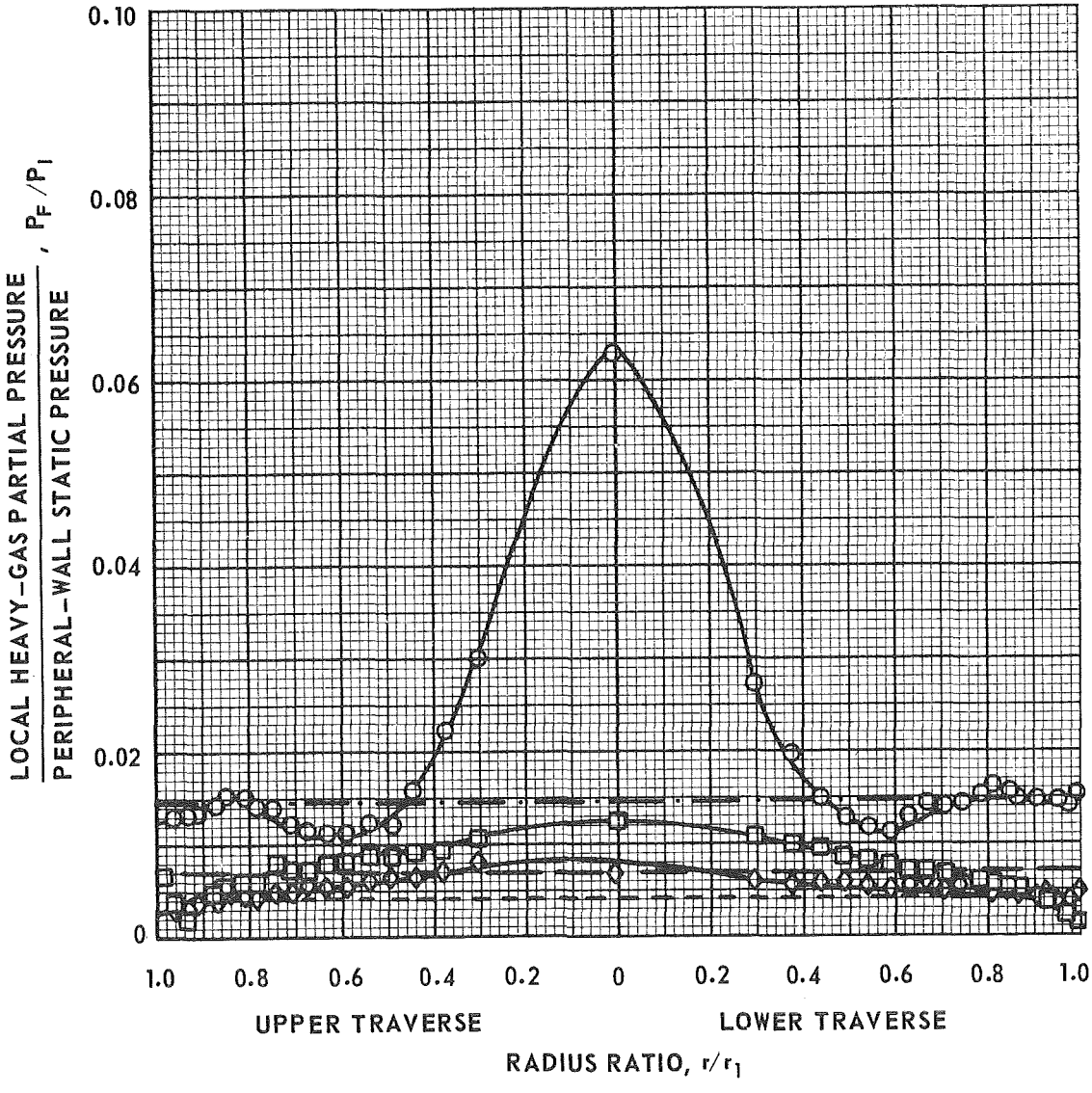

H-910091-20

EFFECT OF HEAVY-GAS INJECTION FLOW RATE ON AVERAGE HEAVY-GAS PARTIAL PRESSURE

FIG. 26

CONSTANT LIGHT-GAS FLOW RATE, $W_B = 5.9 \times 10^{-2}$ LB/SEC ($Re_J = 2.2 \times 10^5$)
PERIPHERAL-WALL LIGHT-GAS INJECTION (SEE FIG. 5)
PERIPHERAL-WALL HEAVY-GAS INJECTION (SEE FIG. 7a)
ARROWS INDICATE POINTS FOR WHICH RADIAL DISTRIBUTIONS ARE PRESENTED IN FIG. 27
SEE TABLE III FOR OPERATING CONDITIONS

SYMBOL	HEAVY GAS	FULLY MIXED (SEE TEXT)
△	$He + I_2$	- - - - -
○	$N_2 + I_2$	— · — · —
□	$SF_6 + I_2$	———

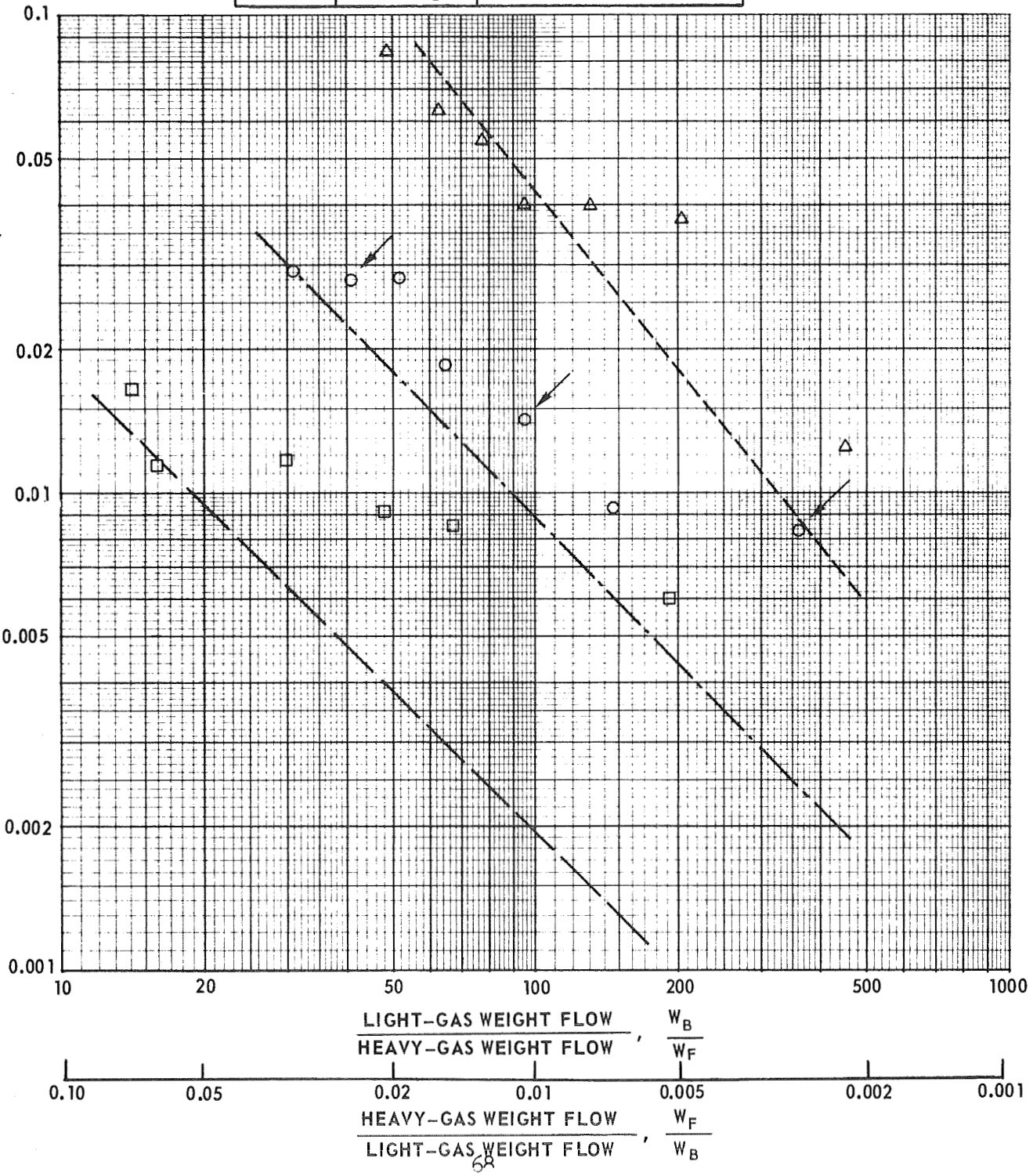

AVERAGE HEAVY-GAS PARTIAL PRESSURE / PERIPHERAL WALL STATIC PRESSURE, $\bar{P}_F / P_1$

LIGHT-GAS WEIGHT FLOW / HEAVY-GAS WEIGHT FLOW, W_B / W_F

HEAVY-GAS WEIGHT FLOW / LIGHT-GAS WEIGHT FLOW, W_F / W_B

RADIAL DISTRIBUTIONS OF HEAVY-GAS PARTIAL PRESSURE AT SEVERAL HEAVY-GAS FLOW RATES--NITROGEN/IODINE HEAVY GAS

PERIPHERAL WALL LIGHT-GAS INJECTION (SEE FIG. 5)
PERIPHERAL WALL HEAVY-GAS INJECTION (SEE FIG. 7a)
CONSTANT LIGHT GAS FLOW RATE: $W_B = 5.9 \times 10^{-2}$ LB/SEC ($Re_j = 2.2 \times 10^5$)
SEE TABLE III FOR OPERATING CONDITIONS

SYMBOL	W_B/W_F	W_F/W_B	$\overline{P}_F/P_I$	$\overline{P}_F/P_I\|_{MIX}$
—○—	41	0.0244	— — — —	0.022
—□—	94	0.0106	—·—·	0.0095
—△—	360	0.0028	—— ——	0.0024

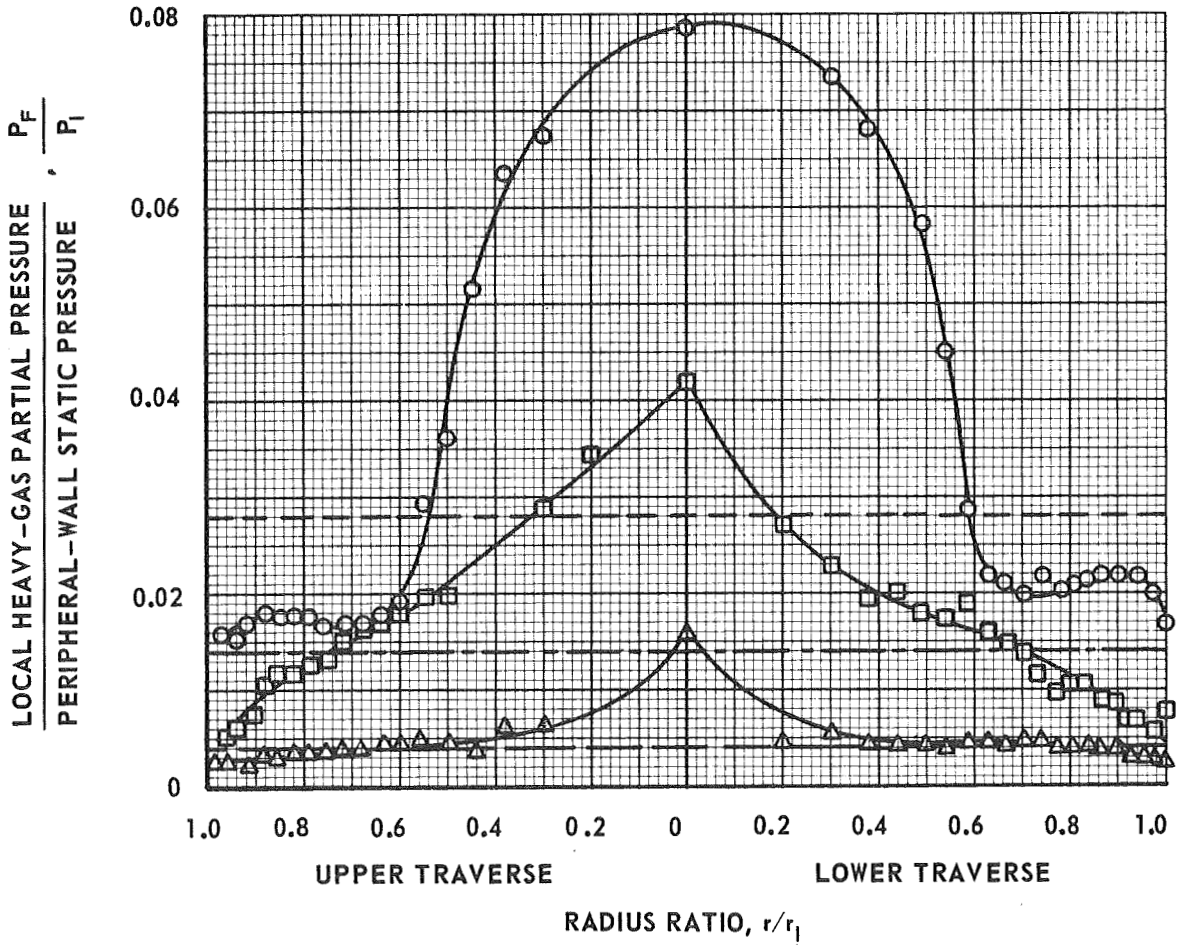

FIG. 28

EFFECT OF HEAVY-TO LIGHT-GAS INJECTION VOLUME FLOW RATES ON AVERAGE HEAVY-GAS PARTIAL PRESSURE

PERIPHERAL-WALL LIGHT-GAS INJECTION (SEE FIG. 5)
PERIPHERAL-WALL HEAVY-GAS INJECTION (SEE FIG. 7a)

TYPE OF TEST	SYM	HEAVY-GAS	W_B - LB/SEC	W_F - LB/SEC	DATA FROM
VARIABLE W_B, CONSTANT W_F	△	$He+I_2$	0.008→0.08	$0.4X10^{-3}$	FIG. 22
	○	N_2+I_2	0.008→0.08	$1.1X10^{-3}$	FIG. 22
	□	SF_6+I_2	0.008→0.08	$0.8X10^{-3}$	FIG. 22
CONSTANT W_B, VARIABLE W_F	▲	$He+I_2$	0.059	$0.13→1.2X10^{-3}$	FIG. 26
	●	N_2+I_2	0.059	$0.17→2.0X10^{-3}$	FIG. 26
	■	SF_6+I_2	0.059	$0.2→4.3X10^{-3}$	FIG. 26

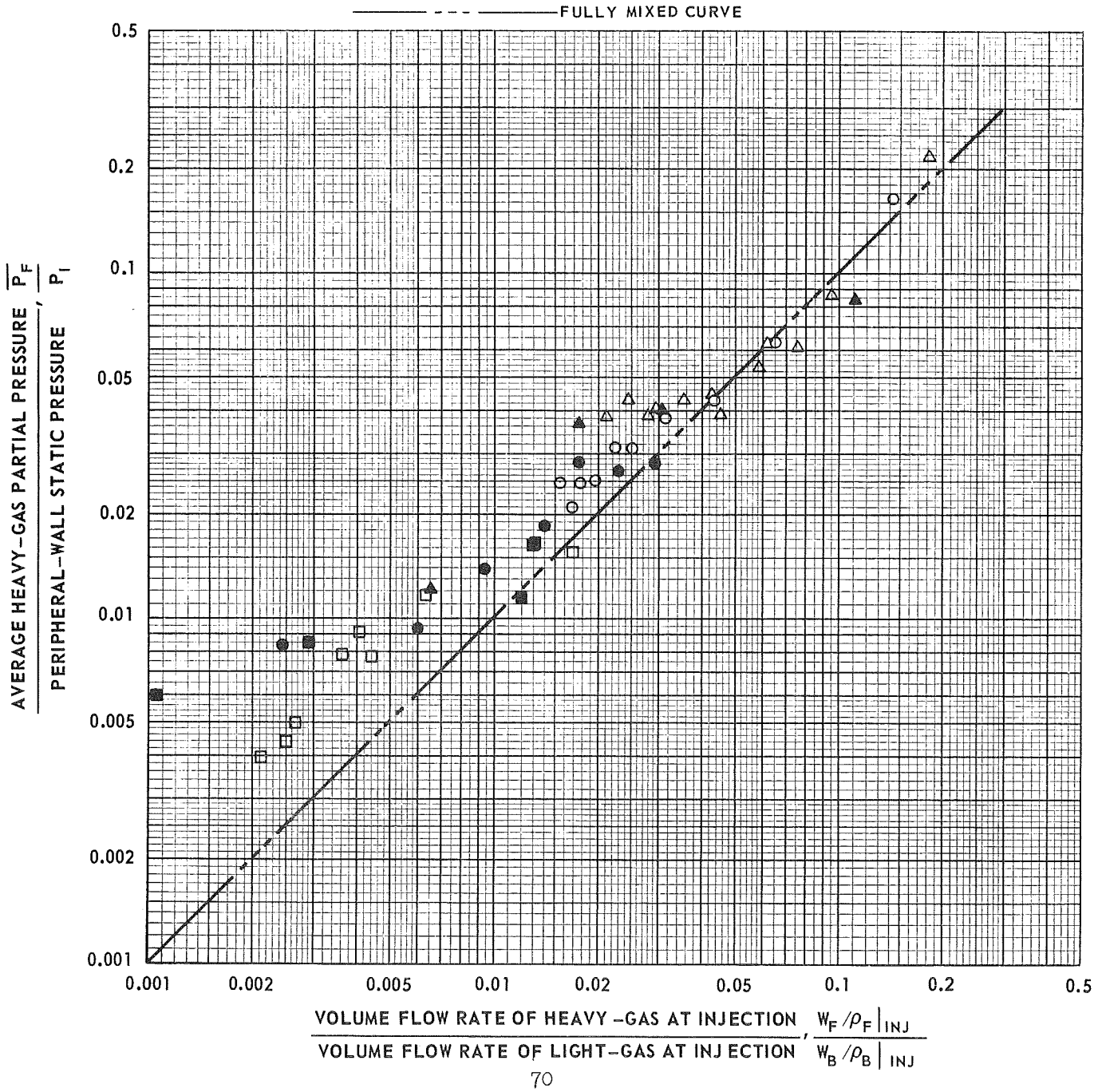

FIG. 29

EFFECT OF BYPASS ON AVERAGE HEAVY-GAS PARTIAL PRESSURE FOR CONSTANT LIGHT-GAS FLOW RATE -- NITROGEN/IODINE HEAVY GAS

BYPASS WITHDRAWN THROUGH PERIPHERAL WALL AT BOTH ENDS OF VORTEX TUBE (SEE FIG. 5a)
PERIPHERAL-WALL LIGHT-GAS INJECTION (SEE FIG. 5)
CONSTANTS: $W_B = 6.0 \times 10^{-2}$ LB/SEC, $Re_j = 2.25 \times 10^5$
ARROWS INDICATE POINTS FOR WHICH RADIAL DISTRIBUTIONS ARE PRESENTED IN FIG. 30
SEE TABLE II FOR OPERATING CONDITIONS

SYMBOL	HEAVY-GAS INJECTION LOCATION	W_F - LB/SEC
□	PERIPHERAL WALL (SEE FIG. 7a)	1.23×10^{-3}
◇	END WALL (SEE FIG. 7b)	1.21×10^{-3}

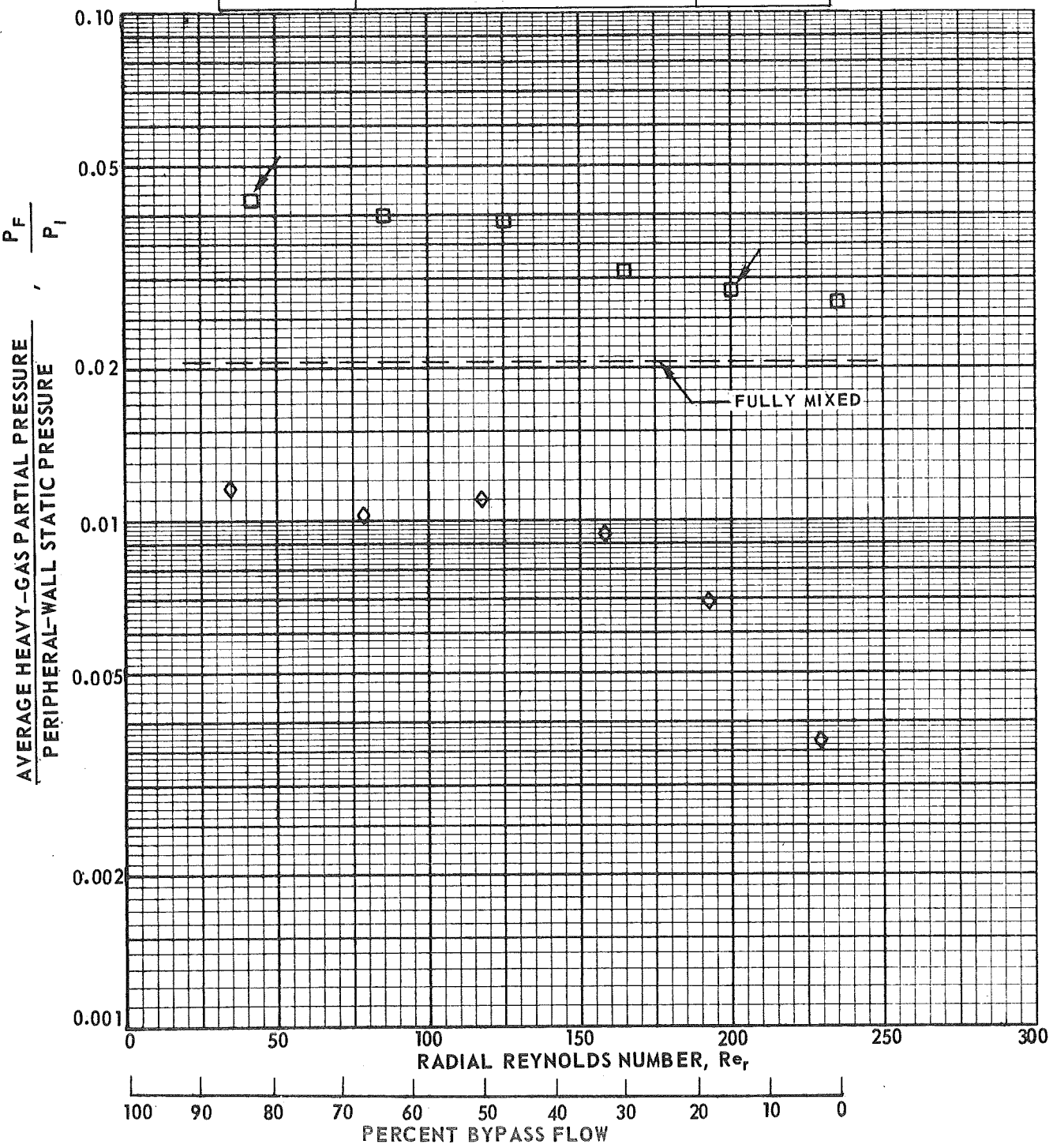

EFFECT OF BYPASS ON THE LOCAL HEAVY-GAS PARTIAL PRESSURE - - NITROGEN/IODINE HEAVY GAS

PERIPHERAL-WALL LIGHT-GAS INJECTION
PERIPHERAL-WALL HEAVY-GAS INJECTION
CONSTANTS: $W_F = 1.23 \times 10^{-3}$ LB/SEC
$Re_j = 2.25 \times 10^5$
SEE TABLE II FOR OPERATING CONDITIONS

SYMBOL	% BYPASS	$\overline{P_F}/P_l$	$\overline{P_F}/P_l \mid_{MIX}$
—○—	82.8	—·—·	0.02
—□—	14.4	— — — —	0.02

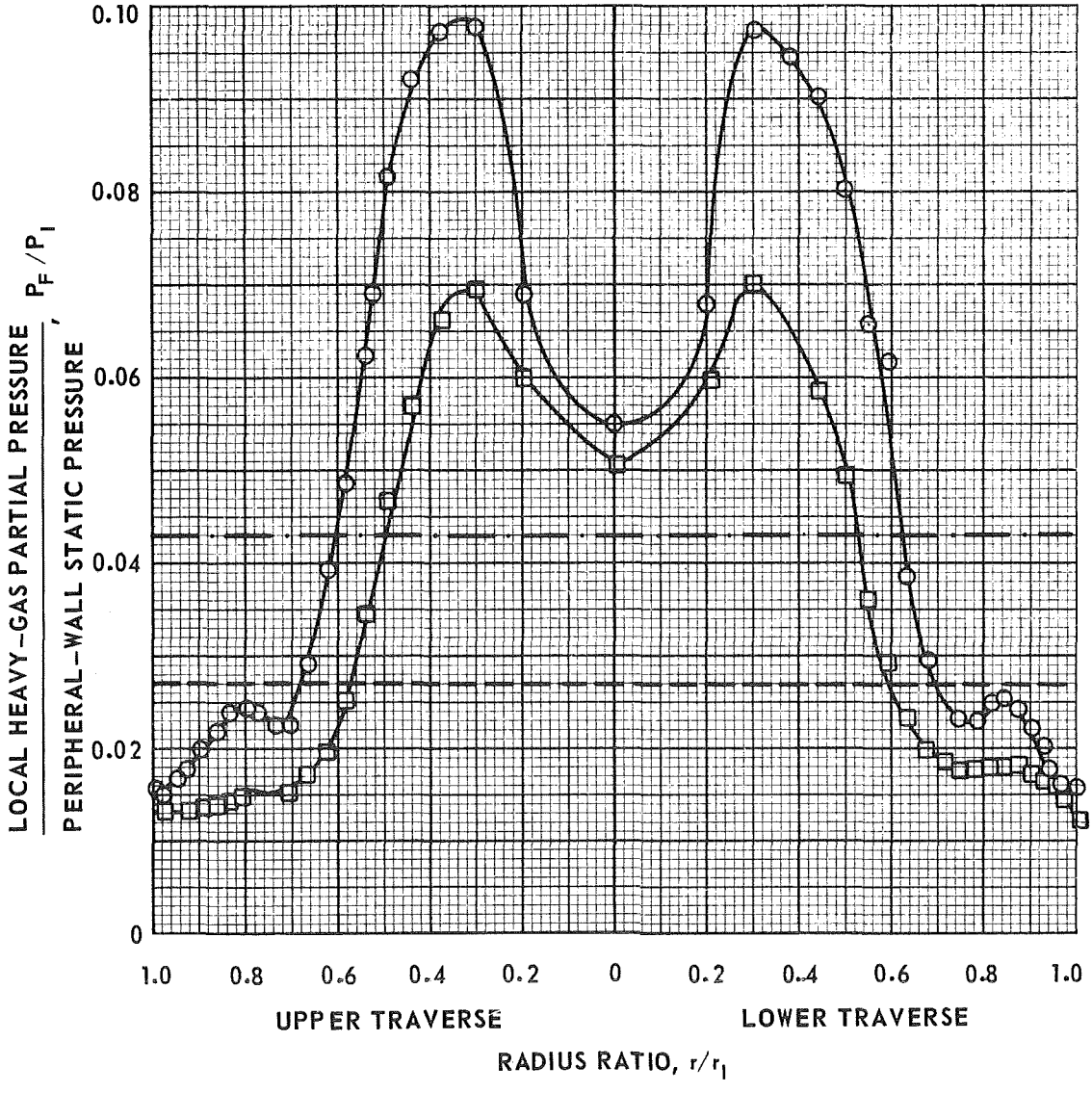

FIG. 31

EFFECT OF LIGHT-GAS INJECTION CONFIGURATION ON HEAVY-GAS CONTAINMENT FOR CONFIGURATIONS HAVING END-WALL HEAVY-GAS INJECTION -- NITROGEN/IODINE HEAVY GAS

CONSTANT HEAVY-GAS FLOW RATE

SEE FIG. 7b FOR END-WALL HEAVY-GAS INJECTION CONFIGURATION

ARROWS INDICATE POINTS FOR WHICH RADIAL DISTRIBUTIONS ARE PRESENTED IN FIG. 32

SEE TABLE III FOR OPERATING CONDITIONS

SYMBOL	LIGHT-GAS INJECTION CONFIGURATION	W_F - LB/SEC
◇	PERIPHERAL WALL (SEE FIG. 5)	1.3×10^{-3}
□	END WALL (SEE FIG. 6)	1.6×10^{-3}
○	DATA FROM FIG. 22 (PERIPHERAL-WALL LIGHT-GAS INJECTION, PERIPHERAL-WALL HEAVY-GAS INJECTION)	

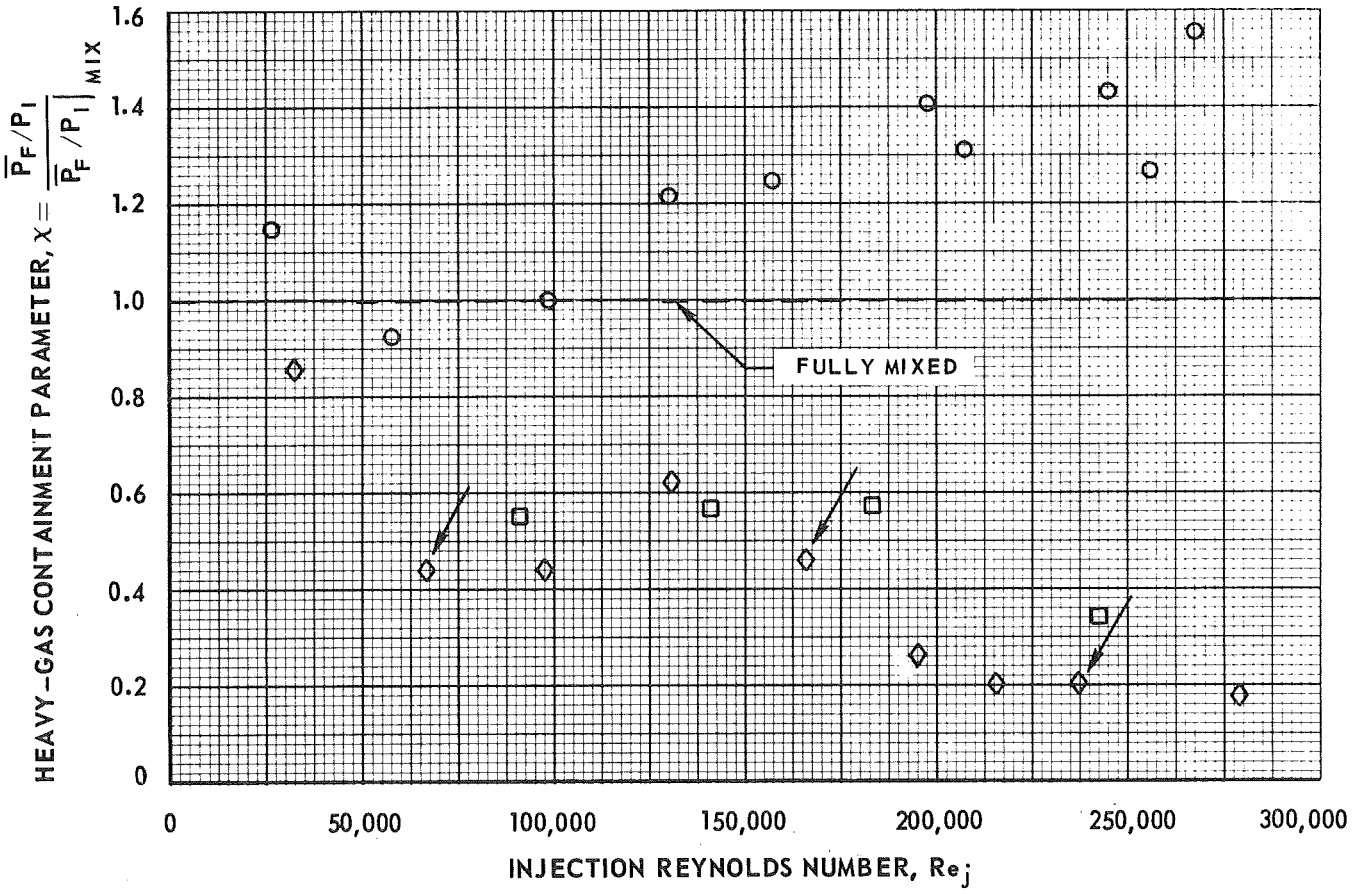

FIG. 32

RADIAL DISTRIBUTIONS OF HEAVY-GAS PARTIAL PRESSURE AT SEVERAL INJECTION REYNOLDS NUMBERS -- NITROGEN/IODINE HEAVY GAS

PERIPHERAL-WALL LIGHT-GAS INJECTION (SEE FIG. 5)
END-WALL HEAVY-GAS INJECTION (SEE FIG. 7b)
CONSTANT HEAVY-GAS FLOW RATE: $W_F = 1.3 \times 10^{-3}$
SEE TABLE II FOR OPERATING CONDITIONS

SYMBOL	Re_j	$\bar{P}_F/P_I$	$\bar{P}_F/P_I\|_{MIX}$
—△—	0.7×10^5	- - - -	0.07
—□—	1.7×10^5	—·—·	0.028
—○—	2.4×10^5	—— ——	0.02

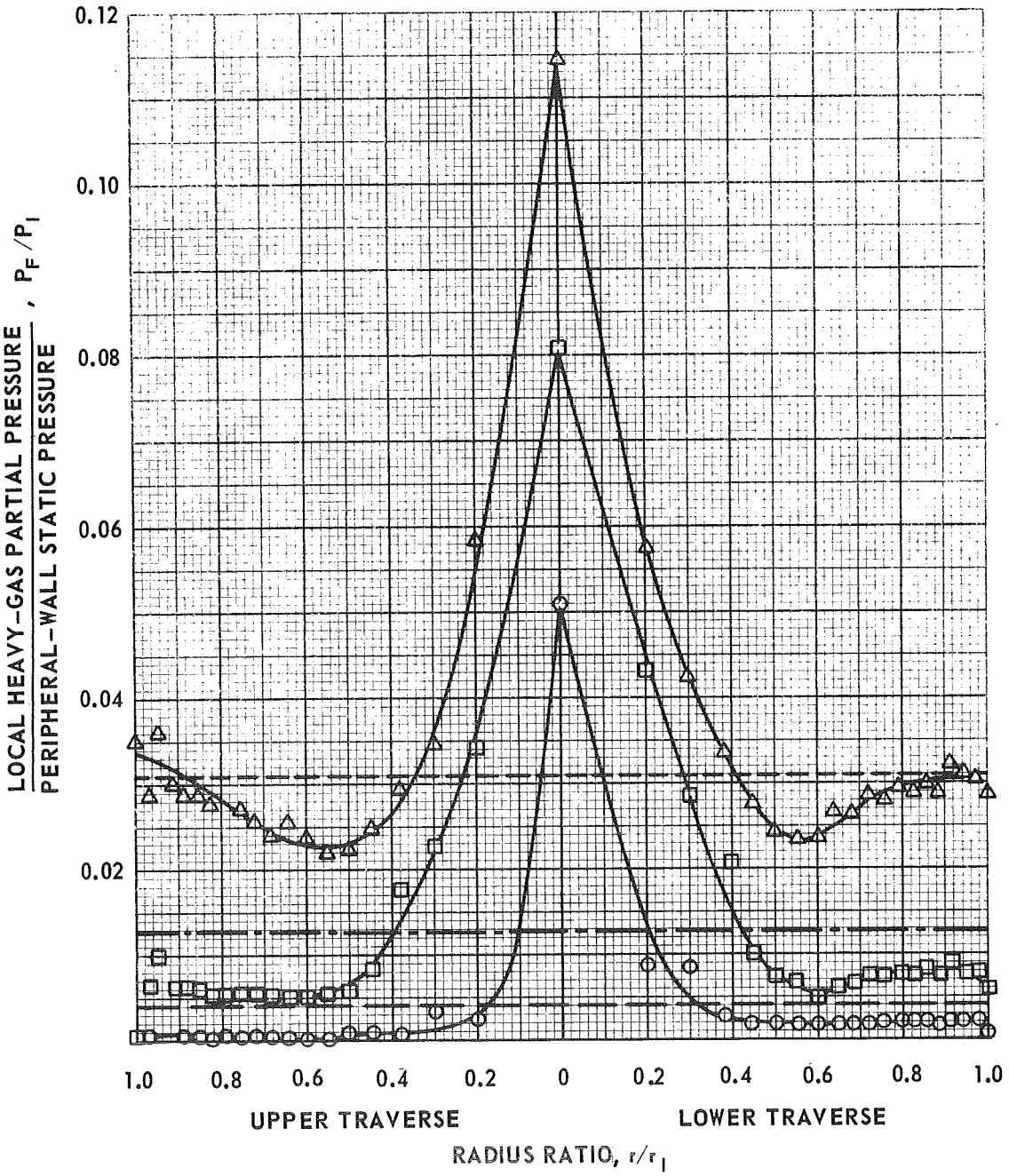

FIG. 33

AXIAL AND RADIAL STATIC PRESSURE DISTRIBUTIONS IN HEATED AND UNHEATED ARGON VORTEXES

1.26-IN.-ID VORTEX TUBE
END-WALL LIGHT-GAS INJECTION (SEE FIG. 1a)
FLOW AND POWER CONDITIONS LISTED IN TABLE I, COLUMN 1
GEOMETRY AND FLOW RATES ARE SAME IN BOTH HEATED AND UNHEATED VORTEXES

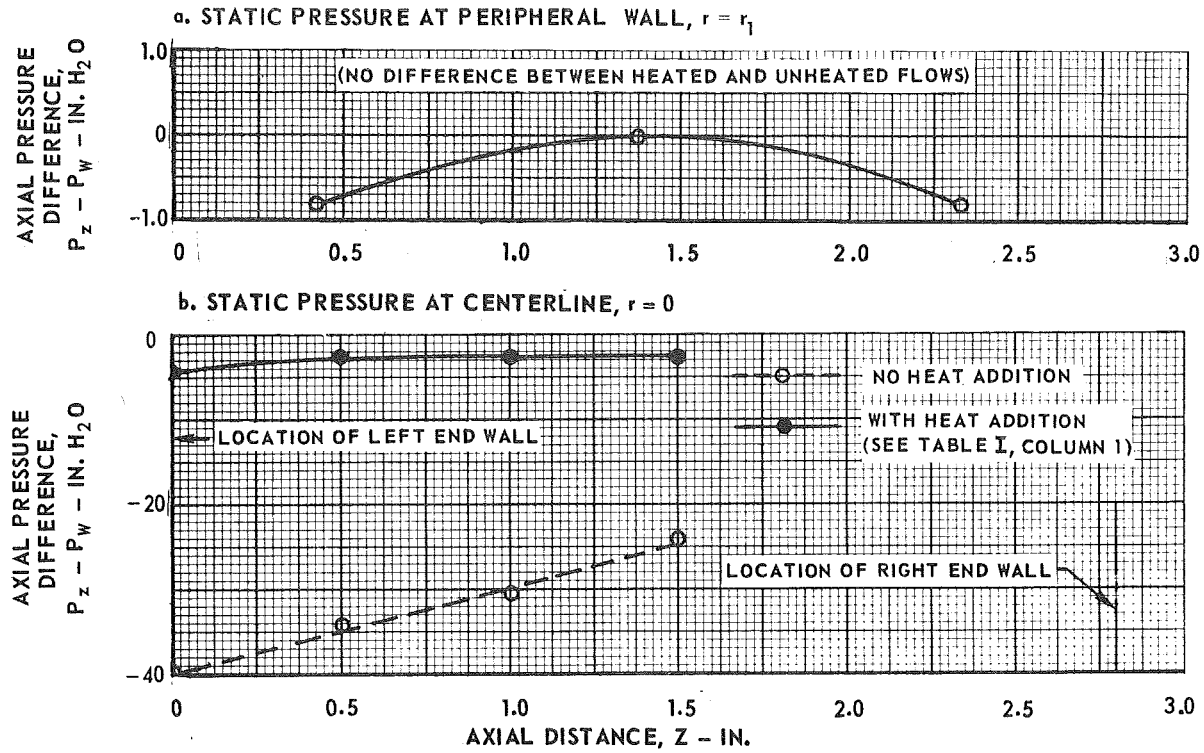

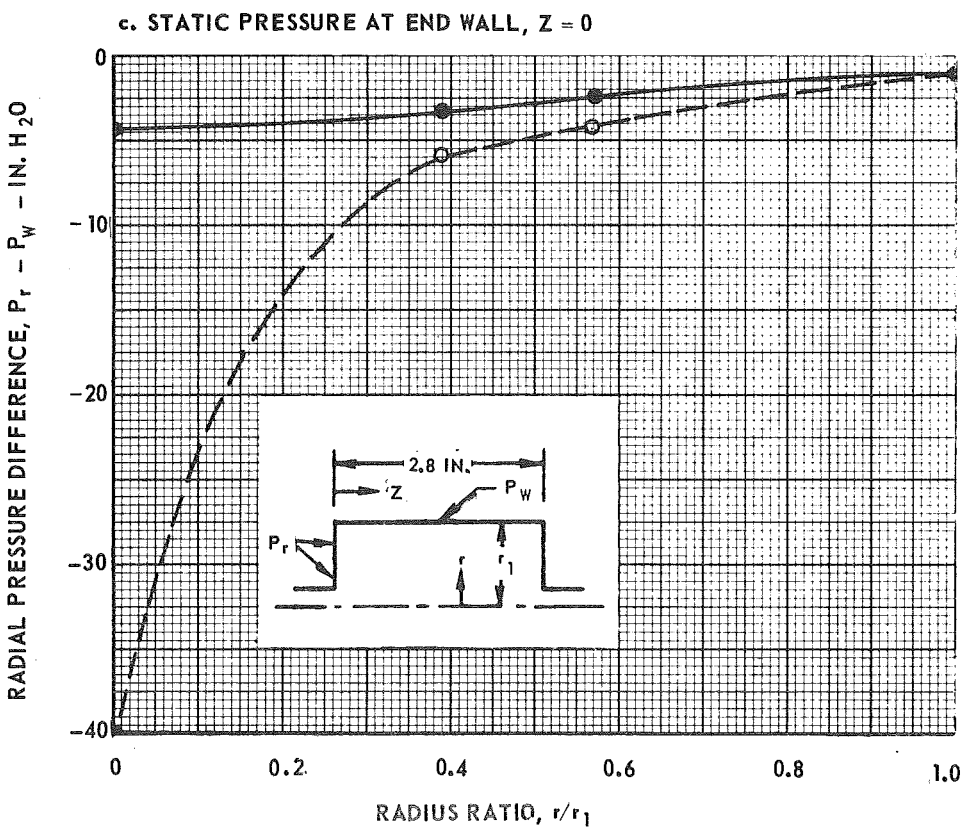

RADIAL DISTRIBUTIONS OF HEAVY-GAS PARTIAL PRESSURE IN HEATED AND UNHEATED VORTEXES

PERIPHERAL-WALL LIGHT-GAS INJECTION
PERIPHERAL-WALL HEAVY-GAS INJECTION

LINE	FACILITY	W_B/W_F	M_F/M_B	Re_j	DATA FROM
———	80-KW R-F	66	3.3	1.0×10^5	FIG. 20
– – – –	HRN	46	5.0	1.3×10^5	FIG. 25

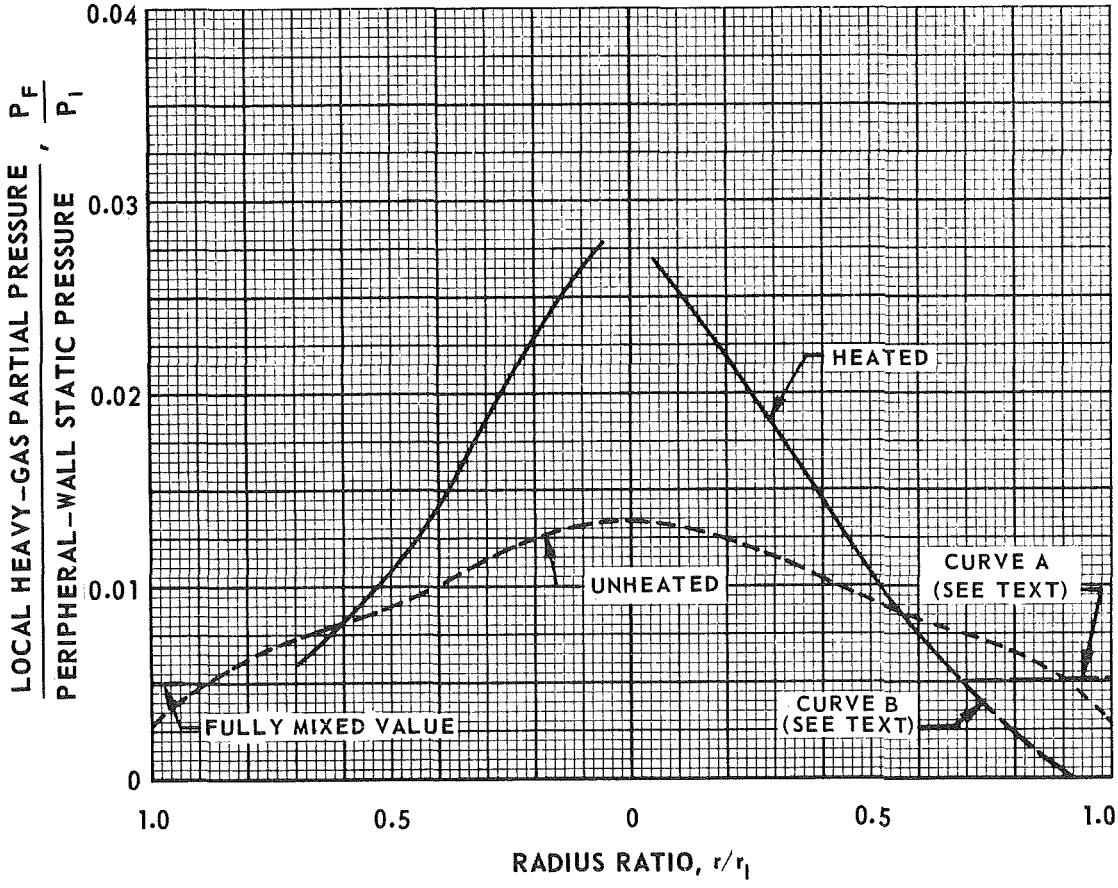

FIG. 35

COMPARISON OF AVERAGE HEAVY-GAS PARTIAL PRESSURE IN HEATED AND UNHEATED TWO-COMPONENT VORTEXES

PERIPHERAL-WALL HEAVY-GAS INJECTION
PERIPHERAL-WALL LIGHT-GAS INJECTION
/// APPROXIMATE RANGE OF DATA FROM UNHEATED TESTS (FROM FIG. 28)
▽ VALUE DETERMINED FROM INTEGRATION OF CURVE A FROM FIG. 34
△ VALUE DETERMINED FROM INTEGRATION OF CURVE B FROM FIG. 34

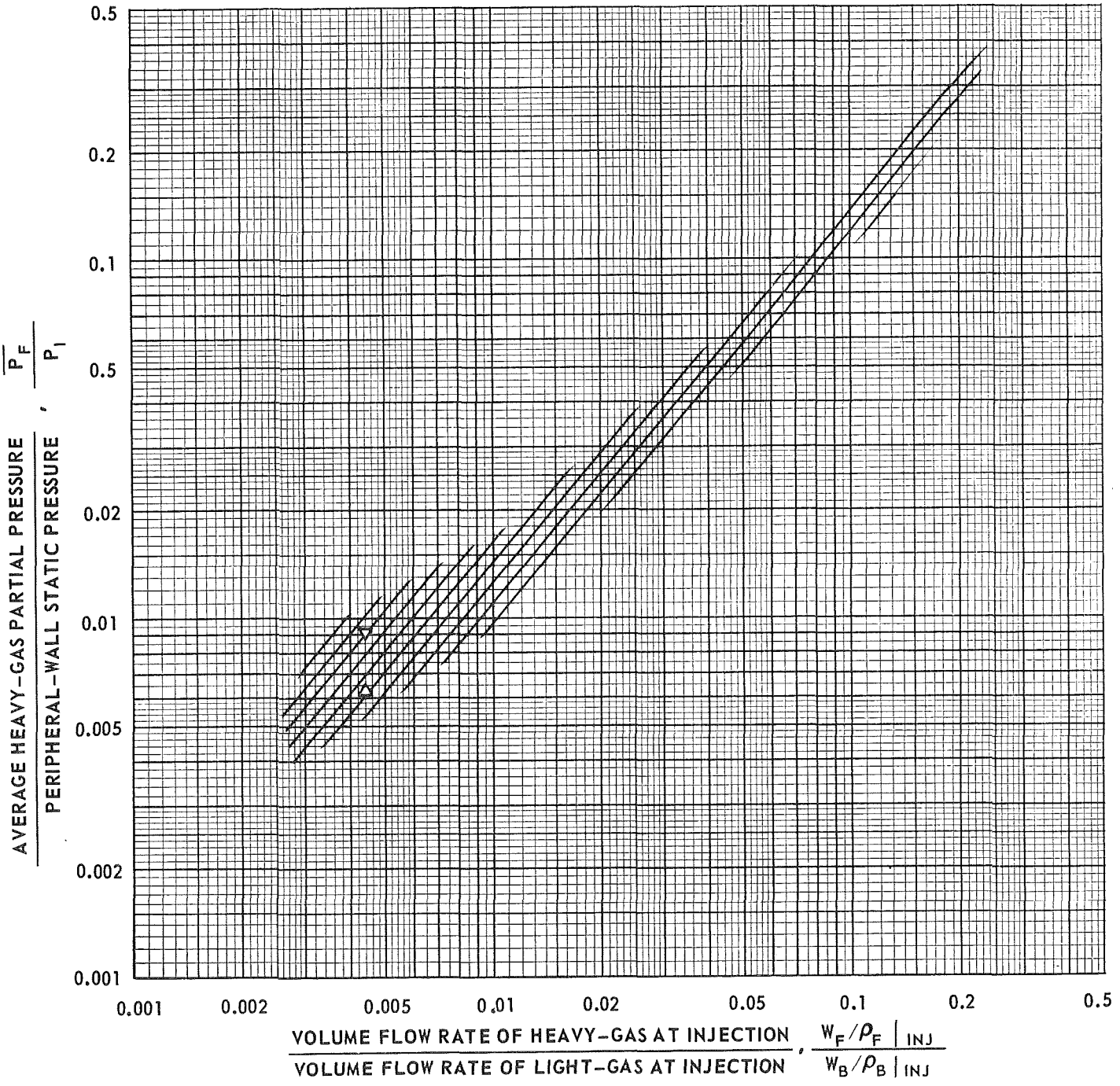

COMPARISON OF MAXIMUM TO FULLY MIXED VALUES OF HEAVY-GAS PARTIAL-PRESSURE RATIO IN HEATED AND UNHEATED VORTEXES

SEE TEXT FOR CONFIGURATIONS USED

SYM	TYPE OF TEST	HEAVY GAS	DATA FROM	$A_{F,J}/A_{B,J}$
△	UNHEATED	$He + I_2$	FIG. 23	0.0132
○	↓	$N_2 + I_2$	FIG. 24	↓
□	↓	$SF_6 + I_2$	FIG. 25	↓
●	↓	$N_2 + I_2$	FIG. 27	↓
◈	HEATED	Xe	FIG. 17b	0.102
◈	↓	↓	FIG. 18b	0.056
◈	↓	↓	FIG. 20b	0.102

$$\frac{V_{F,J}}{V_{B,J}} = \left(\frac{W_F/\rho_F\,|_{INJ}}{W_B/\rho_B\,|_{INJ}}\right)\left(\frac{1}{A_{F,J}/A_{B,J}}\right)$$